GENETIC FACTORS INFLUENCING OLIGODENDROCYTE DEMYELINATION

By

QILI YU

A dissertation submitted to the

School of Graduate Studies

Rutgers, the State University of New Jersey

In partial fulfillment of the requirements

For the degree of

Doctor of Philosophy

Graduate Program in Neuroscience

Written under the direction of

Renping Zhou

And approved by

_____

_____

_____

_____

_____

New Brunswick, New Jersey

January, 2018

ABSTRACT OF THE DISSERTATION

Genetic Factors Influencing Oligodendrocyte Demyelination

by QILI YU

Dissertation Director:

Renping Zhou

Oligodendrocytes are an important cell type in the central nervous system (CNS). Their most prominent function in the brain is to provide axonal processes of neurons with insulation by means of creating myelin sheath that wrap around axons (myelination), which serves to increase the nerve conduction velocity, as well as to provide trophic support.

Due to their high metabolic demand, oligodendrocytes are particularly susceptible to demyelinating pathology, the most prominent ones being multiple sclerosis and various leukodystrophies. Thus understanding the genetic and molecular factors that contribute to oligodendrocyte demyelination is crucial to our understanding of the diseases and identification of therapeutic targets.

In order to address this issue, we conducted two studies in an attempt to elucidate the factors that are involved in regulation of the demyelination process in the CNS. Our first approach involves challenging two different mouse strains (C57BL/6 and CD1), which have different genetic backgrounds, with the neurotoxin

cuprizone to induce a multiple sclerosis (MS)-like demyelinating pathology in the corpus callosum. We show that cuprizone induced demyelination is highly strain-dependent, and thus is under significant influence of genetic background factors. Our second approach involves probing the developmental as well as the cuprizone induced demyelinating phenotype in mice devoid of a gene that is highly expressed within CNS myelin, namely, Ephrin-B3. Our results suggest that Ephrin-B3 knockout animals exhibit relatively normal myelin-related phenotype compared to age-matched control animals, indicating that the gene is not specifically involved in regulation of oligodendrocyte myelination/demyelination in the CNS.

Along the way, we document in this dissertation another separate study that aims to probe the developmental function of a gene named Fbxl15, which is a mammalian homolog of the drosophila jetlag gene, by way of gene-specific knockout study. We report here that Fbxl15 loss of function does not explicitly impact the circadian regulation in mice, and nor does it affect behavioral parameters in mice such as learning and memory, anxiety and depressive behavior. Thus we speculate that the function of Fbxl15 is redundant throughout development and that other F-box proteins could compensate for the absence of Fbxl15.

ACKNOWLEDGEMENT

My foremost thanks go to my thesis adviser, Dr. Renping Zhou, for his great mentorship and support on my thesis work in his laboratory over the past several years. I want to thank him for giving me the invaluable opportunity to explore science on my own as a graduate student. His persistence, passion in science, and great personality has always inspired and encouraged me to become a scientist. Without his kind support, guidance and encouragement, it would be impossible to fulfill my PhD.

I want to convey great thanks to my committee members. I thank Dr. Cheryl F. Dreyfus for all of her numerous kind support and guidance for my work on the cuprizone model. I thank Dr. Alexander Kusnecov for all of his advices and kind help with the cuprizone experiments as well as the various behavioral experiments that I learned. I thank Dr. Zhiping Pang for his great patience and support for my thesis work as well as extensive discussions and insightful advices. I thank Dr. Li Cai for his great support, advice, as well as his time and sacrifice for serving on my thesis committee.

I would like to thank all of the members from the Zhou lab, including Alexander Son, Jeong Eun Park, Michal Sheleg, Gitanjali Sehrawat, Ryan Grippo, Ryan Hui, Jiyoung Jamie Park and Kevin Huang for all of their kind help and support. Being able to work with them has been so enjoyable. I would like to express special thanks to Dr. Yangyang Huang from the Dreyfus lab for her guidance with analyzing corpus callosum samples.

I would also like to thank my program director Dr. John E. Pintar for his patience and kind support with my degree process.

I reserve my last thanks to my friends and family, for their love and support, without which my degree wouldn’t be possible.

This work was supported by grants 2PO1HD023315 (R.Z.), RO1EY019012 (R.Z.), RG4257B4/1 (C.D), NS036647 (C.D.), MH104800 (A.K.) and P30ES005022.

CONTENTS

LIST OF FIGURES

LIST OF ABBREVIATIONS

AIF	apoptosis-inducing factor
APP	amyloid precursor protein
ATP	adenosine triphosphate
bHLH	basic helix-loop-helix
BrdU	Bromodeoxyuridine
CSF	cerebrospinal fluid
CNS	central nervous system
DTT	Dithiothreitol
EAE	experimental autoimmune encephalomyelitis
EM	electron microscopy
EPM	Elevated plus maze
ER	endoplasmic reticulum
ES	embryonic stem
FGF	fibroblast growth factor
GFAP	glial fibrillary acidic protein
GPCR	G protein–coupled receptor
GST-Pi	glutathione S-transferase Pi
H&E stain	hemotoxylin and eosin stain
HDAC	histone deacetylase
Iba1	ionized calcium binding adaptor molecule
IFNG	interferon-gamma
KO	knockout
LDB	Light-dark box test

LFB	luxol fast blue
LFB–PAS	Luxol fast blue–periodic acid Schiff
MAG	myelin-associated glycoprotein
MBP	myelin basic protein
MOG	myelin oligodendrocyte glycoprotein
MRF	myelin gene regulatory factor
MS	multiple sclerosis
NG2	neural/glial antigen 2
NMO	neuromyelitis optica
OPC	oligodendrocyte precursor cell
OVA	ovalbumin
PBS	phosphate buffered saline
PDGF	platelet-derived growth factor
PDI	protein disulfide isomerase
PLP	proteolipid protein
PML	Progressive multifocal leukoencephalopath
PPMS	primary-progressive
PRMS	progressive-relapsing
ROI	region of interest
RRMS	relapsing-remitting
SCF	Skp1–Cul1–F-box-protein
SCH	spinal cord homogenate
SCN	suprachiasmatic nucleus
SGZ	subgranular zone
SPMS	secondary-progressive

SVZ	subventricular zone
TIM	timeless
TNF	tumor necrosis factor
VPA	valproic acid
WD	tryptophan-aspartic acid
WT	wildtype
X-gal	5-bromo-4-chloro-3-indoly-β-D-galactopyranoside

SECTION I: STRAIN DIFFERENCES IN CUPRIZONE INDUCED OLIGODENDROCYTE DEMYELINATION

Summary

Oligodendrocytes are an important cell type in the central nervous system (CNS) whose function is to make up the myelin sheath that wraps around axons of neurons in order to provide trophic support, as well as to facilitate electrical signal conduction within the nerve cells. Due to their high metabolic demands, oligodendrocytes are specifically susceptible to damage and subsequent demyelination, the most prominent case being Multiple Sclerosis or MS, which is a severe neurological disorder caused by oligodendrocyte demyelination and affects about 2.5 million people worldwide. However the mechanisms underlying the pathogenesis of the disease remain unclear.

In this section, we investigated the role of genetic differences in contributing to oligodendrocyte demyelination by using the cuprizone toxicity model with mice of different genetic background (CD1 and C57BL/6). We demonstrate using black gold staining and luxol fast blue (LFB) staining that exposure to diet containing 0.2% cuprizone treatment resulted in less severe demyelination in CD1 mice than C57BL/6 mice. With continuous cuprizone administration, demyelination in CD1 mice was not prominent until after 7 weeks of treatment, in contrast to C57BL/6 mice, in which demyelination was already prominent at week 4 of exposure. Concomitantly, immunohistochemical analysis of the cuprizone treated brain sections of the corpus callosum overlying the fimbria fornix demonstrated significantly more glutathione S-transferase Pi (GST-Pi)-positive oligodendrocytes in the CD1 mice relative to C57BL/6 mice. Moreover, CD1 mice exhibit fewer glial fibrillary acidic protein (GFAP)-positive astrocytes, ionized calcium binding adaptor molecule 1 (Iba1)-positive microglia and neural/glial antigen 2 (NG2)-positive oligodendrocyte progenitor cells. Moreover, we analyzed 4-weeks-cuprizone treated corpus callosum tissue samples and found that CD1 mice show a smaller reduction of

myelin-associated glycoprotein (MAG) and a smaller increase of Iba1, GFAP and NG2. In order to rule out the issue of potential difference in diet consumption between strains, we measured food intake per body weight between CD1 mice and C57BL/6 mice and report no significant differences. Thus, genetic background factors appear to greatly influence the susceptibility to cuprizone induced oligodendrocyte demyelination.

Introduction

The oligodendrocyte lineage: progenitor cells

Myelin is an essential component of the vertebrate central nervous system (CNS), which is a specialized membrane structure that wraps around the axon of a nerve cell in a spiral shaped manner (B. Emery, 2010). Myelin is formed by a specific cell type called oligodendrocyte, which has a separate cell body from which the myelin structure is derived. From a developmental perspective, mature oligodendrocytes are differentiated from committed oligodendrocyte progenitor cells (OPCs) which are in turn generated from subventricular cells in the brain and the spinal cord.

In the forebrain, the first wave of OPCs that appear originate in the medial ganglionic eminence and anterior entopeduncular area of the ventral forebrain (M. Bradl & H. Lassmann, 2010). These OPCs populate the developing telencephalon, which is followed by a second wave of OPCs that originate from the lateral and caudal ganglionic eminences. Lastly, the third wave of OPCs appear postnatally in the cortex (Kessaris et al., 2005). Importantly, these serially occurring waves of OPCs during development appear to be functionally redundant, in that one source of OPCs can serve to compensate for the loss of another induced by targeted expression of genetically encoded toxin by way of migration and spreading to vacant regions, thus restoring the normal OPC distribution (Kessaris et al., 2005). This observation has led to the proposition that different OPC population are fierce competitors of one another (M. Bradl & H. Lassmann, 2010).

A common feature of the three waves of developing OPCs is that they all

migrate long distances before reaching their destination, and this migration is tightly and intricately controlled by various regulatory signals. Among which, three distinct classes of secreted signaling molecules have been identified, including growth factors such as fibroblast growth factor (FGF) (Redwine, Blinder, & Armstrong, 1997), platelet-derived growth factor (PDGF) (Spassky et al., 2001) and hepatocyte growth factor (Yan & Rivkees, 2002); chemotropic molecules such as netrins and semaphorins (Jarjour et al., 2003); and the chemokine CXCL1 (de Castro & Bribian, 2005). In addition to the above mentioned secreted molecules, extracellular matrix proteins and cell surface molecules are also reported to be involved in regulation of OPC migration (Frost, Kiernan, Faissner, & ffrench-Constant, 1996; Kiernan, Gotz, Faissner, & ffrench-Constant, 1996; Milner et al., 1997; Niehaus, Stegmuller, Diers-Fenger, & Trotter, 1999; Prestoz et al., 2004; Schnadelbach et al., 2000; Tiwari-Woodruff et al., 2001; C. Wang, Rougon, & Kiss, 1994).

Once the OPCs have located at their final destination, the majority of them differentiate into myelinating oligodendrocytes, while a minor portion of them stay and persist into adulthood.

The oligodendrocyte lineage: differentiation

The differentiation into oligodendrocytes is tightly regulated by a number of sophisticated mechanisms, including axonal surface ligands, secreted molecules and axonal activity.

Axonal surface ligands appear to be the simplest form of regulation, which would allow the myelination to be finely regulated at the subcellular level.

Interestingly, the axonally expressed ligands for contact with oligodendrocytes have so far been identified as all being inhibitory, which would prevent myelination to occur and inhibit OPC differentiation (B. Emery, 2010). These inhibitory signaling components include Jagged (S. Wang et al., 1998) which signal through Notch in the OPC, as well as LINGO-1 (Mi et al., 2005) and PSA-NCAM (Charles et al., 2000). Interestingly, neuregulins, which function as a permissive cue in the peripheral nervous system for Schwann cells are not required in the CNS (Ben Emery, 2010). However, overexpression of neuregulins in the CNS does induce excess myelination to occur.

An important signaling pathway within OPCs to induce myelination has been demonstrated to be the Wnt/β-catenin pathway. Upon the initiation of myelination, canonical Wnt signaling is activated transiently within the OPC, which is followed by a down-regulation ofβ-catenin activity and a down-regulation of the expression of Tcf4/Tcf7l2, which are transcription factors that mediate the effect of Wnt signaling (Fancy et al., 2009; Fu et al., 2009). This transient down-regulation of Wnt signaling has been shown to be crucial for the subsequent myelination events to occur by the fact that sustained elevation of canonical Wnt signaling in mice lacking one functional copy of the endogenous Wnt pathway inhibitor APC would result in myelination blockage and subsequent hypomyelination (Fancy et al., 2009). It is important to note that these experimental observation of the involvement of Wnt/β-catenin signaling in regulation of myelination is of relevance to the human demyelinating disorder multiple scleroris (MS), and that various Wnt signaling components have been identified at the site of MS lesions in patients.

The second category of mechanisms that regulate OPC differentiation is secreted molecules acting as extracellular ligands. To date, a number of such signaling

as been identified, one example being the orphan G protein–coupled receptor (GPCR) Gpr17, which is transiently expressed during oligodendrocyte differentiation in the CNS. This expression of Gpr17 is restricted to the oligodendrocyte lineage (Y. Chen et al., 2009), and is down-regulated during the peak of myelination and adulthood. Consequently, transgenic animals overexpressing Gpr17 exhibit inhibition of oligodendrocyte differentiation and myelination, and that Gpr17 knockout animals on the contrary, exhibit onset of oligodendrocyte myelination that is earlier than normal. Thus Gpr17 expression has been suggested to orchestrate the switching from premyelinating oligodendrocytes to mature myelinating oligodendrocytes. Although the ligands of Gpr17 remain to be identified, it is clear that Gpr17 regulate myelination by way of inhibition.

Another example is that in vitro co-culture experiments have shown that inhibition ofγ-secretase activity within oligodendrocytes during their myelination period promotes the formation of myelin segments around axons (Watkins, Emery, Mulinyawe, & Barres, 2008). Importantly, this effect acts independently of the γ-secretase substrate Notch, indicating the involvement of additional extracellular signaling molecules.

In addition to axonal surface ligands and secreted molecules, axonal electrical activity is also critically involved in regulation of the myelination process. In an early study, the proliferation of OPCs in the developing rat optic nerve has been shown to depend on the electrical activity in neighboring axons (Barres & Raff, 1993). Subsequent studies further showed that application of neurotoxins, which can either block (tetrodotoxin) or increase (alpha-scorpion toxin) neuronal firing can inhibit or enhance myelination, respectively (Demerens et al., 1996), clearly linking neuronal electrical activity to myelinogenesis.

A number of potential mechanisms could be utilized by the variation of neural activity to influence the extent of myelination. First of all, neuronal activity could modulate the surface expression of ligands and secretion of extracelluar molecules (B. Emery, 2010). Second, axonal activity leads to release of adenosine that acts on functional adenosine receptors expressed in OPCs (Stevens, Porta, Haak, Gallo, & Fields, 2002), acting as a potent neuron-glial transmitter to inhibit OPC proliferation, stimulate OPC differentiation, and promote the formation of myelin. Third, action potential in neurons causes release of ATP, which in turn leads to astrocytic release of the cytokine leukemia inhibitory factor (LIF), which eventually serves to promote myelination by mature oligodendrocytes (Ishibashi et al., 2006).

In addition to the above mentioned mechanisms, OPCs may be directly synaptically connected with neurons in order to receive input and respond accordingly (B. Emery, 2010). For instance, Low-affinity AMPA (alpha-amino-3-hydroxy-5-methyl isoxazole propionic acid) and kainate glutamate receptors have been shown to be expressed in OPCs (Bergles, Roberts, Somogyi, & Jahr, 2000), and that stimulation of excitatory axons in the hippocampus elicits AMPA receptor-mediated inward currents in OPCs. Interestingly, some of the AMPA receptors present are calcium-permeable, thus providing a link between axonal neural activity and calcium signaling within OPCs (Bergles et al., 2000). In addition to AMPA receptors, GABA receptors are also present at defined synaptic junctions between NG2-expressing OPCs and GABAergic interneurons in the hippocampus (Lin & Bergles, 2002). Specifically, action potentials have been shown to induce the axonal release of glutamate in the corpus callosum, which is a heavily myelinated axon fiber region responsible for communication across hemispheres (Ziskin, Nishiyama, Rubio, Fukaya, & Bergles, 2007). This corpus callosum release of

glutamate involves vesicular fusion, which induces quantal AMPA receptor-mediated currents in NG2 positive OPCs at anatomically defined synaptic junctions between axons and the OPC. Interestingly, glutamate release from axons can be facilitated by repeated stimulation. It is important to note that in response to stimulation, the OPCs undergo regenerative action potentials that are similar to those observed in neurons (Bergles et al., 2000), due to the fact that they express ionotrophic glutamate receptors and voltage-gated ion channels (Barres, Koroshetz, Swartz, Chun, & Corey, 1990). Upon differentiation into mature oligodendrocytes, however, this electrical feature is lost (De Biase, Nishiyama, & Bergles, 2010), which indicates that the property of action potentials in the oligodendrocyte lineage is specific to OPCs in order to regulate OPC function and differentiation. For instance, studies have shown that in vitro application of glutamate to OPCs inhibit both the proliferation and differentiation of OPCs (Gallo et al., 1996), possibly serving to maintain a reserve pool of quiescent OPCs.

Thus far we have mentioned extrinsic signaling that regulates the differentiation of OPCs. On the other hand, OPC differentiation is also tightly controlled by cell intrinsic mechanisms. These intrinsic factors include transcriptional/posttranscriptional regulation and epigenetic mechanisms.

Olig2, for instance, which is a basic helix-loop-helix (bHLH) transcription factor that is expressed in a restricted domain of the spinal cord ventricular zone that sequentially generates motorneurons as well as oligodendrocytes, has been shown to promote oligodendrocyte differentiation in collaboration with Nkx2.2 (Zhou, Choi, & Anderson, 2001). In addition, targeted disruption of both Olig1 and Olig2 have shown that whereas Olig2 is required for motor neuron and oligodendrocyte specification in the spinal cord, Olig1 plays important roles in the development and maturation of

oligodendrocytes, especially within the brain (Lu et al., 2002). In addition to Olig1 and Olig2, a number of other downstream transcription factors have been identified, including Ascl1, Nkx2.2, Sox10, YY1, and Tcf4, all of which required for oligodendrocyte differentiation, maturation, and subsequent myelination (Wegner, 2008). In contrast to these promyelinating factors, a separate category of transcription factors including Id2, Id4, Hes5, and Sox6, have been shown to be active in maintaining OPCs in their undifferentiated state and suppress myelin gene expression (B. Emery, 2010).

Recently, it has been demonstrated by DNA microarray analysis that myelin gene regulatory factor (MRF) expression is specific to terminally differentiated oligodendrocytes (Cahoy et al., 2008; Heiman et al., 2008). Importantly, knockdown of MRF in oligodendrocytes by RNA interference downregulates expression of the majority CNS myelin genes (Emery et al., 2009). In contrast, overexpression of MRF in in vitro cultured OPCs can promote myelin gene expression. Oligodendrocyte lineage-specific MRF knockout mice show normal premyelinating oligodendrocytes but they display severe myelin gene expression deficits and subsequently fail to myelinate axons. In addition, these knockout mice die early due to severe seizures.

Oligodendrocyte differentiation is also controlled under chromatin remodeling, and that histone deacetylase expression has been detected in the developing corpus callosum (Shen, Li, & Casaccia-Bonnefil, 2005). Importantly, administration of valproic acid (VPA), the specific inhibitor for histone deacetylase (HDAC) activity, results in significant myelination deficit with delayed expression of terminal differentiation marker and preserved expression of OPC markers. However, when a recovery period was allowed, oligodendrocyte differentiation can resume (Shen et al., 2005). Importantly, the effect of VPA administration is specific to OPCs, as upon

myelination onset, VPA administration no longer effects myelin gene expression.

Subsequent further investigations have shown that both HDAC1 and HDAC2 are required for the formation of oligodendrocytes (F. Ye et al., 2009). It has been demonstrated that oligodendrocyte lineage-specific HDAC1 and HDAC2 double knockout animals exhibit stabilization and nuclear translocation of β-catenin, which in turn functions to repress Olig2 expression, and thus inhibiting oligodendrocyte differentiation. In addition, the oligodendrocyte-specific transcription factors TCF7L2/TCF4 are identified as co-effectors of β-catenin and that disruption of Tcf7l2 in mice results in oligodendrocyte maturation deficit. Thus, HDAC1 and HDAC2 functionally compete withβ-catenin for interaction with TCF7L2 to regulate downstream gene expression that are involved in oligodendrocyte differentiation and maturation (F. Ye et al., 2009).

In addition to transcriptional regulation and epigenetic mechanisms, posttranscriptional regulation by microRNAs is also critically involved in the intracellular signaling of oligodendrocyte differentiation. Studies using transgenic mice in which microRNA processing is specifically disrupted in the oligodendrocyte lineage by way of Dicer enzyme knockout have shown that microRNA processing is indispensible for normal CNS myelination (Dugas et al., 2010), and that in vitro OPCs also fail to differentiate in the absence of mature microRNAs. Specifically, three microRNAs including miR-219, miR-138, and miR-338 are found to be elevated by 1-2 orders of magnitude during OPC differentiation into oligodendrocytes, and that miR-219 when induced alone, is sufficient to promote the differentiation (Dugas et al., 2010). The downstream target of miR-219, ELOVL7, is also identified as a main molecular component involved in the development of the Dicer mutant phenotype (Shin, Shin, McManus, Ptacek, & Fu, 2009), and that overexpression of ELOVL7

results in lipid accumulation, which is in turn suppressed by co-overexpression of miR-219. Other important target genes of the above mentioned microRNAs include PDGFRa, Sox6, and Hes5 (Dugas et al., 2010; X. Zhao et al., 2010), all of which serve to maintain OPCs in their undifferentiated state.

Mature oligodendrocyte myelination: plasticity

There have been abundant evidences for a dynamic regulation of myelin content within the adult CNS. For instance in humans, diffusion imaging studies have shown a localized increase in fractional anisotropy, which is a measure of microstructure, in white matter underlying the intraparietal sulcus following repetitive visual-motor skill training (Scholz, Klein, Behrens, & Johansen-Berg, 2009). In addition, extensive piano practicing also has regionally specific effects on white matter development, with pyramidal tract being more structured in pianists compared to non-musicians (Bengtsson et al., 2005). These observations have led to the proposition that myelin plasticity should be considered as a form of neural plasticity (Fields, 2005), and that myelination could serve to strengthen and synchronize long range inputs.

Oligodendrocyte pathology: risk factors

Oligodendrocytes are vulnerable to pathology due to its high metabolic demands (McTigue & Tripathi, 2008). Specifically, the consumption of large amount of adenosine triphosphate (ATP) as well as oxygen in oligodendrocytes causes the

production of hydrogen peroxide as a byproduct, together with reactive oxygen species (McTigue & Tripathi, 2008), both of which needs to be tightly metabolized. Moreover, oligodendrocytes are also the predominant iron-containing cells in the brain (Connor & Menzies, 1996), which puts them at risk of free radical formation and lipid peroxidation. Importantly, both a direct and an indirect relationship exist between iron acquisition and myelin production in oligodendrocytes. Iron is directly involved as co-factor for cholesterol and lipid biosynthesis in the production of myelin and also indirectly involved due the requirement for oxidative metabolism to occur at a much higher rate in oligodendrocytes compared to other cell types in the brain. As a result, cytokine factors and iron deficiency conditions that may reduce iron acquisition in oligodendrocytes can cause them to be susceptible to oxidative injury (Connor & Menzies, 1996). Many known effect of pathological conditions affecting oligodendrocyte survival rate and myelination may thus be mediated through decreasing iron availability and iron homeostasis within oligodendrocytes.

On top of these, oligodendrocytes contain only low concentrations of the anti-oxidative enzyme glutathione (Thorburne & Juurlink, 1996), and lastly, oligodendrocytes are also especially susceptible to endoplasmic reticulum (ER) stress upon slight variations in the amount of a single protein (Bauer et al., 2002). For instance, mice overexpressing the myelin protein proteolipid protein (PLP) which show impairment of PLP transport from the olidodendrocyte cell body to the myelin sheath also show impairment of the transportation of other myelin proteins including myelin-associated glycoprotein (MAG) and myelin oligodendrocyte glycoprotein (MOG), but sparing the peripherally translasted myelin basic protein (MBP). Importantly, the transportation of other non-myelin proteins are also affected, including the amyloid precursor protein (APP) (Bauer et al., 2002). Ultrastuctural

study of the ER showed swelling of the cisternae, together with intense presence of the ER chaperone molecule BiP/GRP78 and ER folding enzyme protein disulfide isomerase (PDI). Taken together, disturbed metabolism with oligodendrocytes readily puts them at risk of pathogenesis and programmed cell death.

Oligodendrocyte pathology: cell death mechanisms

As mentioned, due to its high metabolic rate, the massive presence of toxic byproducts, the high ionic concentration, and the lack of sufficient glutathione, oligodendrocytes are specifically vulnerable to oxidative stress and damage (Juurlink, 1997; Thorburne & Juurlink, 1996). This oxidative damage is a common cause of oligodendrocyte damage as well as demyelination in many disease conditions such as MS and ischemia (M. Bradl & H. Lassmann, 2010) and it can impose its action jointly with the sphingomyelinase/ceramide pathway. Ceramides are a family of waxy lipid molecules (Obeid, Linardic, Karolak, & Hannun, 1993) that are composed of sphingosine, which is a primary part of the important sphingomyelin phospholipid, and a fatty acid. Ceramides are found in high concentrations within the cell membrane, since they are component lipids that make up sphingomyelin. The function of ceramides is not only to supporting structural elements, but also to participate in a variety of cellular signaling, including regulation of cell differentiation, proliferation, and programmed cell death (Obeid et al., 1993). Importantly, ceramides are released by the action of sphingomyelinase and can activate pro-apoptotic signaling cascades eventually leading to oligdendrocyte loss in case of oxidative stress, inflammation, injury or infection. For instance, upon treatment with IL-1 beta to CG4

oligodendrocyte cells, which induces a dose-dependent increase of the intracelluar ceramide, cell survival MTT assay showed that an increase in the concentration of ceramide causes depletion of up to 40% of the CG4 cell population within 6 hours (Brogi, Strazza, Melli, & Costantino-Ceccarini, 1997). Similar results can also be obtained using primary differentiated oligodendrocytes, and that evidences such as chromatin condensation, nuclear fragmentation, and apoptotic bodies formation all point to apoptosis as the main cause of cell death (Brogi et al., 1997).

In addition to ceramide, oligodendrocytes also express AMPA receptors (Targett et al., 1996), kainite (Sanchez-Gomez & Matute, 1999) and NMDA receptors (Salter & Fern, 2005), making to them vulnerable to glutamate excitotoxicity, together with the ATP receptor P2X7 (Matute et al., 2007), also rendering them vulnerable to extracellular ATP induced toxicity.

Moreover, inflammatory cytokines can act directly on oligodendrocytes to induce apoptosis. For instance, tumour necrosis factor (TNF) induces oligodendrocyte cell death, acting through TNF receptor p55 (TNFR-p55) (Jurewicz et al., 2005). Upon ligand binding, apoptosis-inducing factor (AIF) translocation to the nucleus is observed, together with subsequent large-scale DNA fragmentation that is characteristic of AIF-mediated cell death. Importantly, disruption of AIF using antisense strategy prevents this TNF-induced cell death of human oligodendrocytes (Jurewicz et al., 2005), and that this apoptotic pathway is non-caspase dependent, as evidenced by a lack of presence of caspases 8, 1 and 3; lack of cleavage of caspases 1 and 3 fluorogenic substrates. In addition to TNF, interferon-gamma (IFNG) also induces programmed cell death in OPCs (Horiuchi, Itoh, Pleasure, & Itoh, 2006). In this study, the direct effects of IFNG on purified rat oligodendroglial cultures at different developmental stages are examined. IFNG had direct cytotoxic effects on

actively proliferating OPCs but less so on immature oligodendrocytes and not at all on terminally differentiated mature oligodendrocytes. Importantly, this stage-specific susceptibility of OPCs to IFNG-induced cell death is tightly linked to the progression of the cell cycle. Inhibition of the MEK-ERK pathway, also known as the Ras-Raf-MEK-ERK pathway, by U0126 partially reverses this IFNG-induced cytotoxicity in OPCs (Horiuchi et al., 2006), suggesting the involvement of this pathway.

Inflammatory mediators can also damage oligodendrocytes indirectly by promoting the production of radical in microglia and also in astrocytes. For example, Nitric oxide (NO) is a free radical that is found at concentrations higher than normal within inflammatory MS lesions (Smith & Lassmann, 2002), their presence due to the appearance of the nitric oxide synthase (iNOS) in cells such as microlia/macrophages and astrocytes. Robust evidences suggest that NO play a role in induces several MS features, including disruption of the blood-brain barrier, oligodendrocyte damage and demyelination, as well as degeneration of axons.

As aforementioned, due to high metabolic demands, oligodendrocytes are specifically vulnerable to oxidative stress in the mitochondria, as well as ER stress. A prominent example is the cuprizone animal model, which uses cuprizone as a oligodendrocytes-specific neurotoxin that induces CNS demyelination in mice, specifically in the corpus callosum (Torkildsen, Brunborg, Myhr, & Bo, 2008). Importantly, cuprizone acts as a chopper chelator that interferes with complex IV of the mitochondrial respiratory chain, which leads to its subsequent cell death, although the exact mechanism of action of cuprizone is still widely debated (Jelle Praet, Caroline Guglielmetti, Zwi Berneman, Annemie Van der Linden, & Peter Ponsaerts, 2014).

It is importantly to note, however, that the above mechanisms is not specific to oligodendrocytes, and that myelinating oligodendrocytes are in general more susceptible to damage than any other cellular components in the CNS. For instance, the possibility that myelin can be damaged as a nonspecific consequence of a specific delayed type of hypersensitivity reaction that is directed at non-neural antigens was investigated by an early study in guinea pigs (Wisniewski & Bloom, 1975). Sensitization to tuberculin with Freund's complete adjuvant, using either sonicated tubercle bacilli or tuberculin purified protein derivative, in the CNS as well as the peripheral nervous system invariably produces local inflammatory response, accompanied by prominent demyelinating lesion. Vesicular disruption of the myelin sheath in the vicinity of the inflammatory infiltrates together with stripping of the myelin by the histiocytes were observed (Wisniewski & Bloom, 1975). Taken together, nonbrain antigens can be the cause of inflammatory demyelinating conditions. Another interesting example is the neuromyelitis optica (NMO), also known as Devic's disease or Devic's syndrome, characterized by simultaneous inflammation and demyelination of the optic nerve as well as the spinal cord (C. F. Lucchinetti et al., 2002). Recent immunological studies have provided evidences that point to astrocytes, instead of oligodendrocytes, as the primary target of the NMO inflammatory lesion (Lennon et al., 2004; C. F. Lucchinetti et al., 2002). Although astrocytes show the first sign of damage in this case, oligodendrocyte cell death and demyelination quickly ensue (Misu, Fujihara, & Itoyama, 2008).

Besides non-specific nonbrain antigens that can cause oligodendrocyte damage, autoantibodies directed against epitope expressed on myelinating oligodendrocytes is more commonly observed to elicit demyelination. A related animal demyelination model of this kind is the experimental allergic encephalomyelitis (EAE) model. EAE

can be induced in a number of species, including mice, rats, pigs, rabbits and primates. Commonly used antigens include purified myelin protein such as MBP, PLP, and myelin/oligodendrocyte glycoprotein (MOG), or peptides of these proteins and spinal cord homogenate (SCH), all of them can serve as distinct models with different disease characteristics of immunological response and pathology (Robinson, Harp, Noronha, & Miller, 2014). For example, monoclonal antibodies against MOG can be injected intravenously into rats, resulting in T-cell-mediated inflammatory response and the formation of large, confluent demyelinated plaques (Linington, Bradl, Lassmann, Brunner, & Vass, 1988). Similarly, cytotoxic T-lymphocytes that are directed against oligodendrocyte also induce demyelinating lesions. For instance, induction of CD8 T-cells specific for the model antigen ovalbumin (OVA) that is sequestered in oligodendrocytes as a cytosolic molecule leads to fulminant demyelinating EAE with MS-like lesions (Na et al., 2008), affecting all parts of the organism including cerebellum, brainstem, optic nerve and spinal cord. Release of interferon-gamma (IFNG) was also identified to precede the disease manifestation, indicating that naïve CD8 T-cells gaining access to an immune-privileged organ is sufficient to elicit autoimmunity via IFN-gamma-assisted self amplification (Na et al., 2008).

Oligodendrocyte pathology: heterogeneity in lesion patterns

The initial stages of oligodendrocyte lesions have been shown to follow three main patterns, possibly reflecting the different mechanisms of action. Nonetheless, all patterns eventually lead to primary demyelination.

The first type of oligodendrocyte lesion is characterized by a simultaneous damage to the oligodendrocyte cell body, as well as its myelin processes. When this type of lesion occurs, myelin sheaths are commonly lost, while oligodendrocyte cell bodies may be partly preserved (Monika Bradl & Hans Lassmann, 2010). Studies utilizing immunogold-labeled peptides of myelin antigens and high-resolution microscopy have identified autoantibodies that are specific for the CNS myelin antigen binding to disintegrating myelin by means of vesicular dissolution in acute MS lesions (Genain, Cannella, Hauser, & Raine, 1999). Other myelin disintegration mechanism involve phagocytosis of myelin fragments by macrophages, as primary demyelination occurs in the vicinity of the invading cells, and close examination by electron microscopy suggests an active stripping of myelin by these cells (Brosnan, Stoner, Bloom, & Wisniewski, 1977). The damage to the cell body on the other hand, follow the pathway of necrosis in case of acute injury, or the pathway of apoptosis, in which case oligodendrocytes lose their myelin processes but survived the initial insult (Wolswijk, 2000).

The second type of oligodendrocyte damage is characterized by primary oligodendrocyte injury. In this case, the damage is frequently due to disturbance to the metabolism within oligodendrocytes, and that demyelination is often observed as incomplete (Monika Bradl & Hans Lassmann, 2010). One such example is the progressive multifocal leukoencephalopathy (PML) (Murayama & Saito, 2007), which was originally reported as a rare complication of hematologic disorders, but later greatly increased in number in association with acquired immunodeficeincy syndrome (AIDS). The pathological features of PML include demyelination with the absence of inflammatory response or oligodendrocyte necrosis. Presence of

oligodendrocyte nuclear inclusions is often observed at the periphery of the lesion site (Murayama & Saito, 2007). Of note, the lesion pattern of the cuprizone model of demyelination also falls into this category (Torkildsen et al., 2008).

A third type of oligodendrocyte lesion is characterized by a dying back pattern in which the most distal portion of myelin is affected first. This type of lesion is evident in a sutbset of MS patients termed pattern III (Aboul-Enein et al., 2003), in which active demyelinating lesions show a preferential loss of myelin-associated glycoprotein (MAG), together with apoptotic-like oligodendrocyte destruction. Other myelin related proteins, however, remain largely unaffected. Of relevance, MAG is located in the inner most layer of the myelin sheath, which is the most distal process from the oligodendrocyte cell body (Mukhopadhyay, Doherty, Walsh, Crocker, & Filbin, 1994), and that this observation has led researchers to propose such "dying back" type of oligodendrogliopathy to be the initial step of demyelination in pattern III MS lesions (Aboul-Enein et al., 2003). Additional characteristic features of such lesions are the preferential damage of small caliber axons and a prominent preservation of axons and their myelin segments at the proximity of large blood vessels, which are indicative of an ischemic nature of the lesion. Similar lesions are also evident in a subset of acute MS patients and in patients with white matter viral infections (Aboul-Enein et al., 2003).

As mentioned above, although these initial stages of demyelination differ in terms of lesion site and time course, they all culminate in demylination spreading throughout the cell as the lesion progresses, and that their individual features are gradually lost. Nonetheless, characterizing and understanding the pathogenesis of the initial stages of demyelinating lesion sheds light on the origin of the myelin damage and is an area of intense research. Such investigations show eventually led to

identification of therapeutic targets as well as design of various therapies.

Given the vulnerability of oligodendrocytes to damage as well as the various mechanisms that potentially contribution to demyelination that are mentioned above, in this section we focus on the cuprizone model, which is commonly used by researchers to address demyelination mechanisms involved in MS. Importantly, cuprizone induces oligodendrocyte dystrophy and damage, over a time course of several weeks, allowing us to examine the detailed demyelination as well as neuroinflammatory response in the cuprizone lesion site.

Multiple sclerosis

Multiple sclerosis (MS) is a chronic, demyelinating disease in which myelin sheath, the insulating cover that wraps around axons of neurons, is damaged. The normal function of myelin involves increasing the speed of action potential propagation in axons as well as providing trophic support (Nave, 2010). Upon damage of myelin, patients suffer from a wide range of signs and symptoms, ranging from benign to devastating.

The disease onset for MS is usually between ages of 20 and 40, which is relatively early compared to other neurological disorders such as Alzheimer's disease and Parkinson's disease. The initial symptoms of MS include blurry vision or double vision, red-green color distortion, or even blindness (Kister et al., 2013). Coordination and balance impairments caused by muscle weakness are also commonly experienced. As the disease progresses, patients are susceptible to partial or complete paralysis, paresthesias, abnormal sensations, speech impediments, hearing loss and cognitive

impairments. Moreover, suffering from MS symptoms typically leads to depression (Nyenhuis et al., 1995).

Heterogeneity of MS

Notably, MS is a disease with prominent heterogeneity in its pathogenesis, its clinical manifestations, its incidence across various racial and ethnic groups and the response to treatment (Langer-Gould, Brara, Beaber, & Zhang, 2013; Lassmann, Bruck, & Lucchinetti, 2001; C. Lucchinetti et al., 2000; C. F. Lucchinetti, Bruck, Rodriguez, & Lassmann, 1996). MS has been shown to exhibit profound heterogeneity in clinical and laboratory tests. Specifically, four fundamentally different patterns of demyelination, namely, patterns I, II, II and IV, have been characterized, which differ from each other in terms of their clinical course, neuroradiological appearance of the lesions, involvement of susceptibility gene loci, and response to therapy (C. Lucchinetti et al., 2000). Two of the patterns, I and II, showed close similarities to T-cell-mediated or T-cell plus antibody-mediated autoimmune encEphalomyelitis, respectively. The other two patterns (III and IV), on the other hand, exhibit a primary oligodendrocyte dystrophy, which bears significant similarity to virus- or toxin-induced demyelination. Autopsy case studies have shown that at a given time point of the MS pathology, the lesion patterns are homogenous within multiple active lesion sites in the same patient, but heterogeneous across different patients, pointing to different genetic backgrounds as one of the causes in triggering the various MS lesion patterns (Lassmann et al., 2001).

In addition to the four different lesion patterns documented, MS is also

categorized into four clinical subtypes by MS specialists (F. D. Lublin & Reingold, 1996): relapsing-remitting (RRMS), primary-progressive (PPMS), secondary-progressive (SPMS), and progressive-relapsing (PRMS). This categorization has guided MS research and clinical practice for many years since. Of the four subtypes, relapsing-remitting MS affects the most of the MS population (85%), and it is characterized by episodic disease exacerbations, or 'attacks', during which symptoms develop over a few days, remain for several weeks or months, and then resolve either completely or partially (remission). On the other hand, a smaller percentage of MS patients fall into the primary-progressive category, which do not exhibit acute relapses. Rather, patients of primary-progressive MS experience disability progression from the onset without any distinct relapses or remissions. The third subtype, secondary-progressive is considered a later stage of RRMS, where relapses gradually disappear, and that neurological disability continues to increase. The identity of the last subtype, progressive-relapsing, is debated (Fred D. Lublin et al., 2014; Fred D. Lublin, Reingold, & Sclerosis*, 1996) and it may simply have indicated a more aggressive course of the relapsing RRMS.

In addition to the different subtypes of MS, different races have been reported to vary dramatically in the incidence of MS, with Africans and Caucasians being much more susceptible to MS compared to Hispanics and Asians (Langer-Gould et al., 2013). Taken together, people with different genetic background can differ in their susceptibility to MS, as well as in the pathogenic pathway and the clinical time course of the disease progression.

MS pathology

The pathology of MS, albeit after years of investigation, is still uncertain and is under debate. Traditionally, MS has been considered to be an autoimmune disorder, which is mediated by T cell attacking myelin in the central nervous system (CNS) (Frohman, Racke, & Raine, 2006; McFarland & Martin, 2007; Noseworthy, Lucchinetti, Rodriguez, & Weinshenker, 2000). Evidence for this hypothesis includes observation of oligoclonal immunoglobulins in the cerebrospinal fluid (CSF), blood-brain barrier breakdown shown in MRI scans and perivascular infiltrates of T cells and macrophages in brain biopsies/autopsies of MS patients (Frohman et al., 2006; McFarland & Martin, 2007; Noseworthy et al., 2000). However, it has been argued that this autoimmune hypothesis is unlikely to explain type III and type IV MS lesions (C. Lucchinetti et al., 2000), and that it only applies to the relapsing-remitting type of MS, rather than the relatively minor primary-progressive subtype (Stys, Zamponi, van Minnen, & Geurts, 2012).

An recent alternative hypothesis (Stys et al., 2012) states that MS is primarily a degenerative disease in which the oligodendrocytes, the myelin-forming glial cells in the CNS, undergo degeneration in the first place. Furthermore, this model proposes that MS can be considered to be an interaction or ‘convolution’ between the underlying cytodegeneration and the host’s aberrant immune response, with the cytodegeneration of oligodendrocytes being the invariant that is shared across various MS subtypes, and that inter-individual variations in the extent of the immune priming produces the broad spectrum of MS presentations, ranging from the Marburg variant of MS which exhibits large tumor-like demyelinating plaques (Capello & Mancardi, 2004) at one extreme, to the primary progressive MS at the other end of the spectrum

which shows a minimal-inflammatory progressive course from the onset. The proposal that the same cytodegeneration is the true invariant underlying all MS subtypes is strongly supported by the clinical observation that the mean age of onset of PPMS is about 10 years later than that of RRMS (Miller & Leary, 2007). Thus, this 'inside out' model of MS which argues for a primary cytodegeneration unifies the different subtypes of MS lesions into a simple explanation: with the same course of cytodegeneration, the immune response differences of the heterogeneous MS population dictate the individualized disease symptoms and time course of disease progression.

Animal models for MS: cuprizone toxicity

Interestingly, there are two most prominent animal models adopted by laboratory researchers that each addresses one of the two hypotheses of MS pathogenesis mentioned above. One of them, the so-called experimental autoimmune encephalomyelitis (EAE) model, involves probing the autoimmune aspect of MS by injecting CNS protein extracts such as myelin basic protein (MBP) into mice (Rao & Segal, 2004). The presence of the aduvant thus elicits the generation of inflammatory response and demyelination. The other model, the cuprizone model, involves administration of the neurotoxin cuprizone to mice to induce oligodendrocyte apoptosis (Matsushima & Morell, 2001; Torkildsen et al., 2008), without directly priming the immune system.

Cuprizone was first described by in 1950 following the observation that cuprizone, as the condensation product of oxalylhydrazide and cyclohexanone,

induced a sensitive blue color reaction upon chelation with copper salts (Nilsson, 1950). Later on in 1966, the first experimental application of cuprizone was done in mice, and that low serum copper levels along with demyelination was observed (Carlton, 1966). From then on, the cuprizone model has been used to induce demyelination in mice, providing a valuable tool to probe the demyelination and remyelination processes in the brain.

Upon treatment of cuprizone, mice typically exhibit profound demyelination within the corpus callosum, the cortex and the superior cerebellar peduncles (Matsushima & Morell, 2001; Torkildsen et al., 2008). Within the corpus callosum, apoptosis of oligodendrocytes are observed, together with recruitment of microglia/macrophages (microgliosis), astrocytes (astrogliosis) and oligodendrocyte precursor cells (OPCs) (Hiremath et al., 1998; Matsushima & Morell, 2001).

Microgliosis starts at week 2 of cuprizone treatment (Hiremath et al., 1998), and gradually accumulates overtime. At the peak, a large number of proliferating microglia is observed, and that 30% of which originates from peripheral progenitors (Remington, Babcock, Zehntner, & Owens, 2007). This cuprizone induced microgliosis has been described as a mixture of pro-inflammatory M1 and anti-inflammatory M2 phenotype. This co-existence is supported by the presence of receptors and cytokines such as TNF-α and IL-β, indicative of an M1 phenotype and IL-13Rα1, IL-4Rα and IL-2Rγ indicative of M2 phenotype (Arnett, Wang, Matsushima, Suzuki, & Ting, 2003; Olah et al., 2012). Based on transcriptome analysis, the functions of microglia have been suggested to include phagocytosis of myelin debris, recruitment of OPCs and trophic support for promoting recovery and remyelination (Biancotti, Kumar, & de Vellis, 2008; Voß et al., 2012). Importantly, in early electron microscopy studies, microglia processes were observed in between

myelin lamellae, possibly actively stripping off myelin from axons (Blakemore, 1972; Ludwin, 1978).

The astrocyte population becomes activated in response to any disruption of brain homeostasis, and that the cuprizone lesion model is not an exception. Following cuprizone treatment, astrocytes increase its enzyme activity as early as week 1 (Cammer & Zhang, 1993; Tansey, Zhang, & Cammer, 1997; Zatta et al., 2005), and that astrogliosis gradually increases overtime (Matsushima & Morell, 2001), and persists during remyelination (M.-K. Chen & Guilarte, 2006; Zaaraoui et al., 2008). Activated astrocytes are believed to help protect against oxidative stress and energy depletion (Liberto, Albrecht, Herx, Yong, & Levison, 2004), maintain ionic homeostasis (Garzillo & Mello, 2002) as well as to provide trophic support for remyelination (M.-K. Chen & Guilarte, 2006; Fulmer et al., 2014; König et al., 2012; J. N. Ye et al., 2013). In addition to its protective role, astrocytes are also believed to contribute to the cuprizone toxicity effect by expressing pro-inflammatory genes through NF-kB signaling (Raasch et al., 2011).

OPCs are also found in the cuprizone lesion site, originating either from nearby tissue or neural proliferation zones such as the subventricular zone (SVZ) and the subgranular zone (SGZ) (J. Praet, C. Guglielmetti, Z. Berneman, A. Van der Linden, & P. Ponsaerts, 2014). These OPCs appear from week 1 of cuprizone treatment and also proliferate and accumulate overtime. The proliferation and migration of OPCs initiate remyelination and differentiation toward mature oligodendrocytes, by activation of a cascade of transcription programs (L. P. Chen et al., 2012; Fulmer et al., 2014; Moll et al., 2013; Othman et al., 2011; Patel, McCandless, Dorsey, & Klein, 2010; Soundarapandian et al., 2011).

In addition to the observed histological pathologies in the brain, mice treated

with cuprizone also exhibit reversible weight loss and behavioral abnormalities (Franco-Pons, Torrente, Colomina, & Vilella, 2007; Xiao et al., 2008). For instance, demyelinated mice on a cuprizone diet have been shown to exhibit impaired running performance on training wheels as compared to control animals, and that this impairment was even more pronounced when demyelinated mice were exposed to complex running wheels which had irregularly spaced crossbars and thus demanded high-level motor coordination (Liebetanz & Merkler, 2006). Interestingly, remyelinated animals that were returned to a cuprizone-free diet fully recovered on the training wheels, but still showed latent motor deficits on the complex wheels. In addition to altered motor coordination, other behavioral abnormalities are reported, including inhibited anxiogenic response to a novelty challenge test and increased sensorimotor reactivity to auditory click stimulus (Franco-Pons et al., 2007), elevated climbing behavior, lower prepulse inhibition, decreased social interaction and impaired spatial working memory (H. Xu et al., 2009). Antipsychotic treatment, however, can reverse some of these effects (H. Xu, Yang, McConomy, Browning, & Li, 2010). Taken together, cuprizone administration in mice induces profound demyelination pathology, along with various impaired behavioral parameters.

the cuprizone model: effects of mouse strain.

The cuprizone model has been used widely in MS research (Kipp, Clarner, Dang, Copray, & Beyer, 2009) and that commonly people have used the standard C57BL/6 strain to study the different molecular signaling components involved in the complex pathogenic process based on the robust demyelination in the corpus callosum

in this strain (Matsushima & Morell, 2001). However, other strains are used as well and significant differences in the demyelinating response between different strains are reported (Skripuletz et al., 2008; Taylor, Gilmore, & Matsushima, 2009). SJL mice for example, do not readily demyelinate at the midline within the corpus callosum but showed greater demyelination immediately lateral to midline, which is different from the reproducible midline demyelination in the C57BL/6 mice (Taylor et al., 2009). In addition, cuprizone induced demyelination in SJL mice is slower and plateau after week 7, which is in contrast to C57BL/6 mice which plateau at week 5 (Matsushima & Morell, 2001). Aside from demyelination differences in the corpus callosum, cortical demyelination differences between strains have also been reported by comparing BALB/cJ mice with C57BL/6 mice (Skripuletz et al., 2008). In this study, only partial cortical demyelination could be induced by cuprizone treatment in BALB/cJ mice, and that cortical microglia accumulation was significantly higher in BALB/cJ mice, compared to C57BL/6.

In this section, we focused on characterizing the cuprizone induced demyelination response in CD1 strain, and by comparing it to the commonly used C57BL/6 strain, we show that CD1 mice exhibit relatively mild demyelination in the corpus callosum, together with blunted neuroinflammatory response. Thus, genetic background differences greatly influence the susceptibility of mice to cuprizone induced damage, which is reminiscent of the heterogeneity in MS pathology that is observed across the human populations.

Results

CD1 mice exhibit less demyelination compared to C57BL/6 mice

The Black gold staining is an easy and widely used approach for visualizing myelin morphology with good resolution of individual myelin fibers (Schmued et al., 2008). We first performed Black gold staining of the 4 week-cuprizone treated samples, focusing on sections of the corpus callosum above the fornix, which is approximately between bregma -0.58 mm and -0.82 mm (Fig I-1A). The C57BL/6 mice showed a dramatic loss of myelin staining at this time point (Fig I-1B), which is consistent with previous reports (Matsushima & Morell, 2001). However, the CD1 mice didn't show significant myelin loss. This difference in response was also observed at later stages of cuprizone treatment (Fig I-1B).

An alternative histological approach that is complementary to the Black gold staining is the Luxol fast blue–periodic acid Schiff (LFB–PAS) method, which not only stains the myelin (in blue) but also stains the demyelinated areas in pink, thus providing a counter stain to contrast with the positive myelin stain. We thus performed LFB-PAS staining to confirm the results obtained with the Black gold staining (Fig I-2A). The LFB-PAS stained sections were scored blind on a scale of 3 (3=intact and 0=full demyelination, Fig I-3). As shown in Fig I-2B, the two strains of mice showed different severity of demyelination at 4 to 6 weeks of treatment. A close examination of the CD1 corpus callosum at 4 to 6 weeks of cuprizone exposure shows that CD1 mice do exhibit mild demyelination which is not apparent in the Black

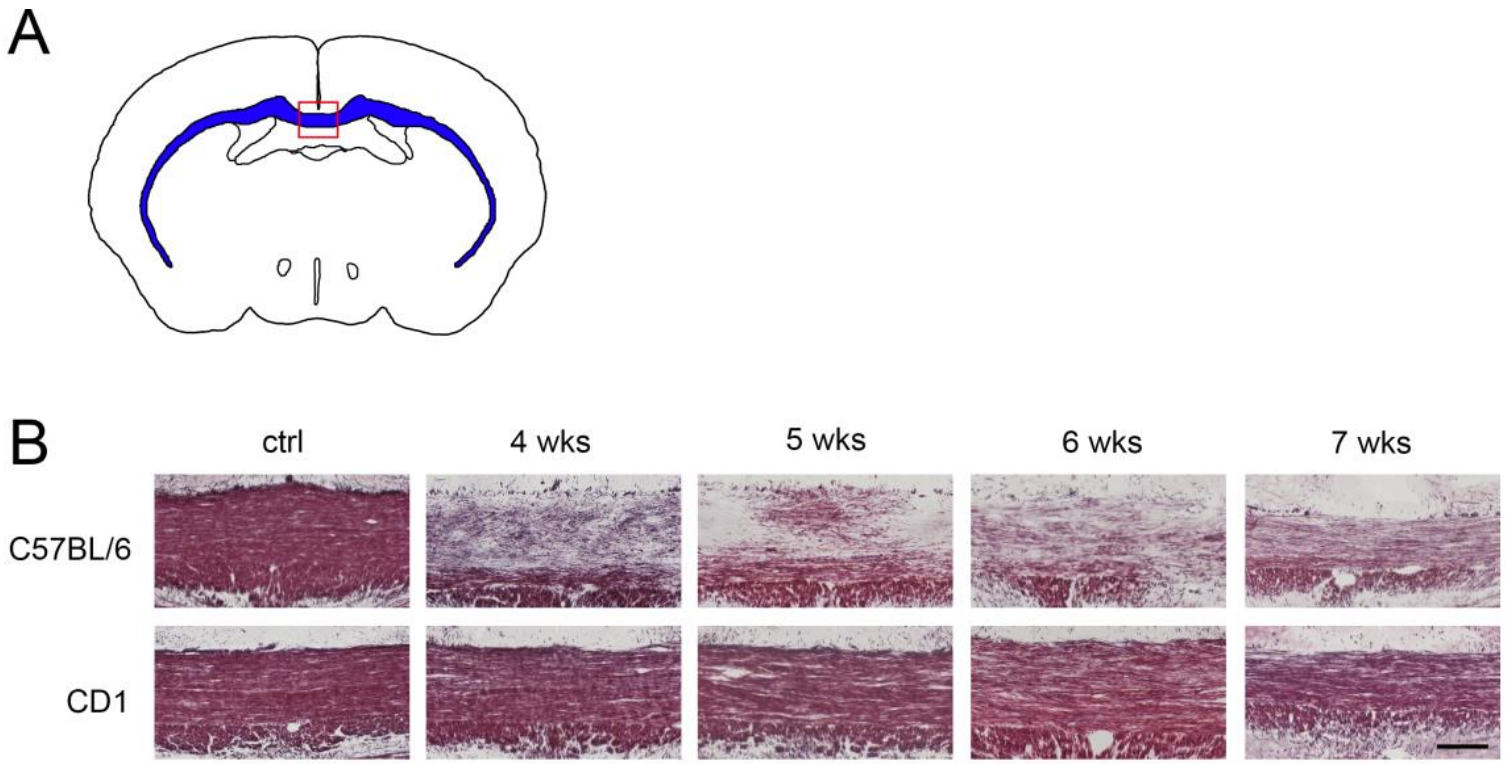

Figure I-1. Black gold staining reveals that CD1 mice exhibit much less demyelination relative to C57BL/6 mice following various length of cuprizone exposure. A, coronal sections of the corpus callosum were taken above the fornix, approximately between bregma -0.58 mm and bregma -0.82 mm, corresponding to Fig 36-Fig 39 in the Mouse Brain in Stereotaxic Coordinates (Franklin, 1997). The boxed area depicts the midline of the corpus callosum that was analyzed in B and all the following figures in this study. B, representative images of Black gold-stained corpus callosum in C57BL/6 mice and CD1 mice. CD1 mice show relatively intact myelin fibers compared to C57BL/6 mice. Scale bar, 100 μm.

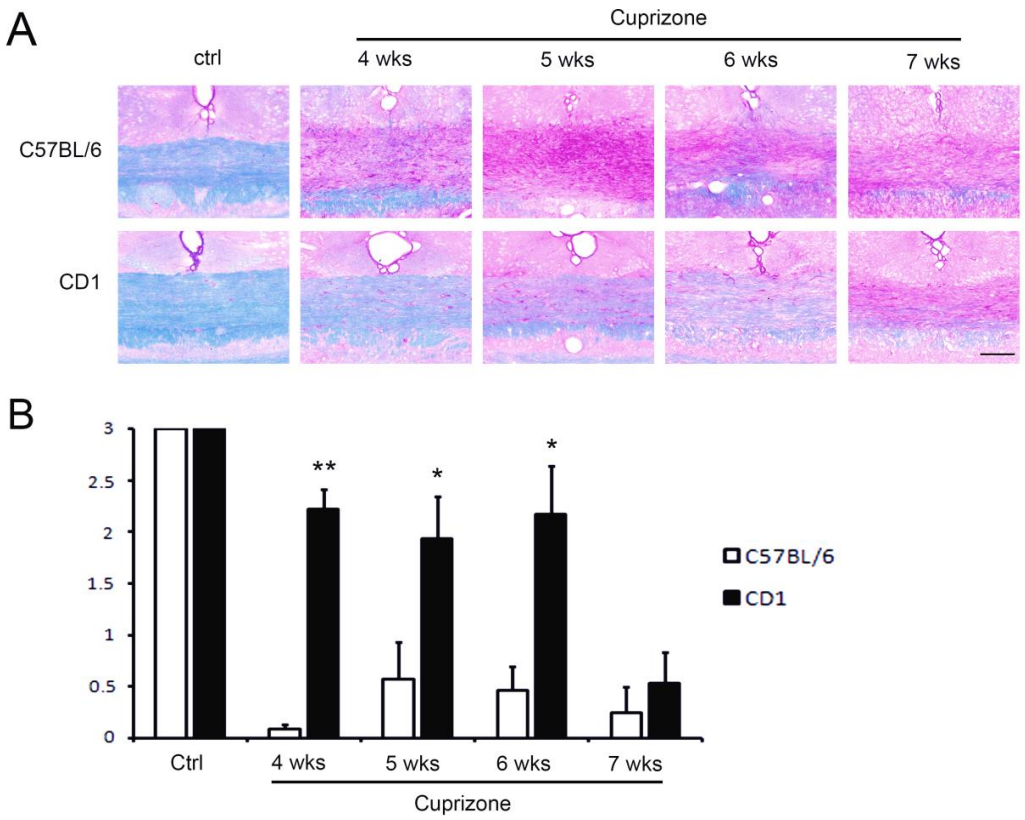

Figure I-2. LFB-PAS staining reveals relatively mild demyelination in CD1 mice in comparison to C57BL/6 mice. A, representative images of the LFP-PAS stained corpus callosum in C57BL/6 mice and CD1 mice. Myelin shows up as blue stain and the demyelinated area shows up as pink. Note C57BL/6 sections show more pink and less blue compared to CD1 mice. Scale bar, 100 µm. C, semi-quantification of demyelination by blind scoring (3=intact and 0=complete demyelination). Data is shown as group averages. N= 4 and 7 at 4 weeks for C57 and CD1, respectively. N= 5 and 5 for 5 weeks, N=4 and 5 for 6 weeks and N=5 and 7 for 7 weeks. Significant differences between strains were observed at 4 to 6 weeks of cuprizone treatment (student's t-test). ** indicates $P<0.001$, * indicates $P<0.05$.

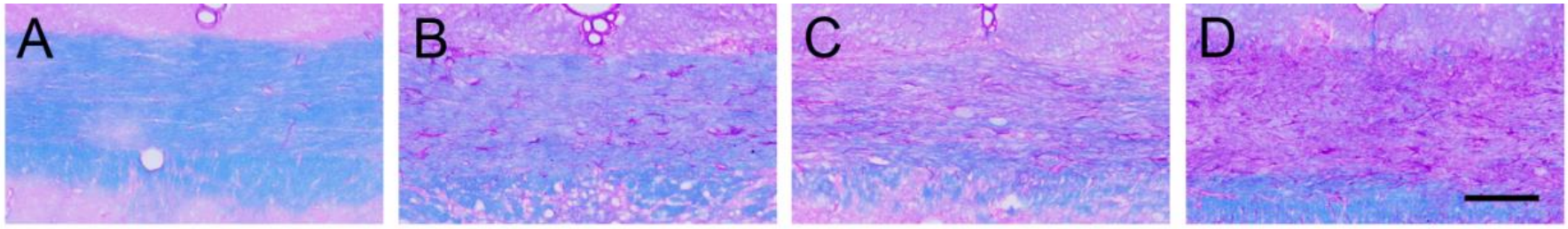

Figure I-3. Standard for blind scoring of LFB-PAS stained midline corpus callosum sections. A corresponds to a score of 3 (intact). B corresponds to a score of 2, C corresponds to 1 and D corresponds to 0 (complete demyelination with minimum blue stain of myelin). Scale bar, 100 μm.

gold histological analysis. By 7 weeks, CD1 mice were slightly less demyelinated compared to C57BL/6 mice, but this difference is not statistically significant, although the Black gold data shows CD1 mice still exhibit more Black gold-stained fibers at this point. This slight discrepancy could be due to the different substrates that these two methods detect (Savaskan, Weinmann, Heimrich, & Eyupoglu, 2009) in that LFB stains phospholipids while Black gold stains myelin proteins. Taken together, the CD1 strain exhibits a delayed and mild demyelination in comparison to C57BL/6 mice.

CD1 mice exhibit more oligodendrocytes and less myelin protein decrease compared to C57BL/6 mice

Because the myelin fibers are formed by oligodendrocytes, we wanted to examine whether the less severe demyelination in CD1 mice is associated with more mature oligodendrocytes being present at the lesion site. We performed immunofluorescence staining using an antibody against GSTpi, a marker for mature oligodendrocytes. As shown in Fig I-4, although both strains fed with cuprizone showed a decrease in GSTpi+ mature oligodendrocytes compared to non-cuprizone fed controls, the decrease for C57BL/6 mice was more severe than for CD1 mice [significant differences were observed at 4, 5, 6 and 7 weeks of treatment ($P<0.05$ in ANOVA at all time points)]. These observations indicate that the lesser demyelination of CD1 mice as shown in the Black gold staining and LFP-PAS stain may be attributed to more oligodendrocytes being present. We also noticed that at 7 weeks of treatment, the number of GSTpi+ oligodendrocytes in the two strains are relatively high, compared to the absence of myelin as shown in the LFB-PAS stain

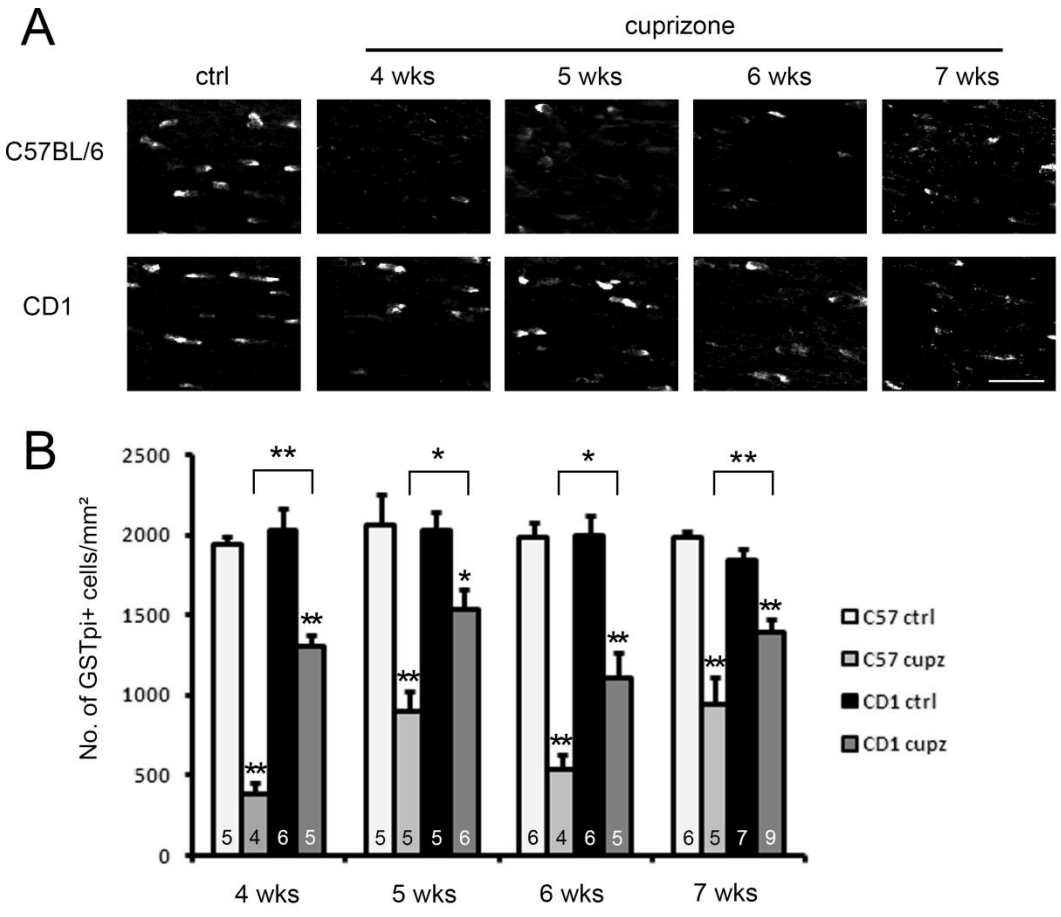

Figure I-4. Immunostaining of GSTpi shows relative abundence of mature oligodendrocytes in CD1 mice relative to C57BL/6 mice after various length of cuprizone exposure. A, representative images of GSTpi+ mature oligodendrocytes at the midline of the corpus callosum. Scale bar, 30 μm. B, quantification of cell density counts. Note CD1 mice and C57BL/6 mice show comparable numbers of mature oligodendrocytes under control conditions. Asterisks above brackets indicate significant differences between strains were observed at all time points of treatment (two way ANOVA analysis for interaction between strain and cuprizone treatment. *, $P<0.05$; **,$P<0.01$). Asterisks above the bars indicate significant difference from respective controls (t-test, *, $P<0.05$; **,$P<0.01$). Error bars show SEM. N numbers are indicated on individual bars.

at this time point (compare Fig I-2 and I-4 at 7 weeks). This discrepancy could be due to oligodendrocyte progenitor cells differentiating into pre-myelinating oligodendrocytes (B. Emery, 2010) (also see below), which are not myelinating the axons due to continuous cuprizone lesion.

Since CD1 mice show more myelin and more oligodendrocytes, we wanted to determine whether this difference is reflective of a quantitative difference in the levels of myelin proteins. To this end, we performed western blot analysis using 4 weeks-cuprizone treated corpus callosum samples (Fig I-5). We first examined the levels of myelin basic protein (MBP). As shown in Fig I-5A and C, on average, CD1 mice showed a milder reduction in MBP protein levels after cuprizone treatment compared to C57BL/6 mice, however the difference did not reach statistical significance ($P>0.05$ in t-test, N=6 for C57BL/6 and N=8 for CD1). A comparison of untreated corpus callosum between CD1 mice and C57BL/6 mice (inset) did not reveal a significant difference (t-test, $P>0.05$, N=6 per group) between strains. We also analyzed the level of myelin associated glycoprotein (MAG). As shown in Fig I-5A and D, the decrease in MAG level was less in CD1 mice compared to C57BL/6 mice (student's t-test, $P<0.05$, N=6 for C57BL/6 and N=8 for CD1), and a comparison of unlesioned corpus callosum sample between the two strains (inset) revealed a similar base line MAG level between the two strains (student's t-test, $P>0.05$, N=6 per group).

CD1 mice exhibit fewer oligodendrocyte progenitor cells compared to C57BL/6 mice

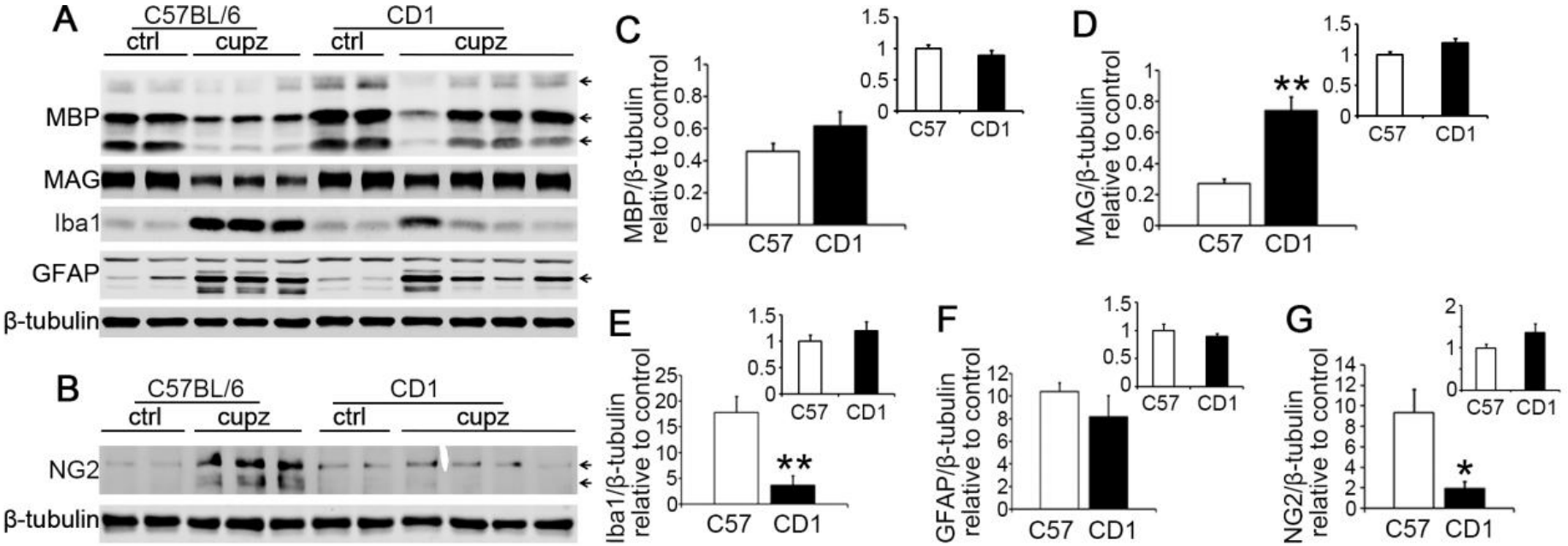

Figure I-5. Western blot analysis confirms the relatively mild effect of cuprizone on CD1 mice compared to C57BL/6 following 4 weeks of cuprizone exposure. A and B, representative western blot images of MBP, MAG, Iba1, GFAP and NG2 protein. Arrows point to the bands used for quantification of MBP, GFAP and NG2, respectively. C-G, statistical analysis of the reduction of MBP, MAG, Iba1, GFAP and NG2. Densitometric data are normalized to β-tubulin and relative to control mice. The decrease in MBP levels are not statistically different in the two strains, while the reduction of MAG level shows significant difference between the two strains (**, $P<0.01$ in t-test, N=6 and 8 for C57 and CD1, respectively). The change in Iba1 and NG2 levels after cuprizone treatment are also significantly different between strains (**, $P<0.01$ in t-test; *, $P<0.05$ in t-test. N=6 and 8 for C57 and CD1 mice, respectively). Error bars show SEM. Insets in C-G shows comparison of protein levels of the two strains using 8-9 weeks old unlesioned corpus callosum samples, with data normalized to average of C57BL/6 mice. None of the comparisons show significant difference between the two strains.

Because the oligodendrocyte loss induced by the cuprizone lesion is usually accompanied by NG2+ oligodendrocyte progenitor cell (OPC) accumulation and differentiation (Mason et al., 2000), we analyzed the number of OPCs in the cuprizone treated mice (Fig I-6). In C57BL/6 mice, NG2+ OPC number peaked at 4 and 6 weeks, while CD1 mice exhibited a gradual increase in NG2+ cell population, coinciding with increasingly severe demyelination. Although CD1 mice showed a much smaller increase in NG2+ cells at 4 and 6 weeks ($P<0.05$ in ANOVA for both 4 and 6 weeks), they do show comparable numbers of NG2+ cells as C57BL/6 strain at 7 weeks. The observation that CD1 mice show less NG2+ OPC recruitment is consistent with the data that CD1 mice show more oligodendrocytes and less demyelination. We also confirmed the morphological data by western blot analysis of NG2 protein level, using 4 weeks-cuprizone treated corpus callosum samples. As shown in Fig I-5 B and G, the induction of NG2 protein is significantly lower ($P<0.05$, student's t-test) in CD1 mice, compared to C57BL/6 mice.

CD1 mice exhibit a smaller neuroinflammatory response compared to C57BL/6 mice

Because cuprizone induced demyelination in the corpus callosum in also known to be associated with microglial/macrophage accumulation and prominent astrogliosis (Hiremath et al., 1998), we then analyzed the degree of the innate neuroinflammatory response, focusing on recruitment of microglia to the site of demyelination in the two strains. As the CD1 mice showed less myelin loss following the cuprizone lesion, we expected that CD1 mice show less microglia compared to C57BL/6 mice. As shown

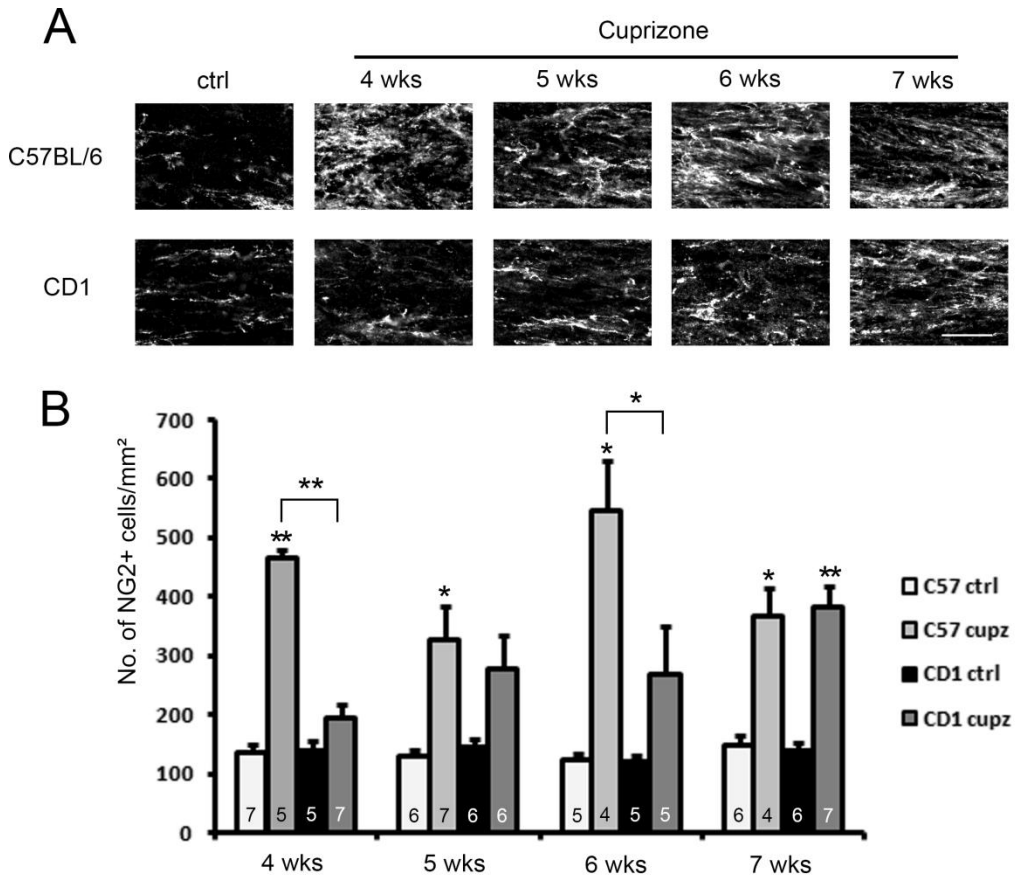

Figure I-6. Immunostaining of NG2 shows blunted recruitment of NG2+ oligodendrocyte progenitor cells (OPCs) in CD1 mice relative to C57BL/6 mice at different length of cuprizone exposure. A, representative images of NG+ OPCs at the midline of the corpus callosum. Scale bar, 30 μm. B, quantification of cell density counts. CD1 mice and C57BL/6 mice show comparable numbers of OPCs under control conditions, and significant differences between strains were observed at 4 and 6 weeks of treatment (asterisks above brackets indicate significant interaction between strain and cuprizone in two-way ANOVA analysis, *, $P<0.05$; **, $P<0.01$). At 7 weeks of treatment, the numbers of OPCs in the two strains appear to be similar. Asterisks above the bars indicate significantly different from respective controls (t-test, *, $P<0.05$; **, $P<0.01$). Error bars show SEM. N numbers are indicated on individual bars.

in Fig I-7, the level of Iba1+ microglia peaked at 4 weeks of cuprizone exposure in C57BL/6 mice, and then gradually decreased in number at 5 to 7 weeks. In contrast, CD1 mice showed a less prominent microglial response, with the relative increase in microglia being less than C57BL/6 mice at 4, 6 and 7 weeks of cuprizone treatment ($P<0.01$ in ANOVA). The numbers of Iba1+ microglia in CD1 mice stayed roughly similar throughout the time points analyzed. A western blot analysis showed that in response to 4 weeks of cuprizone administration, the levels of Iba1 was also lower in CD1 mice compared to C57BL/6 mice (Fig I-5A and E, $P<0.01$ in student's t-test), confirming the morphological observation.

We also analyzed the changes in astrocytes in the cuprizone treated mice. Both strains exhibited a gradual increase in the GFAP+ astrocyte population from 4 to 7 weeks of treatment, with 7 weeks showing the greatest amount of astrogliosis. Compared to C57BL/6 mice, CD1 mice showed on average, a lower degree of astrocyte recruitment at all time points and statistical comparison between strains showed significant difference at 6 and 7 weeks of cuprizone treatment (Fig I-8). Western blot analysis examining GFAP levels in the two strains following 4 weeks of cuprizone treatment showed that CD1 mice exhibited on average a smaller induction of GFAP, which is consistent with the immunohistochemical analysis, but the difference did not reach statistical significance (Fig I-5A and F). Note that the arrow in the figure points to the one band/isoform of GFAP analyzed. Other bands, however, are other GFAP isoforms (Kamphuis et al., 2012).

CD1 mice exhibit comparable amount of cuprizone intake with C57BL/6 mice

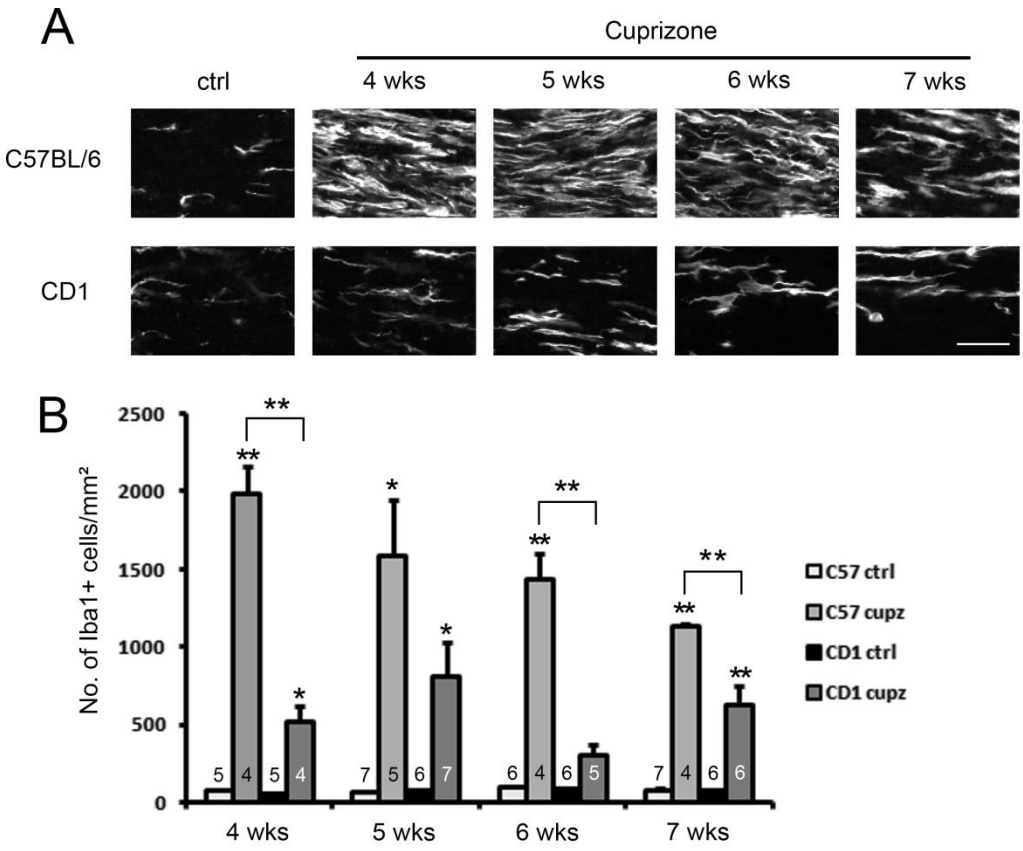

Figure I-7. Immunostaining of Iba1 shows blunted recruitment of Iba1+ microglial cells in CD1 mice relative to C57BL/6 mice after various length of cuprizone exposure. A, representative images of Iba1+ microglia at the midline of the corpus callosum. Scale bar, 30 μm. B, quantification of cell density counts. CD1 mice and C57BL/6 mice show comparable numbers of microglia under control conditions, and significant differences between strains were observed at 4, 6 and 7 weeks of treatment (asterisks above the brackets indicates significant interaction between strain and cuprizone in two way ANOVA analysis, $P<0.01$). Asterisks above the bars indicate significant difference compared to respective controls (t-test, *, $P<0.05$; **, $P<0.01$). Error bars show SEM. N numbers are indicated on individual bars.

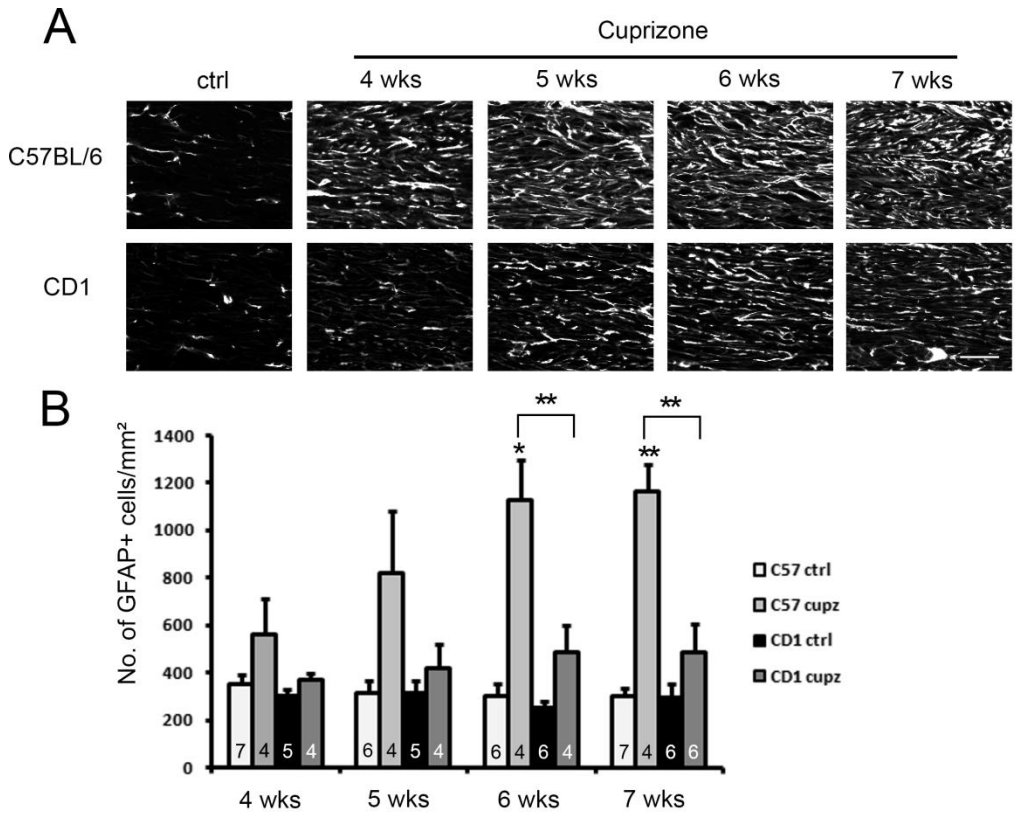

Figure I-8. Immunostaining of GFAP shows blunted recruitment of GFAP+ Astrocytes in CD1 mice relative to C57BL/6 mice after various length of cuprizone exposure. A, representative images of GFAP+ microglia at the midline of the corpus callosum. Scale bar, 30 μm. B, quantification of cell density counts. CD1 mice and C57BL/6 mice show comparable numbers of astrocytes under control conditions, and significant differences between strains were observed at 6 and 7 weeks of treatment (asterisks above brackets indicate significant interaction between strain and cuprizone in two-way ANOVA analysis, $P<0.01$). Asterisks above the bars indicate significant differences from controls (t-test, *, $P<0.05$;**, $P<0.01$). Error bars show SEM. N numbers are shown on individual bars.

Finally, we asked whether the differences in demyelination could be attributed to a difference in cuprizone intake. We noticed that CD1 mice appear to be bigger and weigh heavier compared to C57BL/6 mice, and thus there is a possibility that CD1 intake relatively less cuprizone compared to C57BL/6 mice. In order to rule out this possibility, we tracked the body weight of the cuprizone treated animals across the duration of the treatment and we also measured the amount of food intake by weighing the food pellets in the food tray. The food intake per body weight was then calculated by dividing the amount of food intake by the respective body weight of the animals. As shown in Fig I-9, although CD1 mice are on average bigger than C57BL/6 mice (left panel), they also ingest more cuprizone containing diet (middle panel), resulting in a similar amount of food intake relative to body weight (right panel).

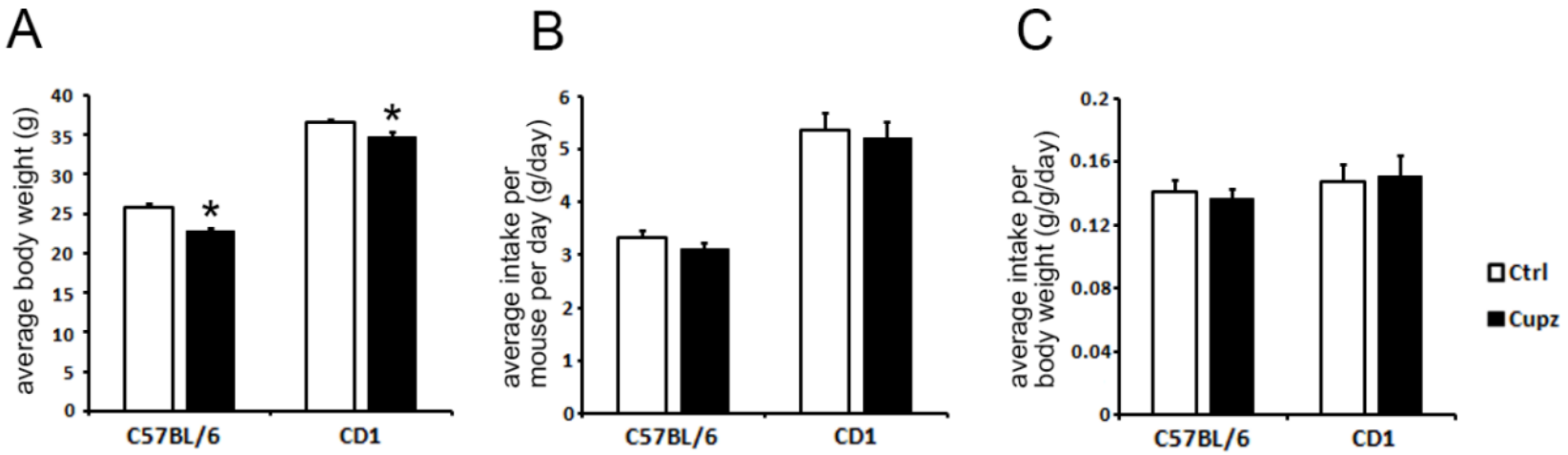

Figure I-9. CD1 mice ingest similar amount of cuprizone compared to C57BL/6 mice. Although CD1 mice on average exhibit higher body weight compared to C57BL/6 mice (A), they also comsume more cuprizone containing diet (B), as a result, the two strains exhibit similar amount of cuprizone diet intake in terms of grams per body weight (C) (No significant differences were seen between groups). Mice were housed in 3-5 animals per cage, and total food intake of individual cages were measured and divided by the number of animals of each individual cage to obtain the average food intake per mouse (B), or divided by the total body weight of animals in the cage to obtain the average food intake per body weight (C). All values are averaged across 4 consecutive weeks of control diet/cuprizone diet treatment. For A, N=10, 11, 13, 11 respectively. Asterisk indicates significant difference from respective controls ($P<0.01$). For B and C, N=3 cages per group.

Discussion

In this section we have demonstrated that CD1 mice display less severe demyelination compared to C57BL/6 mice as demonstrated using several different parameters. First, histology data of black gold and LFB-PAS staining clearly indicates that CD1 mice undergo a mild and slower demyelination process. Second, immunohistochemistry data shows that CD1 mice exhibit less oligodendrocyte decrease and concomitantly less recruitment of microglia/astrocytes/oligodendrocyte progenitor cells following cuprizone intoxication. Third, western blot analysis indicates that while the reduction of MBP is comparable in the two strains, the reduction of MAG is less in CD1 mice. Fourth, western blot analysis also confirms that CD1 mice show less increase in protein levels of Iba1 and NG2. In addition, we showed that CD1 mice consume a similar amount of cuprizone diet per body weight as compared to C57BL/6 mice, and thus the slower rate of myelin damage is unlikely due to less cuprizone consumption.

Strain differences affect cuprizone induced demyelination

The earliest studies characterizing cuprizone induced pathology was done in ICI or Swiss mice, and used a much higher dosage at 0.5%-0.6% (Blakemore, 1972; Ludwin, 1978; Suzuki & Kikkawa, 1969). However, the cuprizone induced demyelination in the corpus callosum is best documented in the commonly used C57BL/6 strain and at a dosage of 0.2% (Hiremath et al., 1998; Mason et al., 2000). Therefore in our study, we adopted a 0.2% dosage to address cross-strain differences.

For C57BL/6 mice, it was observed that the demyelination of C57BL/6 mice is robust at 4 to 6 weeks of cuprizone treatment, and our findings mostly agree with the previously reported observations. However, notably, there have been several other recent studies that have addressed the importance of genetic background factors in influencing the extent of demyelination in the cuprizone model. For instance, SJL mice have been shown to be less susceptible to demyelination in the corpus callosum compared to the established C57BL/6 strain (Taylor et al., 2009). The authors also reported that SJL mice exhibit a unique pattern of demyelination in that the area of the corpus callosum that is immediately lateral to midline seems to demyelinate more prominently than the midline. In our study we observed several cases that some CD1 mice also showed a similar pattern, but not all. In addition to the corpus callosum, cortical demyelination induced by cuprizone has also been shown to be affected by genetic background factors (Skripuletz et al., 2008). In this study the authors challenged BALB/cJ mice with 0.2% cuprizone treatment of 6 weeks, and observed that cortical demyelination of BALB/cJ mice was incomplete, as opposed to C57BL/6 strain which shows no detectable cortical myelin at this stage.

Cuprizone administration specifically affects oligodendrocytes

The cuprizone model of induced demyelination has been a widely adopted approach to study the pathological process of MS for the past 20 years. However, the exact mechanism of how cuprizone induces demyelination still remains elusive (J. Praet et al., 2014). Two opposing hypothesis have been proposed to explain the in vivo action of the cuprizone molecule. The first hypothesis states that the toxic effects

of cuprizone mainly arises from a copper deficient diet (Benetti et al., 2010). In this interesting study, a mass spectrometry was performed on the liver and brain of cuprizone-fed mice and found no detectable cuprizone. In addition, the authors also showed the inability for the cuprizone molecule to cross either the intestinal epithelial barrier or the neuronal cell membrane. The other hypothesis states that the cuprizone molecule has to be present and act directly in the brain for its toxic effect (Zatta et al., 2005). In this study the authors were able to detect cuprizone in blood plasma samples from cuprizone treated mice. In addition, a severely altered copper and zinc homeostasis was observed the central nervous system. Regardless of how exactly cuprizone exerts its action in vivo, a consensus seems to be that cuprizone selectively affects oligodendrocytes. Evidence includes giant mitochondria formation specifically within oligodendrocytes (Acs & Komoly, 2012; Asano, Wakabayashi, Ishikawa, & Kishimoto, 1978; Biancotti et al., 2008; Hiremath et al., 1998; Ludwin, 1978; Tandler & Hoppel, 1973; Wakabayashi, Asano, Ishikawa, & Kishimoto, 1978) and an increased oxidative stress (Acs, Selak, Komoly, & Kalman, 2013; J. Praet et al., 2014; Tandler & Hoppel, 1973, 1975; Wakabayashi, Asano, & Kurono, 1975) and endoplasmic reticulum (ER) stress (Hemm, Carlton, & Welser, 1971; Love, 1988; Wagner & Rafael, 1977) observed in oligodendrocytes, eventually leading to oligodendrocyte apoptosis (Matsushima & Morell, 2001; C. Xu, Bailly-Maitre, & Reed, 2005). Importantly this apoptosis precedes the massive demyelination caused by cuprizone administration (J. Praet et al., 2014), indicating that oligodendrocytes degeneration is the main cause, as opposed to a secondary immune response. This actually makes the cuprizone model particularly suitable for studying Type III and Type IV MS lesions (C. Lucchinetti et al., 2000; Stys et al., 2012).

Neuroinflammatory response contribute to cuprizone induced demyelination

In addition to the direct effect of cuprizone on oligodendrocytes, the involvement of the immune system is believed to be responsible for the massive demyelination occurring at 4 weeks time point of cuprizone exposure (J. Praet et al., 2014). Important supporting evidence includes: 1, a switch from Caspase 3-dependant to Caspase 3-independent form of apoptosis is reported for later stages of cuprizone exposure (Hesse et al., 2010), 2, cuprizone-induced apoptosis in in vitro oligodendrocyte culture was successful only after addition of pro-inflammatory cytokines, which are produced by microglia and astrocytes (Pasquini et al., 2007). 3, inhibition of microglial activation by minocycline prevented cuprizone induced demyelination in vivo (Pasquini et al., 2007). 4, microglial processes were observed in between myelin lamellae, possibly stripping myelin from axons (Ludwin, 1978). In our experiments, we observed a dramatic increase of microglia in C57BL/6 mice following 4 weeks of cuprizone exposure, which is similar to previous reports (Hiremath et al., 1998). However, for the CD1 strain, we did not observe prominent microgliosis (Fig I-6). Even after 7 weeks of treatment, when CD1 mice already show extensive demyelination in the black gold stain and LFB-PAS stain (Figure I-1 & I-2), the levels of Iba1+ cells is still well below that of the C57BL/6 strain. Thus we propose that the strain differences observed in this study can be at least partially accounted for by a difference in the sensitivity of the immune system between the two strains. This is also a mechanism that has been proposed to explain the difference seen between type II and type III MS lesions (Stys et al., 2012). Future experiments addressing the levels of cytokines and growth factors during the cuprizone treatment period and functional interference with specific cells types such as microglia and

astrocytes should help elucidate the role of immune response in contributing to the strain differences observed.

MAG is less affected in CD1 mice compared to C57BL/6 mice

Another notable finding in our experiment is that whereas MBP reduction is comparable between the two strains, MAG reduction is less in the CD1 strain. Given that MAG molecules are localized exclusively in the periaxonal regions of the myelin sheath (Trapp, 1990; Trapp & Quarles, 1984), a relatively abundant MAG level might indicate a relatively intact myelin-axon interface in the CD1 mice, which could contribute to the lack of massive immune response. Indeed, our results indicate that at least, MAG reduction better correlates with the magnitude of immune response including astrogliosis and microgliosis than MBP reduction (comparing Fig I-4 with Fig I-6 & 7). A similar analysis of myelin protein reduction following cuprizone lesion in other strains, especially strains that are less vulnerable might help to address whether this is also the case under other genetic backgrounds.

Future directions

We addressed the important role of genetic background in affecting the demyelination response induced by the neurotoxin cuprizone by comparing CD1 strain versus the commonly used C57BL/6 strain, adding abundance to the current literature on strain differences in the cuprizone model. CD1 mice appear to show relatively mild demyelination and blunted immune response compared to C57BL/6

mice after the same dosage of cuprizone treatment.

In order to further address the strain differences observed, three experiments could potentially be carried out. The first would be to examine the mitochondria morphology using an electron microscopy (EM) study. This approach would enable us to address the pathology within oligodendrocytes specifically at earlier time points of the cuprizone treatment (e.g., after 1 or 2 weeks of continuous cuprizone exposure), with minimal interference of the neuroinflammatory response (Matsushima & Morell, 2001). The rationale is that since cuprizone affects primarily oligodendrocytes, we will need to address whether the oligodendrocytes are similarly affected between the two strains (C57BL/6 and CD1) in the first place. As mentioned earlier, mitochondria morphology is an important parameter of cuprizone-induced oligodendrocyte pathology, and that enlarged oligodendrocyte mitochondria signals oligodendrocyte metabolic stress. Thus, examination of mitochondria morphology will provide clue for the metabolic state of oligodendrocytes, and that if CD1 mice exhibit relatively mild mitochondria pathology compared to C57BL/6 mice, we can easily hypothesize that the strain differences observed in response to cuprizone treatment is primarily due to CD1 oligodendrocytes being less susceptible to cuprizone insult. Further confirmation might include in vitro cell culture experiments using isolated oligodendrocytes from both strains.

The second experiment that could be done is functional ablation of specific cell lineages such as the OPCs, microglia and astrocytes, possibly using a cell type specific promoter and tetracycline-controlled expression system. This would allow for time-controlled inhibition of neuroinflammatory response and specifically examine the cuprizone effect on the pre-existing mature oligodendrocytes, without the interference of oligodendrocyte regeneration, myelin debris clearance and trophic

support from other cell types. The rationale is the cuprizone induced lesion is highly complex, and involves cross-talk among various cell types, and that inhibiting specific cell lineages would enable us to address fewer processes at a time

SECTION II: POTENTIAL ROLES OF EPHRIN-B3 IN OLIGODENDROCYTE MYELINATION

Summary

In Section I, we showed that different genetic backgrounds lead to dramatic difference in oligodendrocyte pathologic response to a demyelinating lesion. In this section, we focus on probing the function of the Ephrin-B3 ligand in oligodendrocytes, which is highly expressed in myelin processes. We do so by examining physiological phenotype of mice carrying Ephrin-B3 null mutation.

Ephrin-B3 belongs to the family of Ephrins, or Eph family receptor interacting proteins. This Ephrin/Eph signaling has been shown to regulate a wide variety of physiological processes including neural development and adult CNS function. In this section, we show that Ephrin-B3 is strongly expressed in the adult mouse brain, overlapping with myelin tracks. However, oligodendrocyte and myelin development does not seem to be affected by Ephrin-B3 deletion. In addition, we challenged Ephrin-B3$^{-/-}$ mice with cuprizone, which induces demyelination in the corpus callosum, and analyzed myelin morphology at 4 weeks of cuprizone treatment. Ephrin-B3$^{-/-}$ mice showed profound demyelination which is similar to Ephrin-B3$^{+/+}$ littermates. Moreover, Ephrin-B3$^{-/-}$ mice showed recovery (remyelination) upon cuprizone withdrawal (6 weeks of cuprizone treatment which induces full demyelination, followed by 3 weeks of recovery using cuprizone-free control diet) which is also similar to Ephrin-B3$^{+/+}$ littermates. Taken together, Ephrin-B3 loss of function alone does not seem to dramatically affect oligodendrocyte development as well as its myelination processes, or the demyelination/remyelination response induced by cuprizone toxin induced lesion.

Introduction

Ephrins and Eph receptors

Ephrins are a family of ligands for the Eph group of receptors, which is one of the largest members in the family of receptor tyrosine kinases. The Ephrin ligands are divided into two subclasses of Ephrin-As and Ephrin-Bs based on their structure and linkage to the cell membrane. Ephrin-A ligands are GPI-linked proteins, and the Ephrin-B ligands are transmembrane proteins (Eph Nomenclature, 1997). On the other hand, the Eph receptors can also be divided into two groups based on the relatedness of their extracellular domain sequences, which appears to correspond to the ability of the receptors to bind preferentially to the Ephrin-A or Ephrin-B ligands. Therefore, the group of Eph receptors that preferentially interact with Ephrin-A ligands are called EphAs, and that the group that preferentially interact with Ephrin-Bs are called EphB receptors. However, there is some promiscuity in their binding affinities. For instance, Ephrin-B ligands are shown to bind to EphA4 receptor (Pasquale, 2004), and that EphB2 receptor shows attraction towards Ephrin-A5 ligand (Himanen et al., 2004).

As for many receptor tyrosine kinases, Ephrin binding to Eph receptors induces so-called ‘forward signaling’, mostly through phosphotyrosine-mediated pathways (Kullander & Klein, 2002). However, Ephrins can also signal back into their host cell-referred to as ‘reverse signaling’, in which the Ephrin cytoplasmic tail can be phosphorylated and thereby recruit signaling effectors. The Eph/Ephrin signaling is known to play multifunctional roles in regulating the processes of tissue segmentation (Poliakov, Cotrina, & Wilkinson, 2004), angiogenesis (Cheng, Brantley, & Chen,

2002), axonal guidance (Egea & Klein, 2007) and synaptic plasticity (Klein, 2009).

Ephrin-B3 in oligodendrocytes

Ephrin-B3 has been shown to be expressed in postnatal myelinating oligodendrocytes (Benson et al., 2005), and its forward signaling through the EphA4 receptor has been shown to prevent contralateral corticospinal axons from recrossing the spinal cord midline during neural development, allowing for unilateral motor control. Consequently, Ephrin-B3$^{-/-}$ mice exhibit a hopping gait behavior. Other reported developmental and physiological functions of Ephrin-B3 include neuronal migration (Aycan Senturk, Sylvia Pfennig, Alexander Weiss, Katja Burk, & Amparo Acker-Palmer, 2011), regulation of axon pruning, (N.-J. Xu & Henkemeyer, 2009), synapse formation (N.-J. Xu, Sun, Gibson, & Henkemeyer, 2011), regulation of synaptic transmission (Antion, Christie, Bond, Dalva, & Contractor, 2010), regulation of synaptic plasticity (Armstrong et al., 2006), and endogenous neurogenesis following cerebral ischemia (Doeppner et al., 2011).

In this section, we make use of two strains of mice, the Ephrin-B3^{LacZ} mutant (Yokoyama et al., 2001) and Ephrin-B3$^{-/-}$ complete mutant. The Ephrin-B3^{LacZ} mutant is constructed such that the intracellular domain of Ephrin-B3 is deleted and replaced by a bacterial lacZ cassette, which enables X-gal detection of β-gal activity to examine the expression patterns of the Ephrin-B3 molecule. The extracellular domain of Ephrin-B3, however, is maintained, and thus the ‘forward signaling’ component is preserved while the ‘reverse signaling’ is disrupted. On the other hand, in the Ephrin-B3$^{-/-}$ complete knockout mice (Yokoyama et al., 2001) the Ephrin-B3

expression is completely absent.

By utilizing the Ephrin-B3^{LacZ} mutant mice, we first show that the Ephrin-B3 expression is strikingly reminiscent of myelin fiber tracks, which indicate that its expression is strongly specific to myelinating oligodendrocytes. Then we address the question whether Ephrin-B3 signaling plays a role in normal myelination during development and in mediating demyelination/remyelination following cuprizone lesion, by treating Ephrin-B3$^{-/-}$ mice with cuprizone and examining the pathological phenotype at two different stages.

Results

Myelin specific expression of Ephrin-B3

We utilized the Ephrin-B3$^{+/LacZ}$ heterozygous mutant mice in which the cytoplasmic domain of Ephrin-B3 is replaced by a LacZ cassette and carried out LacZ staining to examine the expression (Fig II-1). Ephrin-B3 showed particularly strong expression in myelin tracks, and that the LacZ staining strikingly resembles the Black gold staining of Ephrin-B3 wild type animals, indicating that Ephrin-B3 is strongly expressed in myelin forming oligodendrocytes, in agreement with previous reports (Benson et al., 2005).

Effects of Ephrin-B3 loss of function on myelin fiber track development

Given the extensive expression of Ephrin-B3 in myelin, we wondered whether Ephrin-B3 loss of function affects normal development of myelinated axon tracks. To this end, we performed Black gold staining of 2 months old Ephrin-B3$^{+/+}$ and Ephrin-B3$^{-/-}$ mice (Fig II-2 and Fig II-3), but observed no obvious abnormalities in terms of morphological development and intensity of the myelin staining. We thus concluded that Ephrin-B3 function is dispensable for the majority of CNS axon development and myelination.

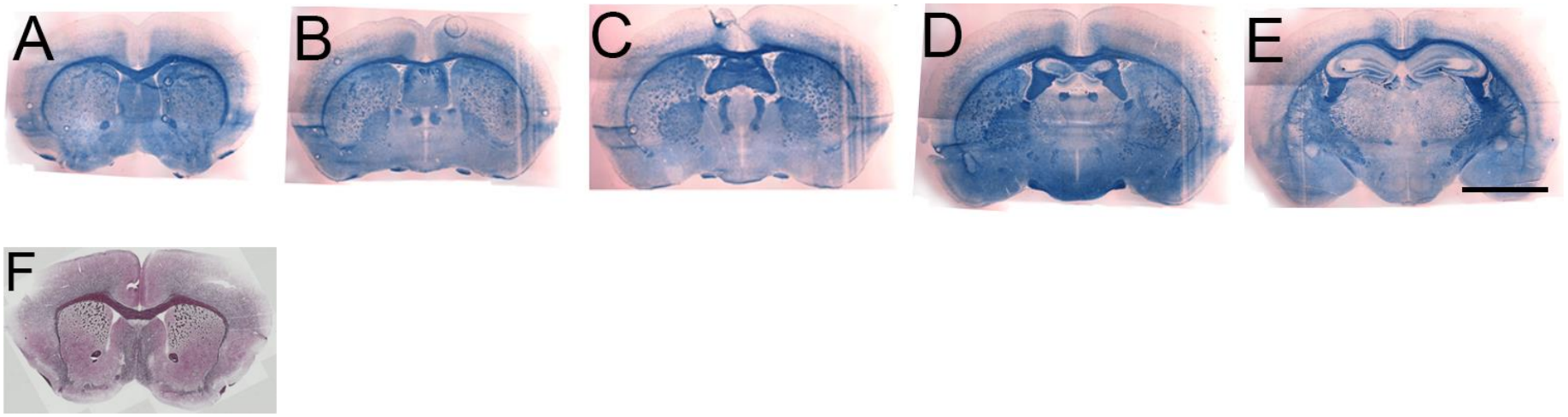

Figure II-1. LacZ staining of 2 months old Ephrin-B3$^{+/LacZ}$ brain. A-E, Ephrin-B3 expression exhibit striking resemblance of myelin tracks, which indicates that Ephrin-B3 is strongly expressed in oligodendrocytes. F, example Black gold staining of myelin tracks of an Ephrin-B3 wild type brain section for comparison. Scale bar, 3 mm.

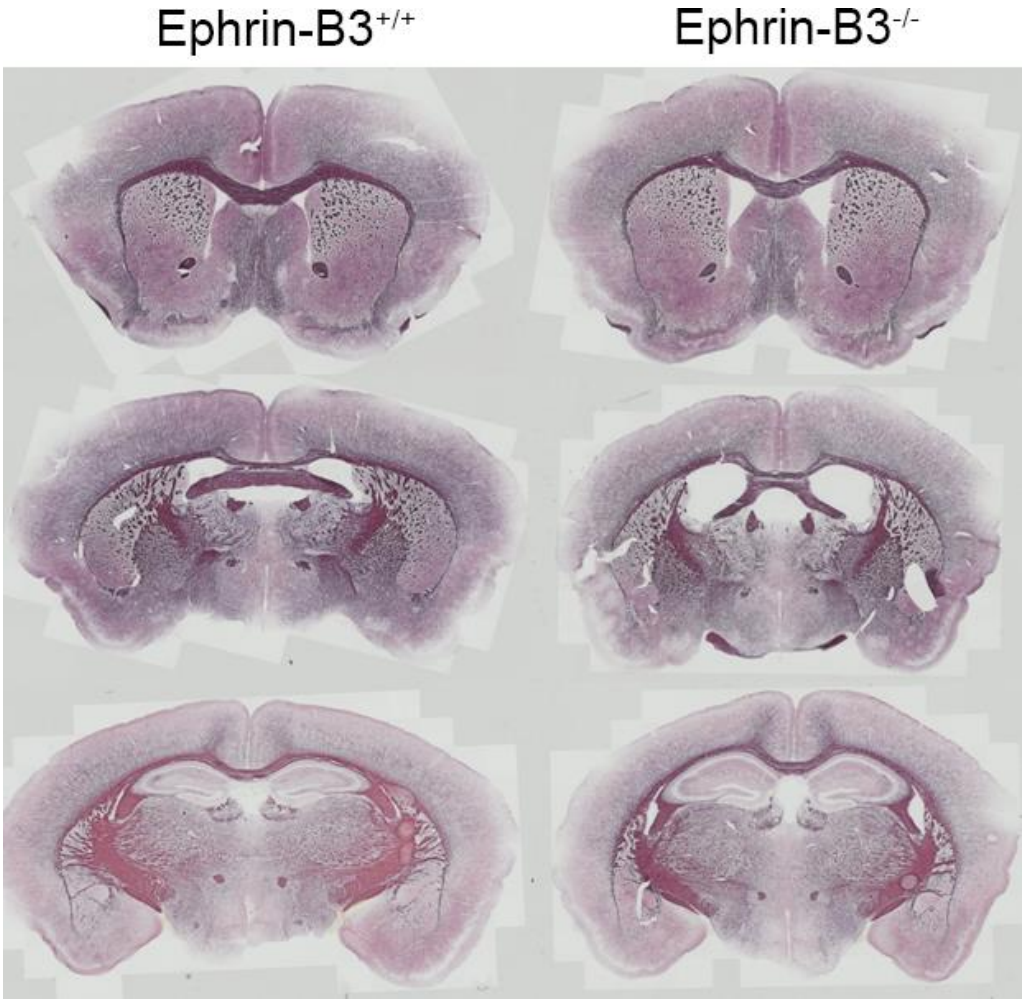

Figure II-2. Black gold staining of 2 months old coronal mouse brain sections shows that Ephrin-B3 loss of function does not dramatically affect myelin development. Left, wildtype. Right, Ephrin-B3 knockout. No obvious abnormality in myelin track development is observed.

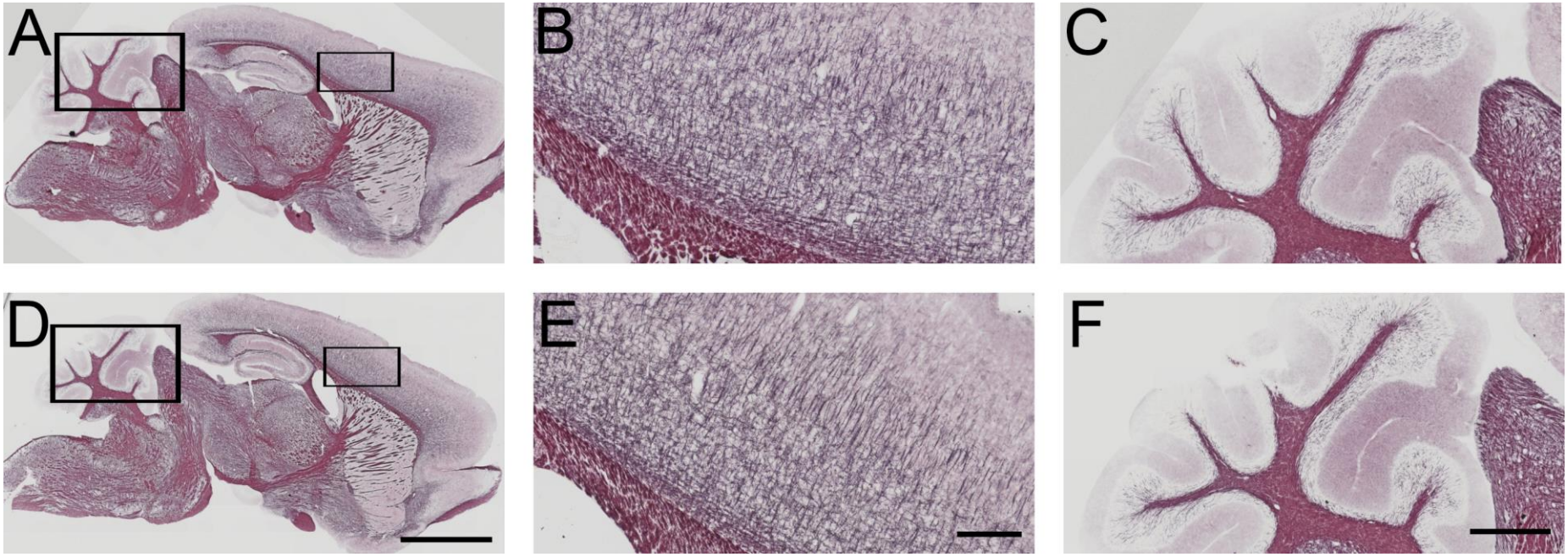

Figure II-3. Black gold staining of 2 months old sagittal mouse brain sections shows that Ephrin-B3 loss of function does not dramatically affect myelin development. Upper panels A, B and C are example wild type images. Lower panels D, E and F are from knockout. B, C, E and F are higher magnifications of the rectangle areas in A and D. No obvious abnormality in myelin track development is observed. Scales bars, from left to right: 2 mm, 200 μm and 500 μm, respectively.

Ephrin-B3 signaling in oligodendrocytes: cuprizone treatment study

We next reasoned that since Ephrin-B3 is strongly expressed in myelinating oligodendrocytes, it might be involved in oligodendrocyte cell signaling pathways for demyelination and remyelination. And that a cuprizone challenge might induce a demyelination and inflammation process that would recruit Ephrin-B3 forward/reverse signaling. We thus performed cuprizone treatment of wildtype and Ephrin-B3$^{-/-}$ mice. We first analyzed corpus callosum tissue samples of mice that underwent continuous cuprizone treatment for 4 weeks (Fig II-4). Both Ephrin-B3$^{+/+}$ and Ephrin-B3$^{-/-}$ mice similarly showed extensive demyelination as indicated by the loss of blue myelin stain and the vast recruitment of cell bodies, which are possibly a mixture of OPCs, microglia and astrocytes. Thus, Ephrin-B3 does not appear to influence the extent of cuprizone-induced demyelination at 4 weeks of treatment.

We then asked whether Ephrin-B3 loss of function impairs the remyelination process. To this end, we first exposed mice to continuous cuprizone treatment for a full length of 6 weeks to achieve complete demyelination (Matsushima & Morell, 2001), after which they were returned to a cuprizone-free control diet for 3 weeks to allow for recovery. Corpus callosum tissue section samples of wildtype and Ephrin-B3$^{-/-}$ mice were then analyzed by Black gold staining (Fig II-5). Both Ephrin-B3$^{+/+}$ and Ephrin-B3$^{-/-}$ mice showed remyelination recovery and were not different from each other.

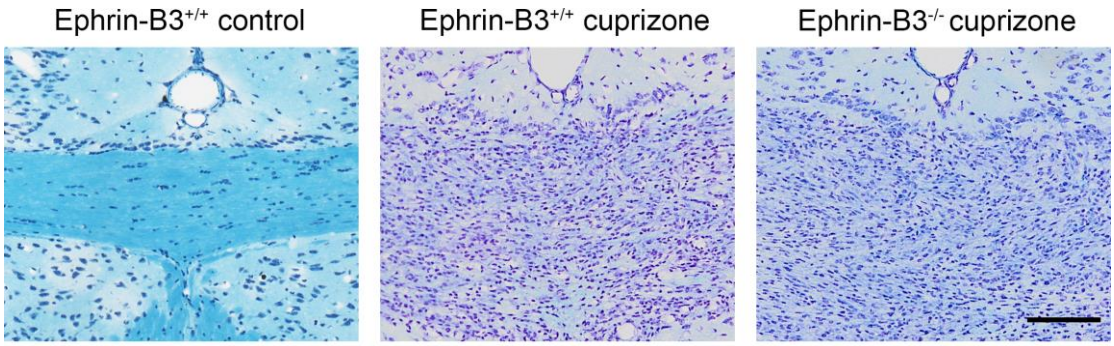

Figure II-4. Example LFB-cresyl violet staining of midline corpus callosum sections from mice treated with cuprizone diet for 4 weeks. Left, wildtype; right, knockout. Both genotypes similarly exhibit profound demyelination, with minimal blue and extensive recruitment of cresyl violet-stained cell bodies. Scale bar, 100 μm.

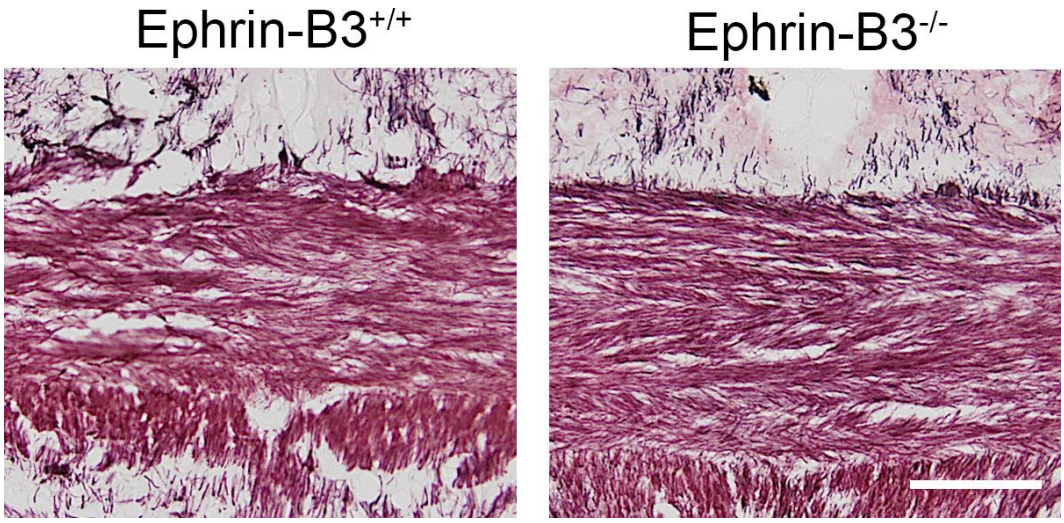

Figure II-5. Example Black gold staining of midline corpus callosum sections from mice treated with cuprizone diet for 6 weeks, followed by 3 weeks of recovery. Left, wildtype; right, knockout. Both genotypes similarly exhibit remyelination, and do not appear to differ from each other. Scale bar, 100 μm.

Discussion

During embryonic development, the expression of Ephrin-B3 has been shown to be concentrated at the spinal cord midline (Yokoyama et al., 2001), and that Ephrin-B3 loss of function leads to a striking motor deficit as manifested by a hopping gait locomotion. Anterograde and retrograde tracing studies further showed that in the absence of Ephrin-B3, contralateral corticospinal tract can aberrantly traverse the spinal cord midline and reenter the ipsilateral side, resulting in bilateral innervations. Importantly, the Ephrin-B3 LacZ mutant which lack the cytoplasmic domain show normal gain appearance (Yokoyama et al., 2001), implying that the reverse signaling of Ephrin-B3 back into the Ephrin-B3 expressing cell is dispensable for its function as a midline-anchored repellent.

In adulthood, a similar function of Ephrin-B3 has also been reported (Benson et al., 2005). In this study, Ephrin-B3 has been shown to be expressed in postnatal myelinating oligodendrocytes and that it partially accounts for the inability of CNS axons to regenerate following traumatic spinal cord injury. Importantly, this inhibition of neurite outgrowth also depends on the forward, and not the reverse, signaling of Ephrin-B3.

Taken together, the forward signaling of Ephrin-B3 has been well documented as an inhibitor of neurite outgrowth. However, the reverse signaling of Ephrin-B3 back into the myelin-forming oligodendrocytes has remained unexplored. In our study, we set out to examine myelin-related developmental phenotype as well as pathology following cuprizone-induce myelin damage in the absence of Ephrin-B3. However, we did not observe any significant differences between wildtype and Ephrin-B3 knockout mice in terms of myelination during development, cuprizone-induced demyelination, and remyelination after cuprizone withdrawal. Thus Ephrin-B3 does

not seem to be critically involved in regulation of myelination within oligodendrocytes, and that the reverse signaling of Ephrin-B3 back into its host cell is still a mystery.

Nevertheless, our study does not preclude Ephrin-B3's function in oligodendrocyte demyelination/remyelination in general, as it is known that intrafamily compensatory mechanisms exist among different Ephrin-Bs (Hu, Li, Jiang, Li, & Zhou, 2014), and that all of Ephrin-B1, Ephrin-B2 and Ephrin-B3 can share the same receptor such as EphA4 (Luxey et al., 2013). Thus, in order to address the function of Ephrin-Bs in general, triple Ephrin-B1, B2, B3 knockout animals (A. Senturk, S. Pfennig, A. Weiss, K. Burk, & A. Acker-Palmer, 2011) will be needed and examined in similar experiments.

SECTION III: EXAMINING THE FUNCTION OF FBXL15 USING FBXL15$^{-/-}$ MICE

Summary

In the first two sections, we presented studies to address the myelination/demyelination processes of oligodendrocytes, one being the affect of genetic background, the other being the potential function of an important signaling molecule Ephrin-B3.

In parallel, our lab has been investigating the roles of other Ephrin/Eph signaling molecules in regulation of neural circuit function. Our previous study indicated that Ephrin-A5 is highly expressed in the suprachiasmatic nucleus (SCN), and thus potentially regulates the circadian rhythm. Interestingly in the literature, Fbxl15, a mammalian homolog of the drosophila jetlag protein, is also implicated in circadian regulation. We thus investigated the physiological phenotype of Fbxl15 loss of function in this separate section, in an attempt to probe its role in circadian rhythm and development.

Fbxl15, or F-box and LRR domain-containing protein 15, is a member of the F-box protein family, and functions as the substrate recognition unit for the Skp1–Cul1–F-box-protein (SCF) ubiquitin ligase complex. Upon binding to its substrate, the SCF ubiquitin complex directs it to proteosomal degradation through ubiquitination. In the literature, Fbxl15 has been implicated to function in various physiological processes, including regulation of circadian rhythm and bone mass homeostasis. Here we generated mice that carry null alleles of Fbxl15 ($Fbxl15^{-/-}$) and report that Fbxl15 loss of function does not explicitly influence several easily assessable behavioral parameters including circadian rhythm, anxiety levels, learning and memory, motor coordination and depressive behavior. Given the expression of Fbxl15 in adult gastrointestinal track, we also analyzed intestinal morphology and report no significant morphological abnormalities. Analysis of trabecular bone mass

also did not reveal genotypic differences between Fbxl15$^{+/+}$ and Fbxl15$^{-/-}$ mice. Thus we conclude that Fbxl15 is not specifically involved in the physiological processes that were addressed, and that compensatory mechanisms might exist in the absence of Fbxl15, possibly involving other F-box family members.

Introduction

Fbxl15 and the F-box protein family

Fbxl15 (F-box and leucine-rich repeat protein 15) is a member of the family of F-box proteins, which are components of SCF E3 ubiquitin-ligase complexes. SCF complexes contain four components: Skp1, a cullin, Rbx1/Roc1/Hrt1 and an F-box protein (Kipreos & Pagano, 2000). SCF complexes facilitate interaction between substrate and ubiquitin conjugating enzymes, which then covalently transfer ubiquitin onto substrates. Poly-ubiquitinated substrates are subsequently degraded by the 26S proteosome (Hershko & Ciechanover, 1998). The F-box protein is a subunit of the SCF complex that binds specific substrates with its carboxyl terminal substrate recognition domain (most commonly leucine-rich repeats or tryptophan-aspartic acid (WD) repeats), and it links to the complex by binding Skp1 through the F-box motif. In other words, the F-box proteins, including Fbxl15, are the substrate recognition unit of the SCF complex and it specifies the target protein to be degraded in the cell.

The F-box protein family in mice consists of 74 identified members, all sharing a common F-box motif and differ in their substrate recognition domains. The various F-box proteins can be divided into three main classes, namely Fbxw (w for WD repeats), Fbxl (“l” for leucine-rich repeat) and Fbxo (“o” referring to “other” domains) (Jin et al., 2004). Among them, the Fbxl subfamily consists of 22 different members, namely Fbxl1 through Fbxl22.

Physiological function of various Fbxl proteins: Cirdadian rhythm

Previously it has been reported that the drosophila homolog of the mammalian Fbxl15, namely, *jetlag (jet)*, plays a crucial role in circadian regulation in drosophila (Koh, Zheng, & Sehgal, 2006). Compared to wildtype, mutations in *jetlag* resulted in a slower phase shift in daily activity in response to an 8 hour light shift (a "jet lag" experiment) and also a substantially reduced light-dependent degradation of the clock protein timeless (TIM). Further analysis revealed that JET promoted ubiquitination of TIM in a light sensitive manner. We thus hypothesized that Fbxl15 might be in involved in circadian regulation in mammals as well.

Two other studies also point to a potential function of Fbxl proteins in mammalian circadian regulations. Godinho and colleagues (Godinho et al., 2007) screened a set of N-ethyl-N-nitrosourea–mutagenized mice and reported that a homozygous mutation in Fbxl3 results in a prolonged (27 hours) circadian rhythm in a constant darkness experiment. Circadian fluctuations of mRNA levels of Cry1, Per1 and Per2, which are all molecular components of the mammalian circadian clock, together with Per2::Luciferase expression, are all disrupted in $Fbxl3^{-/-}$ mice. An accompanying study (Busino et al., 2007) further demonstrated that both Cry1 and Cry2 proteins are ubiquitinated and degraded via the SCF^{Fbxl3} ubiquitin ligase complex.

In addition to Fbxl3, Fbxl21 is also shown to play a role in circadian regulation. In the diurnal sheep, Fbxl21 has been shown to be expressed specifically in the suprachiasmatic nuclei (SCN) of the hypothalamus, a key structure involved in circadian regulation (Dardente, Mendoza, Fustin, Challet, & Hazlerigg, 2008). Similar to Fbxl3, Fbxl21 also binds Cry1 and promotes its degradation. In mice, Fbxl21 was

shown to ubiquitinate and stabilize Crys, antagonizing the destabilizing action of Fbxl3 (Hirano et al., 2013). At the behavioral level, the prolonged circadian rhythm phenotype of $Fbxl3^{-/-}$ mice is shown to be attenuated in Fbxl3/Fbxl21 double knockouts.

To summarize, Jet, Fbxl3 and Fbxl21 have all been shown to be involved in circadian regulation. We thus hypothesized that Fbxl15 might also be involved in the mammalian circadian rhythm.

Physiological function of various Fbxl proteins: BMP signaling and adult bone formation

It has been shown that Fbxl15 targets Smurf1 for ubiquitination and proteasomal degradation (Cui et al., 2011). Smurf1, which is also an E3 ubiquitin ligase, is implicated in the regulation of bone cell function (Xing, Zhang, & Chen, 2010), and that studies from biochemical analyses and genetically modified mouse models reveal that Smurf1 negatively regulates the proliferation, differentiation, and maturation of osteoblast lineage cells in three potential mechanisms.

First, Smurf1 targets phosphorylated Smad1 for ubiquitination and proteosomal degradation, contributing to downregulation of BMP signaling (Sapkota, Alarcon, Spagnoli, Brivanlou, & Massague, 2007). Second, Smurf1 targets the osteoblast lineage specific Runx2 for degradation (M. Zhao, Qiao, Oyajobi, Mundy, & Chen, 2003). Overexpression of Smurf1 induced proteasomal degradation of Smad1 and Runx2 proteins in 2T3 osteoblast precursor cells and in C2C12 myoblast/osteoblast precursor cells. Consistent with this notion, Col1a1-Smurf1 transgenic mice in which Smurf1 overexpression was targeted to osteoblasts, exhibit decreased bone volume

and reduced bone formation rates at 3 months of age (M. Zhao et al., 2004). BrdU-positive osteoblast-like cells were also decreased on the surface of the calvariae of these mice. As such, Smurf1 functions to inhibit osteoblastogenesis leading to decreased bone formation. Third, Smurf1 targets phosphorylated MEKK2 for degradation and consequently downregulating the activity of the Runx2 coactivator AP-1 through the MEKK2-JNK pathway (Yamashita et al., 2005). In this previous study, Smurf1 knockout mice were generated and exhibited a phenotype of age-dependent increase in bone mass. Accumulated phosphorylated form of MEKK2 was found in Smurf1$^{-/-}$ embryonic fibroblasts, which resulted in over-activated JNK and AP-1 family transcription factors. As a result, the collagen matrix production in the mature osteoblast was largely increased. Taken together, Smurf1 not only functions to reduce the proliferation of osteoblasts, but also limits the bone forming activities of mature osteoblasts.

Given the negative role of Smurf1 in osteoblast lineage cells, the fact that Fbxl15 targets Smurf1 for degradation implicates the positive role of Fbxl15 in adult bone formation. Indeed, Cui and colleagues (Cui et al., 2011) showed that 6 months old female rats that were treated Fbxl15 siRNA exhibited significantly reduced bone mineral density and trabecular bone volume compared with age-matched control groups. We thus reasoned that Fbxl15 might also function as a positive regulator of osteogenesis in vivo, and that Fbxl15$^{-/-}$ mice might help us address the impact of Fbxl15 loss of function on bone development.

Taken together, Fbxl15 has been implicated in regulation of circadian rhythm as well as regulation of bone mass homeostasis. We thus generated Fbxl15 knockout animals and examined various physiological parameters.

Results

The generation of Fbxl15 knockout animals

We purchased embryonic stem cell (ES cell) carrying Fbxl15 deletion from KOMP (knockout mouse project). The ES cells were injected into developing mouse embryos, and the progenies are screened for the Fbxl15 null allele. Two heterozygous for Fbxl15 deletion was identified, and one of them was subsequently used to derive the entire Fbxl15 knockout colony.

The expression pattern of Fbxl15

We first performed LacZ staining using 2.5 months old adult mice heterozygous for Fbxl15 knockout ($Fbxl15^{+/-}$). As shown in Figure III-1, Fbxl15 is expressed ubiquitously throughout the brain. Structures such as all layers of the cortex, the hippocampus, the striatum, the thalamus and the cerebellum are all positive for the LacZ staining. We were not able to detect any particular structure that was specifically high in expression, which makes it difficult to pinpoint the specific neurocircuits/function that Fbxl15 is involved in.

Interestingly, we also noticed that Fbxl15 is expressed along the adult gastrointestinal track (Figure III-2), most prominently in the muscle cell layer, which implicates a potential function of Fbxl15 in intestinal morphogenesis.

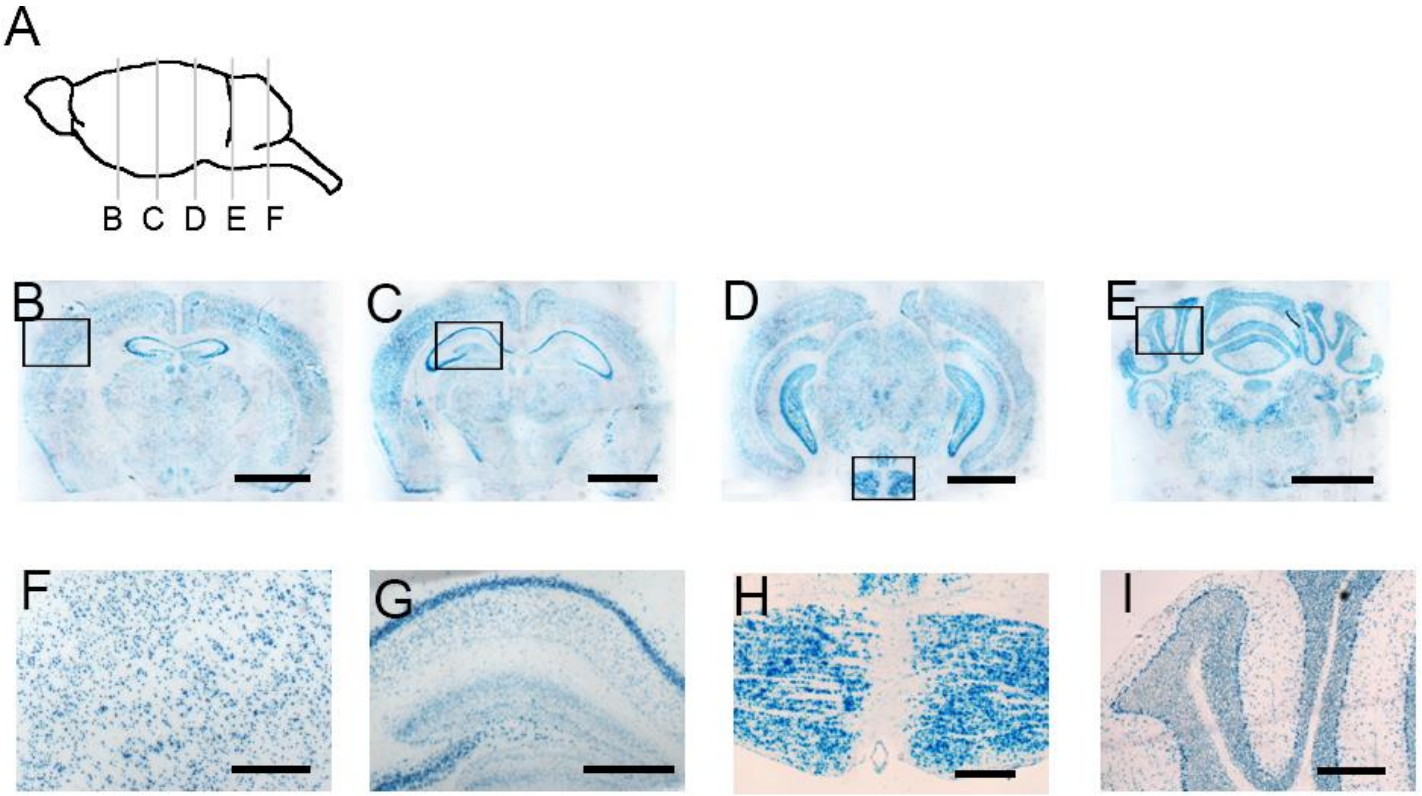

Figure III-1. LacZ expression study shows that Fbxl15 is expressed ubiquitously thoughout the adult brain. Coronal brain sections of 2.5 months old Fbxl15$^{+/-}$ mice were collected and representative images at various levels are shown. Rectangular boxes highlight the areas that are magnified in G-I, showing broad expression in the cortex, hippocampus and cerebellum, respectively. Scale bars, B-F, 2 mm. G-I, 250 μm.

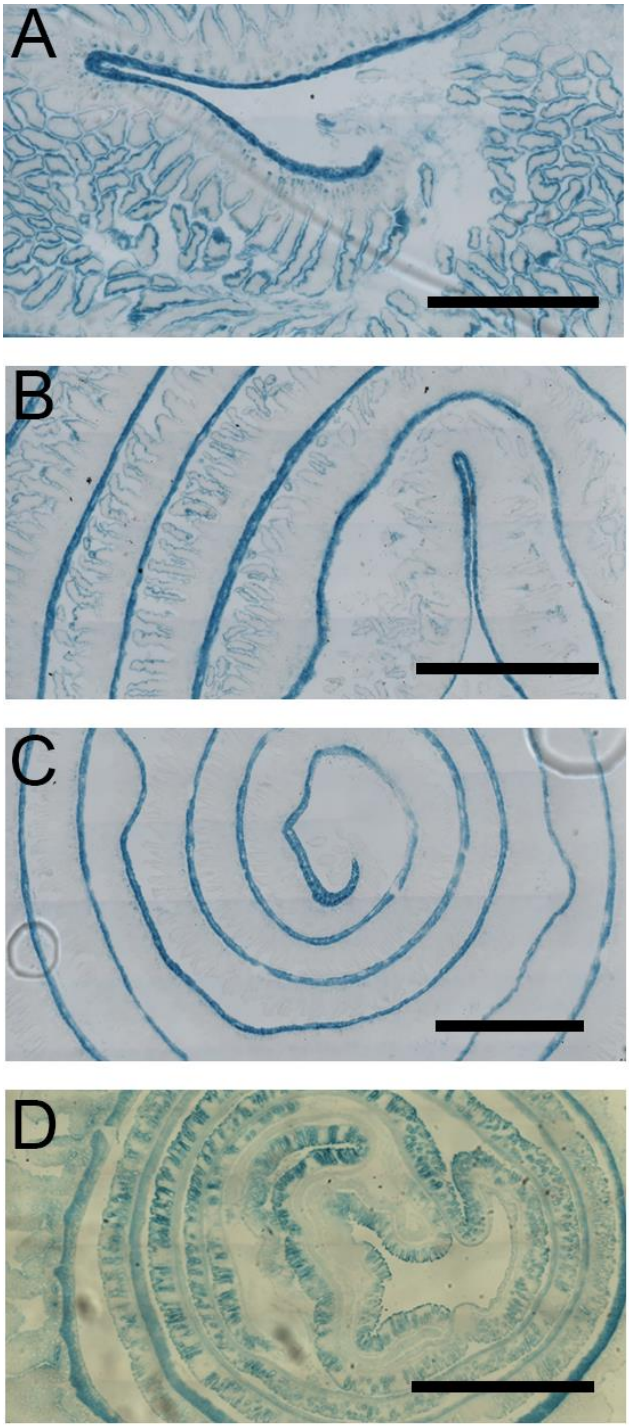

Figure III-2. LacZ expression study also indicates that Fbxl15 is expressed along the gastrointestinal track in two months old adult mice, most prominently in the intestinal muscle cell layer. Cross-sections of “Swiss rolls” are shown. A, duodenum. B, jejunum. C, ileum. D, colon.

The circadian rhythm of Fbxl15$^{-/-}$ mice

Because Fbxl15 was previously implicated in circadian regulation (Koh et al., 2006), we analyzed the circadian cycle in Fbxl15$^{+/+}$ and Fbxl15$^{-/-}$ mice. We first acclimated the mice in the running wheel cages on a regular 12 hour light-12 hour dark circadian cycle for 2 weeks, and then we changed the light schedule to a 24 hour constant darkness free running period, lasting for two weeks. During this period, Fbxl15$^{+/+}$ animals shifted their activity onset time to progressively earlier time points, indicating that in the absence of light entrainment, their internal "body clock" has a natural cycle tau that is shorter than 24 hours (Fig III-3A). The Fbxl15$^{-/-}$ mice showed a similar pattern (Fig III-3B). An analysis of 6 males from each genotype showed that there is no significant difference (student's t-test) in terms of the free running period 'tau' (Fig III-3C). Analysis of wheel running parameters including peak running rates (counts per minute), average activity bout length (minutes), and average bout activity (counts per bout) also showed no significant difference between wildtype and knockout. We thus conclude that Fbxl15 loss of function does not significantly impair the expression of circadian rhythm in mice.

Analysis of anxiety levels in Fbxl15$^{-/-}$ mice

Because Fbxl15 is broadly expressed across the brain, we reasoned that Fbxl15 could potentially be involved in a wide range of different brain circuits underlying different behaviors, and that Fbxl15 deletion could potentially impact these behaviors. In order to address this possibility, we performed a battery of different behavioral

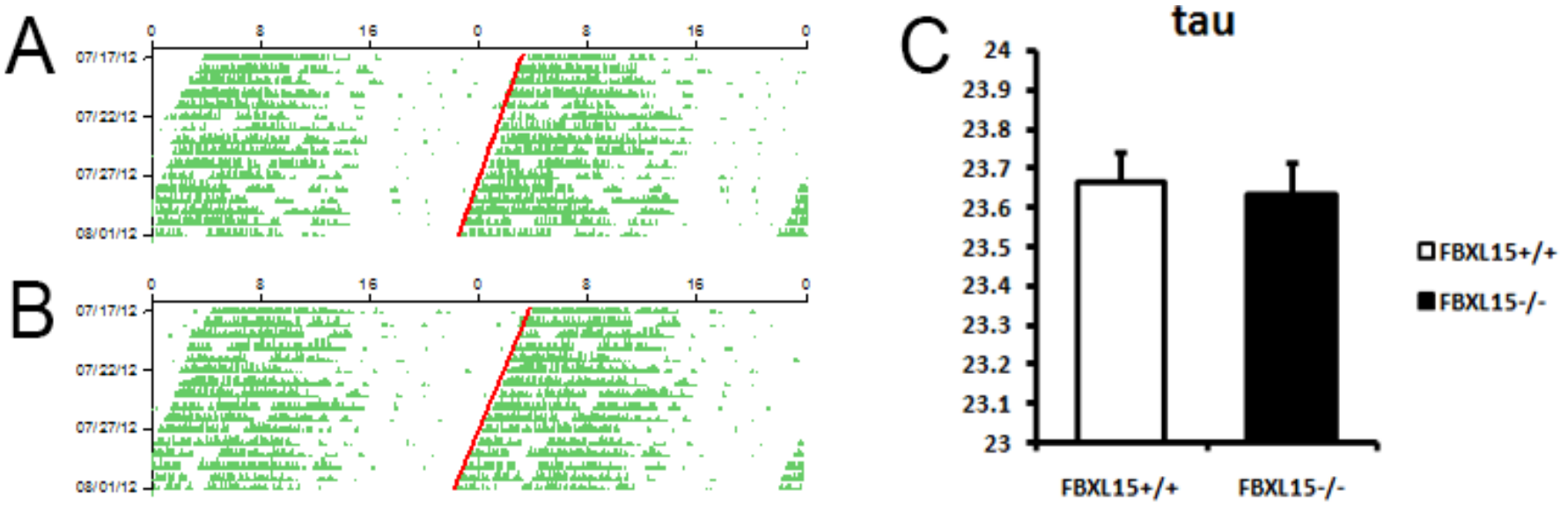

Figure III-3. Fbxl15 knockout mice show normal circadian rhythm as shown in wheel running activity in constant darkness. A, representative circadian actogram for an example adult Fbxl15$^{+/+}$ mouse. B, same as A, but for an Fbxl15$^{-/-}$ mouse. The activity bars are double plotted for visualization and comparison. Red line indicates the time of activity onset during each day gradually advances, which is similar in the wild type and knockout. C, the circadian period tau is similar between wildtype and knockout. N=6 per group, and error bars shows SEM.

tests, interrogating different behavioral parameters that Fbxl15 loss of function might affect.

We first focused on anxiety, applying the commonly used elevated plus maze (EPM) and the light-dark box test. In brief, mice were allowed to freely explore a cross-shaped maze, elevated from the floor, with two of the arms closed and two open. Due to the animal's proclivity toward dark and enclosed spaces, and an unconditioned fear of heights and open spaces (Walf & Frye, 2007), the animal would naturally prefer the closed arms over the open arms, and that the ratio of time the animal explores the open arm, and the ratio of entries into the open arm would be an indicator of the animal's anxiety level. Specifically, an increase in the time spent in the open arm and an increase in the number of entries into the open arm would indicate anxiety reduction or an anxiolytic effect, and vice versa.

As shown in Figure III-4A, the Fbxl15 knockout mice showed a slightly lower open arm preference compared to wild type littermates. However, student's t-test did not show statistical significance in between genotypes (N=8 for wildtype and N=7 for knockout). The total number of entries into either open or closed arms which served as a measurement of general locomotor activity did not show difference between genotypes either. We then turned to the light-dark box (LDB) test, which is also a measurement of anxiety levels. Briefly, animals were placed in the dark compartment of a two compartment enclosure, with one compartment dark and the other brightly illuminated. Based on the innate aversion of mice to light areas (Bourin & Hascoet, 2003), the latency to emerge into the light box as well as the number of entries and time that the mouse spent exploring the light box would be an indicator of its anxiety level. As shown in Figure III-4B, the knockouts were faster to emerge into the light box on average, and that they also showed slightly higher light box preference

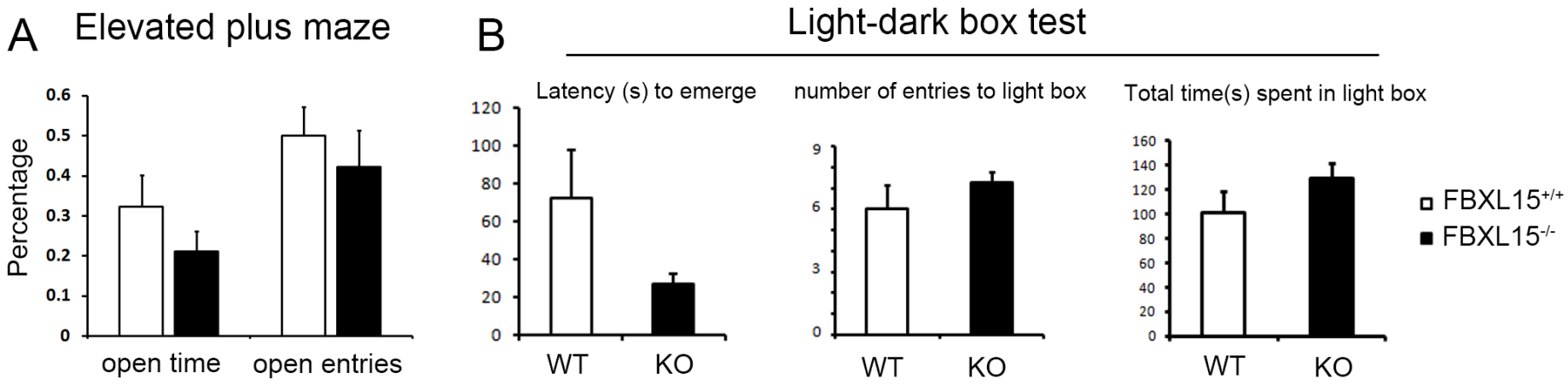

Figure III-4. Fbxl15 deletion does not significantly affect anxiety level. A, elevated plus maze to assess anxiety in wild type versus knockout mice. The group average shows slightly reduced open arm preference in the knockout, but the difference is insignificant. B, group average shows that although Fbxl15 knockout mice spend less time before initiation of exploration in the light box (difference is insignificant (P>0.05)), both wildtype and knockout exhibit similar numbers of entries into the light box and also spent similar length of time exploring the light box. N=8 and 7 for wildtype and knockout, respectively. Statistical comparison was done by student's t-test, and all P values are insignificant (>0.05). Error bar shows SEM.

compared to wildtypes, which would indicate a slightly lower anxiety level on average. However, student's t-test did not show statistical significant difference. Considering the seemingly conflicting results in these two different anxiety tests (EPM showed slightly higher anxiety in the knockout and the LDB showed slightly reduced anxiety in the knockout), we concluded that Fbxl15 deletion does not explicitly impact the animal's anxiety level.

Analysis of learning and memory in Fbxl15$^{-/-}$ mice

We performed a standard water maze test to assess the ability of spatial learning and navigation in Fbxl15 knockout animals. We trained the mice to swim in a circular water tank which was made opaque by non-toxic white paint. On the first two days, an invisible escape platform that was hidden below the water surface but was marked by a mini-flag was present and the animals quickly learned to swim to and climb onto the platform for escape from the water (Fig III-5A, visible days). On the third day, the flag was removed, and the location of the platform was switched to a random place. As a result, the animals had to explore around the pool in order to find the hidden platform (Fig III-5A, invisible days). The animals gradually learned the location of the platform over a course of 4-5 days, as shown by the progressively shorter escape latencies (Fig III-5A, invisible days). This was the case in both Fbxl15$^{+/+}$ and Fbxl15$^{-/-}$ mice, and that the learning curve was not significantly different between genotypes in any of the time points analyzed, indicating that Fbxl15 loss of function does not appear to influence spatial learning and spatial memory.

After the last day of the water maze training, we performed a probe trial in

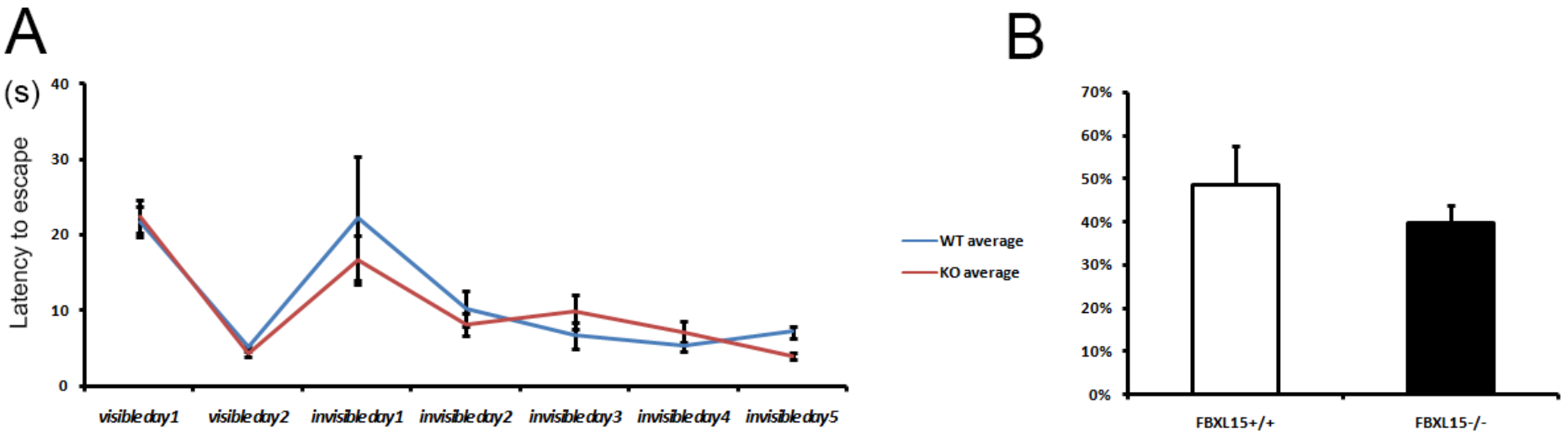

Figure III-5. Water maze test shows that Fbxl15 deletion has no effect on learning and memory. A, Standard water maze test in which animals are first trained with visible platform (visible days) and then with hidden platform (invisible days) at a constant location. Maximum time allowed per trial was 1 minute. $Fbxl15^{+/+}$ and $Fbxl15^{-/-}$ mice show similar learning curve over days. B, Probe test after the last day of water maze learning. With the escape platform removed, the animal was allowed a 1 minute free exploration in the pool. The percentage of time that the animal spent exploring the quandrant in which the hidden platform was located was recorded, and used as an indicator of the memory of the location of the platform.

which the hidden platform was removed from the pool. As shown in Figure III-5B, the Fbxl15$^{-/-}$ mice spent slightly less time exploring the quadrant containing the location of the previous platform, but student's t-test did not show statistical significant difference between genotypes.

Analysis of motor coordination and balance in Fbxl15$^{-/-}$ mice

The rotarod test is a widely used approach to evaluate motor coordination and motor skill learning in rodents (Shiotsuki et al., 2010). We challenged Fbxl15$^{+/+}$ and Fbxl15$^{-/-}$ mice by placing them on a rotating rod and recorded the latencies for them to fall off. The speed of rotation was set to a constant at 12 rpm. Over trials and days, the animals all learned how to stay on the rod for a longer period of time (Fig III-6), and we didn't observe any difference in the learning curve over the 3 day training period between wildtype and knockout animals, indicating that Fbxl15 loss of function does not explicitly impact motor coordination skill, despite its broad expression in the cerebellum.

Analysis of depression-like behavior in Fbxl15$^{-/-}$ mice

We also tested the mice in a forced swim paradigm in order to assess depression-like behaviors (Slattery & Cryan, 2012). In brief, mice were placed inside a glass cylinder filled with water for 4 minutes and during which time it cannot escape. The percentage of immobile time, defined as exhibiting no movements beyond those

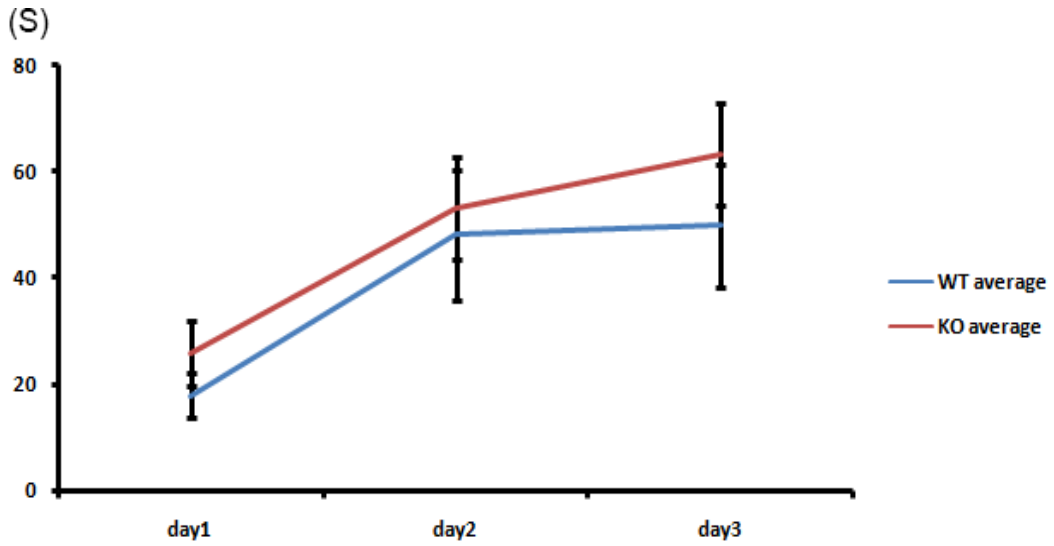

Figure III-6. Rotarod performance test reveals unimpaired motor cordination in Fbxl15$^{-/-}$ mice. Mice were placed on a rotating cylinder at ~12 rpm, and the average latency to fall (s) in three separate trials on each day was measured. The learning curve shows that both the wildtype and the knockout show better performance (longer duration) with training over time. N=6 per group. Error bar shows SEM. No significant difference is seen with any of the time points analyzed.

required to stay afloat was measured and used as an indicator of depression (Porsolt, Le Pichon, & Jalfre, 1977). As shown in Figure III-7, both wildtype and knockout animals spent similar amount of immobile period on the two consecutive test days, indicating that Fbxl15 loss of function does significantly impact depression-like behaviors in mice.

Analysis of intestinal morphology of Fbxl15$^{-/-}$ mice

Given the intestinal expression of Fbxl15$^{-/-}$ mice, we wondered whether Fbxl15 loss of function impacts intestinal morphology. To this end, we performed hemotoxylin and eosin stain (H&E stain) of the intestinal fine structures of the wildtype and knockout animals (Figure III-8). We did not observe prominent difference between wildtype and knockout animals in terms of general morphology and size of the intestinal villi and crypts.

Analysis of trabecular bone volume in Fbxl15$^{-/-}$ mice

Because Fbxl15 was previously implicated in regulation of bone mass and bone mineral density (Cui et al., 2011), we asked whether there would be any developmental abnormalities in bone mass in Fbxl15$^{-/-}$ mice. To this end, we did microCT analysis of 16 months old male proximal tibia samples. As shown in Figure III-9, the wildtype and knockout animals showed similar bone volume percentage. We thus concluded that Fbxl15 loss of function does not significantly affect bone

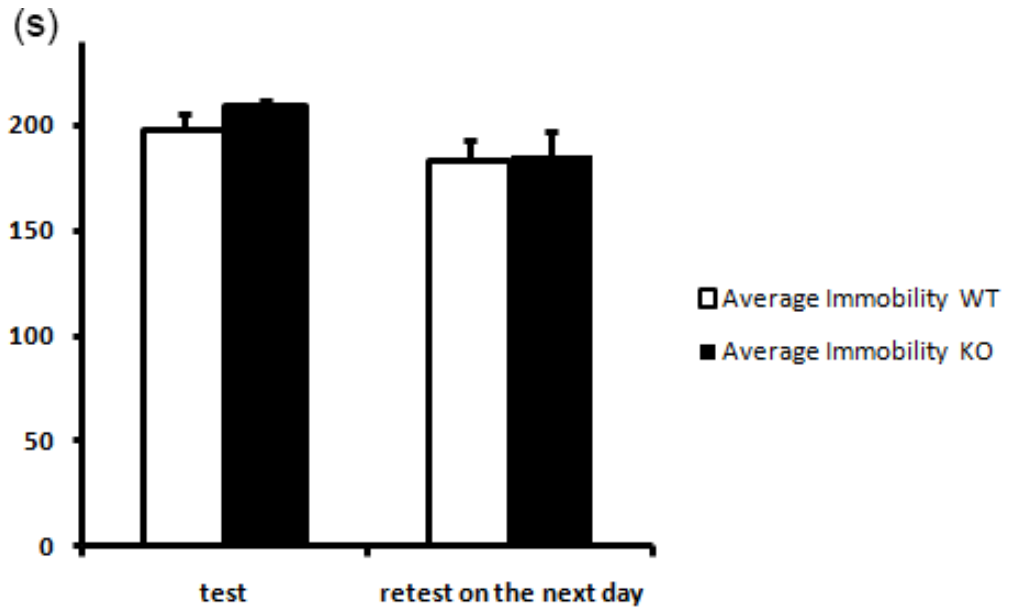

Figure III-7. Forced swim test shows that Fbxl15$^{-/-}$ mice render similar depressive-like performance as wildtype mice. Mice were placed inside a glass cylinder from which they cannot escape for 4 minutes, during which the immobility (defined as showing no movements beyond those required to keep its head above water) time was measured. N=8 for wildtype and N=7 for knockout. Error bars show SEM. No significant difference between genotypes is seen.

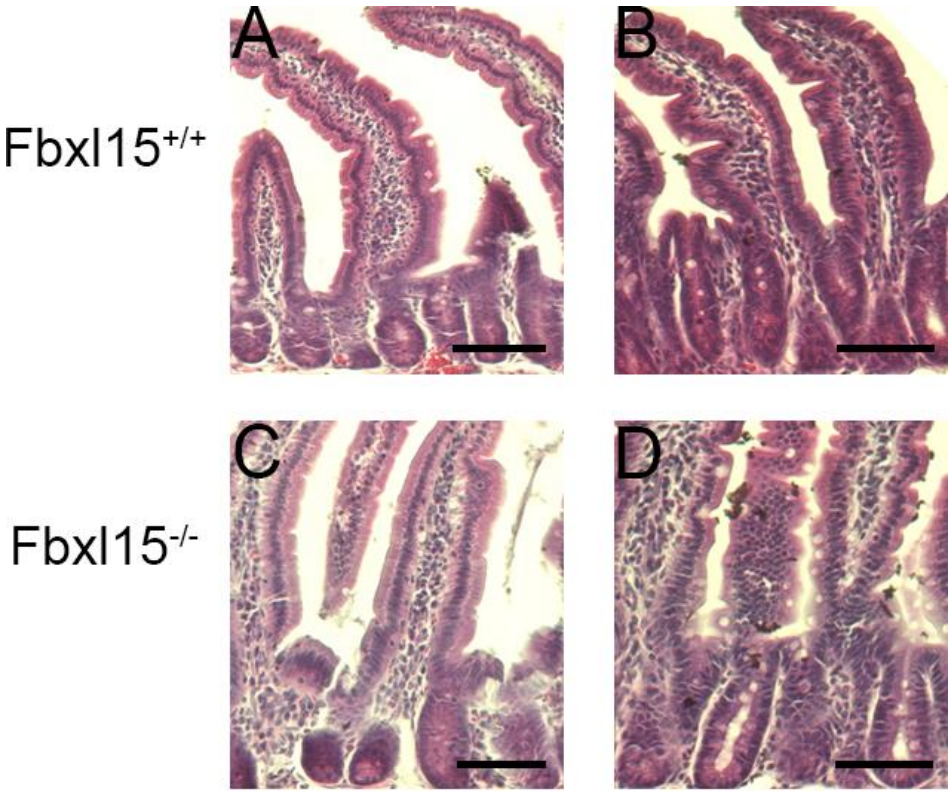

Figure III-8. H&E staining shows that intestinal morphology appears to be normal in Fbxl15$^{-/-}$ mice. A and B, example wildtype sections. C and D, example knockout sections. No obvious difference in terms of general morphology is observed.

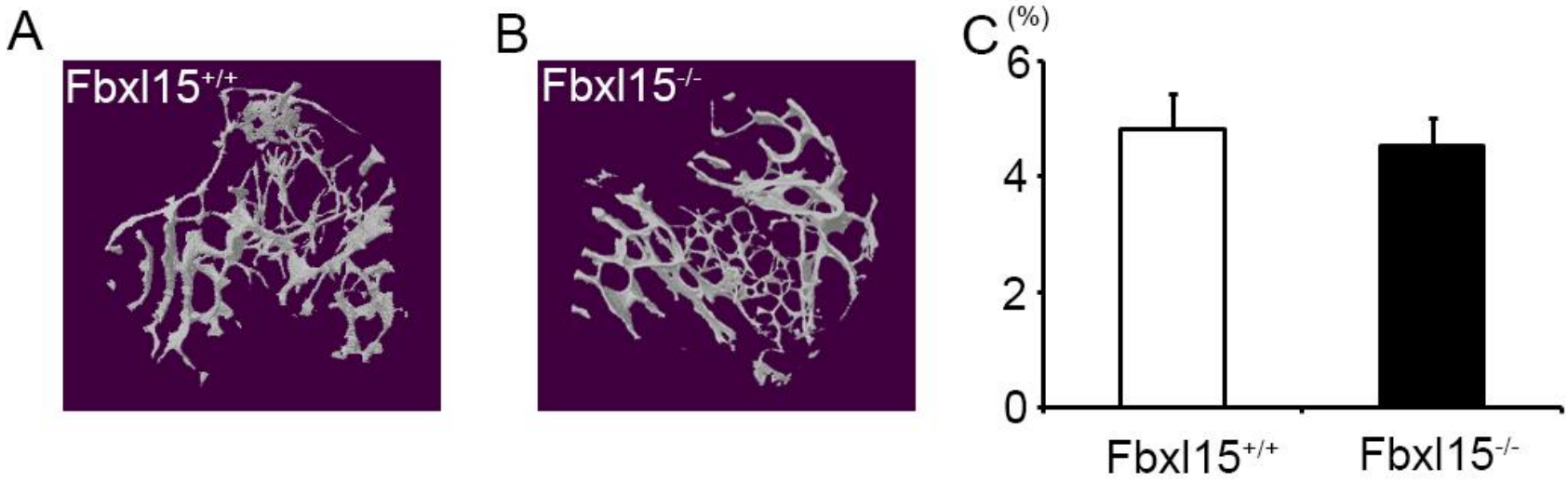

Figure III-9. MicroCT analysis of the trabecular bone at the proximal tibia of Fbxl15$^{-/-}$ mice shows similar bone volume percentage compared to wildtype. A, example 3D reconstruction of trabecular bone structure of a wildtype mouse. B, same as A, but for a knockout mouse. C, bone volume percentage was analyzed and compared between genotypes. No significant difference is seen. N=5 per group.

development or bone homeostasis.

Discussion

After various attempts to address the physiological function of Fbxl15 using Fbxl15 knockout mice, we failed to detect any significant behavioral phenotypes or developmental phenotypes in gastrointestinal morphology, bone morphology, and bone mass homeostasis. Therefore, the function of this protein could possibly be redundant in mouse, or that the loss of function of this protein could potentially be compensated by other members of the F-box protein family (Kipreos & Pagano, 2000). For instance, Fbxo3, another member from the F-box protein family, has recently been reported to target Smurf1 for ubiquitination and degradation (Li et al., 2015), thus sharing the same target with Fbxl15 (Cui et al., 2011). It could well be that Fbxo3 serves to compensate for part of the function of Fbxl15 when Fbxl15 is absent, and that a double knockout of Fbxl15 and Fbxo3 might be helpful in addressing the physiological function of these two proteins.

On the other hand, the substrates of Fbxl15 might not be limited to Smurf1, and that a proteomic approach for analysis of $Fbxl15^{-/-}$ tissue samples might be useful to identify other potential targets that might be affected by Fbxl15 deletion.

MATERIALS AND METHODS

Section I methods

Mouse strains and cuprizone administration

Animal care and use in this study was performed in accordance with Rutgers University Institutional Animal Care and Use Committee (IACUC) standards (approval number 93-052). CD1 mice were purchased directly from Charles River Laboratories (strain code 022) and C57BL/6J mice were purchased from the Jackson Laboratory (stock No. 000664). Both strains of mice were purchased at 8 weeks of age and kept in a pathogen-free facility. Mice were allowed one week of acclimation to the environment upon arrival, and then fed with a 0.2% cuprizone-containing diet (Catalog No. TD.01453, Envigo) or a control diet without cuprizone (Catalog No. TD.00217, Envigo). Feeding was ad libitum for a duration ranging from 4 to 7 weeks. For analysis of cuprizone-containing diet intake, both body weights (recorded 3 times weekly) and food consumption (recorded daily) were closely monitored.

Tissue sample preparation

For histology and immunohistochemistry, mice were deeply anesthetized by ketamine (Henry Schein, Melville, NY) injection, and transcardially perfused with saline and then with 4% Paraformaldehyde (PFA) solution. Mouse brains were then collected and placed in 4% PFA solution for overnight fixation, followed by incubation in 30% sucrose containing phosphate buffered saline (PBS) for cryoprotection. Mouse brains were then frozen in O.C.T. (VWR, Radnor, PA) and cut

at 14 μm thickness with a cryostat (Leica, Buffalo Grove, IL). Coronal brain sections were collected focusing on the corpus callosum above the fornix, which is approximately between bregma -0.58 mm and -0.82 mm (The Mouse Brain In Sterotaxic Coordinates(Franklin, 1997)) (Fig I-1A). For any of the subsequent analyses, including histology and immunohistochemistry, at least 3 sections were stained per mouse and the average luxol fast blue myelin scoring or cell count/mm2 was taken to represent a single mouse.

For western blot analysis, mice were sacrificed by cervical dislocation and mouse brains were collected and placed in a 1 mm brain matrix (Alto Acrylic). A 2 mm section of the corpus callosum tissue overlying the fornix (approximately between bregma 0.14 mm and -1.86 mm) was dissected out and frozen at -80°C. Lysis of the tissue was carried out by homogenizing in diluted NP40 Cell Lysis buffer (ThermoFisher, Bridgewater, NJ) in the presence of protease inhibitor cocktail (1:200, Sigma, St. Louis, MO) and protein concentration was quantified using a BCA protein assay kit (Pierce, Waltham, MA).

Black gold staining and Luxol fast blue–periodic acid Schiff (LFB–PAS) stain

Black gold stain was carried out using Black-Gold II compound (Histo-Chem, Jefferson, AR) following the manufacturer’s instructions. LFB staining was carried out using LUXOL FAST BLUE - PAS kit (Hitobiotec, Kingsport, TN) following the manufacturer’s instructions followed by PAS counterstaining with a PAS kit (Sigma, St. Louis, MO). Sections were eventually dehydrated with graded ethanol and mounted with permount (Fisher Scientific, Waltham, MA). Images of the midline of

the corpus callosum were taken using Virtual Slide microscope 120 (Olympus, Center Valley, PA). For analysis, the sections were scored blind on a scale of 0-3 (Fig I-9) by judging the relative intensity of blue (myelin content) and pink (demyelinated area).

Immunohistochemistry

For visualization of mature oligodendrocytes, sections were boiled in citrate buffer solution for antigen retrieval, followed by one hour blocking in PBS solution containing 10% goat serum and 0.3% Triton and incubated overnight with glutathione S-transferase Pi (GST-π) antibody (Enzo Life Sciences, Farmingdale, NY) at 4°C. Sections were then rinsed in PBS for washing and further incubated for 3 hours in fluorescent secondary antibody (Alexa Fluor Goat anti Rabbit 543, ThermoFisher, 1:200) and to-pro-3 (1:1000, Thermo Fisher) for nuclear stain.

For visualization of oligodendrocyte progenitor cells (OPCs), sections were blocked with 30% goat serum/0.3% triton in PBS for one hour, followed by overnight incubation with NG2 antibody (1:750, Millipore, Billerica, MA) at 4°C. After rinsing in PBS, sections were then incubated with Alexa Fluor goat-anti-rabbit secondary antibody (1:200, Thermo Fisher) together with to-pro-3 for nuclear stain.

For visualization of microglia/macrophages, sections were blocked with 5% goat serum and 0.3% Triton in PBS for one hour, followed by overnight incubation at 4°C in rabbit-anti-Iba1 (1:500, Wako, Richmond, VA). After rinsing in PBS, secondary antibody incubation was carried out using Alexa Fluor goat-anti-rabbit 488 (1:200, Thermo Fisher). To-pro-3 was also added for nuclear stain (1:1000, Thermo Fisher).

For visualization of astrocytes, sections were boiled in citrate buffer solution for antigen retrieval, followed by blocking in 0.1% Triton/2% goat serum containing PBS for one hour. Glial fibrillary acidic protein (GFAP) antibody (1:200, ThermoFisher) was used as primary antibody for overnight incubation at 4°C. After rinsing (3 x 5 min) in PBS, secondary antibody incubation was carried out using Alexa Fluor goat-anti-rat 488 (1:400, ThermoFisher) together with to-pro-3 for nuclear stain.

Finally, slides mounted with clear-mount (Electron Microscopy Sciences, Hatfield, PA) were examined and fluorescence images of the midline of the corpus callosum were taken using a three-channel confocal microscope system (Eclipse C1, Nikon, Melville, NY). For cell counting, positively stained cells are identified by antibody-to-pro-3 colocalization (Fig I-10).

Western blot

For analysis of myelin basic protein (MBP), myelin-associated glycoprotein (MAG), ionized calcium-binding adapter molecule 1 (Iba1) and Glial fibrillary acidic protein (GFAP) levels, both CD1 and C57BL/6 tissue lysates (6 μg) were combined with 5x Laemmli loading buffer containing 0.1% bromophenol blue, 7.7% Dithiothreitol (DTT), 10% SDS, 50% Glycerol and 60 mM Tris-Cl (pH 6.8). Samples were denatured by boiling and then loaded (6 μg/lane) and analyzed in a 12% acrylamide protein gel. Upon completion of gel electrophoresis, protein was wet transferred onto 0.45 μm nitrocellulose membrane (bio rad), followed by blocking in 5% BSA solution and incubation at 4°C overnight with primary antibodies against MBP (mouse-anti-MBP, 1:200, Serotec, Hercules, CA), MAG (rabbit-anti-MAG,

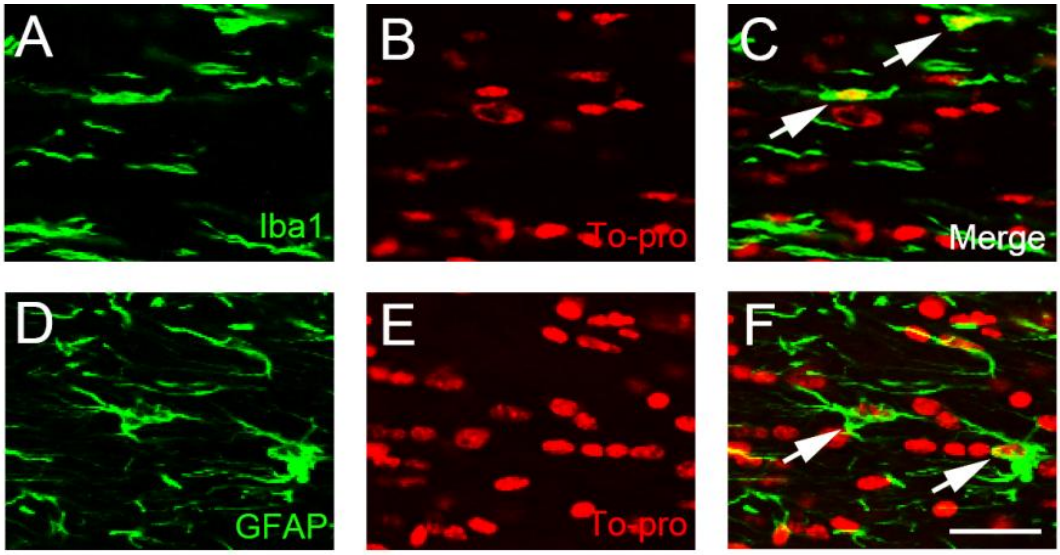

Figure I-10. Examples of positively stained cells. A-C, Example images of Iba1+ cells. A, Iba1 fluorescence. B, To-pro-3. C, overlaid image. Arrows point to Iba1+ cells, which show colocalization of Iba1 fluorescence and nuclear to-pro. D-F, same as A-C, but for GFAP staining. Scale bar, 30 μm.

1:1000, Santa Cruz, Dallas, TX), Iba1 (rabbit-anti-Iba1, 1:1000, Wako), GFAP (rabbit-anti-GFAP, 1:10000, Abcam, Cambridge, MA) and beta-tubulin (mouse-anti-beta-tubulin, 1:5000, Sigma) for loading control. After washing, fluorescent secondary antibody (Li-cor goat-anti-mouse IRDye 680 for MBP and beta-tubulin and Li-cor goat-anti-rabbit IRDye 800 for Iba1, GFAP and MAG) incubation was performed for one hour at room temperature, followed by detection of fluorescence signal using odyssey imaging system (Li-cor, Lincoln, NE).

For analysis of NG2 protein levels, 10 μg of protein samples were loaded and run in a 6% acrylamide protein gel. Primary antibody (Rabbit-anti-NG2, 1:1000, Millipore) and secondary antibody (HRP-linked anti-Rabbit IgG, 1:5000, Cell signaling, Danvers, MA) incubation was performed similarly, and detection of chemiluminescence signal was performed using ECL prime reagent (GE healthcare) and GeneGnomeXRQ imaging system (Syngene, Frederick, MD).

Statistical analysis

Statistical differences between the group data of C57BL/6 and CD1 mice were analyzed using either unpaired student's t-test or two-way ANOVA analysis where appropriate. Statistical differences between cuprizone treated and control groups within individual strains were analyzed using student's t-test. Differences were considered to be significant at $p<0.05$ and data are presented as the mean ±standard error of the mean.

Section II methods

Ephrin-B3 mutant animals

Ephrin-B3^{LacZ} and Ephrin-B3^{Neo} mutant mice were previously described (Yokoyama et al., 2001), and are both from CD1 background. For analysis of Ephrin-B3^{Neo} mutants, Ephrin-B3$^{+/Neo}$ mice were backcrossed into pure C57BL/6 background for 3-4 generations, and mice carrying the Ephrin-B3^{Neo} allele were selected for the Black gold staining analysis of myelin, as well as for the cuprizone experiment.

LacZ staining

The protocol for LacZ staining was described previously (Cooper, Crockett, Nowakowski, Gale, & Zhou, 2009). In brief, brains from adult Ephrin-B3$^{+/LacZ}$ mice were freshly dissected, embedded in Tissue-tek O.C.T. Compound (Sakura Finetek, Torrance, CA) and frozen in dry ice. Coronal sections of 30 μm were cut using a Leica cryostat. Sections were then lightly fixed with 2% paraformaldehyde/0.5% glutaraldehyde solution in phosphate buffered saline (PBS) for 5 minutes, before an 18 hour reaction with 5-bromo-4-chloro-3-indoly-β-D-galactopyranoside (X-gal). The X-gal working solution is at 1 mg/mL X-gal concentration with 5 mM potassium ferricyanide, 5 mM potassium ferrocyanide, 2 mM magnesium chloride, 0.01% sodium deoxycholate, and 0.02% NP-40. After the reaction, sections were subsequently dehydrated in graded ethanol and eventually placed in xylene and

mounted with permount (Sigma).

LFB-cresyl violet staining

LFB-cresyl violet staining was carried out using the Luxol Fast Blue Stain Kit purchased from IHC world, and following the manufacturer's instructions. In brief, tissue sections were incubated in Luxol Fast Blue Solution at 56 ℃ in an oven for overnight, followed by rinsing in 95% alcohol. Differentiation was carried out by incubating sections in Lithium Carbonate solution for 30 seconds, followed by washing in 70% ethanol for another 30 seconds. This differentiation was repeated for multiple cycles and continuously monitored under a light microscope, until the background staining was mostly transparent. When differentiation was complete, sections were counterstained in Cresyl Violet Solution for 1 minute and 30 seconds, followed by washing, dehydration in graded ethanol and mounting using permount (Thermo Fisher).

Section III methods

The generation of Fbxl15$^{-/-}$ mice

Embryonic stem cell (ES cell) carrying Fbxl15 deletion was purchased from KOMP (knockout mouse project, website https://www.komp.org, project ID number CSD67768). Injection of ES cells into mouse embryos generated chimeras, and that mating of chimeras subsequently generated progenies that were screened by PCR

(shared forward primer 5’-cttcctgacaaggattctcagtga-3’, reverse primer for wild type allele 5’-tcgccaagtgcagctga-3’, reverse primer for knockout allele 5’-gtggtatggttatgcgccttagtc-3’). Two progenies heterozygous for Fbxl15 deletion was identified, and one of them was subsequently used to derive the entire Fbxl15 knockout colony. All mice used were on pure C57BL/6 background.

Circadian wheel running experiment

Two months old adult male $Fbxl15^{+/+}$ and $Fbxl15^{-/-}$ mice were placed in wheel running set up (Coulbourn) (one mouse per cage) including wheel running cages and a clocklab 56-channel interface and software. The number of wheel running cycles was recorded in real time by the Clocklab toolbox that runs in MATLAB. The mice were first allowed two weeks of acclimation to the running wheel cages and room conditions, after which the lights are turned off for a 24 hour-constant darkness free running test. Tau analysis and bout analysis were performed using two weeks of free running data, and all analyses were performed using the Clocklab installment within MATLAB.

Elevated plus maze (EPM)

The EPM apparatus was previously described (Sheleg et al., 2017). Briefly, mice were brought into a dimly lit test room and left there for acclimation for half an hour, after which they were taken out of their home cage and placed on the center junction of a four-arm black Plexiglas maze that is elevated 30 cm above the floor,

facing one of the closed arms, which were 65 cm in length and had 8 cm high black Plexiglas walls. The open arms, however, were 30 cm in length and devoid of such walls. The test started when the mouse was released at the center and lasted 5 minutes. The whole experiment was videotaped and an observer recorded the time that the mouse spent in the open arms and closed arms, as well as the number of entries the mouse made into the open and closed arms. The ratio of time spent exploring the open arm and the ratio of entries into the open arms over the total number of entries into open or closed arms served as a parameter of anxiety. The total number of entries serves as a measurement of general locomotor activity. The criteria for an entry to either an open or a closed arm is that all four paws has to be placed into the arm. A total of 7 knockout mice and 8 wildtype littermates were tested.

Light-dark box test (LDB)

The LDB apparatus was previously described (Rossi-George, LeBlanc, Kaneta, Urbach, & Kusnecov, 2004). Briefly, the Plexiglas light-dark box ($47\times24\times21 cm^3$, L×W×H) consisted of two compartments, one black walled and opaque, while the other had transparent walls and had a 20 W light bulb hanging from the ceiling. The two compartments were separated by a wooden wall with a 4×5 cm^2 opening that served as the passage between the two compartments. Before the test, mice (7 $Fbxl15^{-/-}$ and 8 $Fbxl15^{+/+}$ littermates) were brought into the test room for acclimation for half an hour, after which they were individually taken from their home cage and placed in the dark box and were allowed a 5 minute period to freely explore the enclosure. The entire experiment was videotaped and that the latency to emerge from

the dark compartment into the light, the number of entries the mouse made into the light compartment, as well as the total time spent in the light compartment was recorded and used as a measure of anxiety. The criteria for an entry or emerge is that all four paws of the animal has to pass the midline.

Water maze test

The testing apparatus for the water maze was described previously (Woodruff, Schorpp, Lawrenczyk, Chakraborty, & Kusnecov, 2011). Briefly, the water maze pool was a steel circular tub (110 cm in diameter and 59 cm in height) and was filled with tap water and adjusted to approximately 22°C and made opaque with nontoxic white paint. The escape platform consisted of a clear circular Plexiglas plate perforated with small holes that helped the mouse gain stability by grabbing on to them once it reaches the platform. The platform was 1 cm below the water surface and mounted on top of a steel rod affixed to a heavy metal base which was movable to allow different platform locations for the test. A white canvas curtain surrounds the pool and extends from the floor to the ceiling, separating the pool and the experimenter during the trials. The interior of the curtain was decorated by various cues of different cues and sizes to provide spatial cues for orientation for the swimming animal. The curtain also had an opening that allowed the experimenter to place and retrieve the animal from the pool. The entire trials were video-recorded by on overhead camera hanging from the ceiling and above the center of the pool and displayed in real time on a display screen outside of the curtain, where the experimenter monitored the animal's behavior and timed the latency to find the platform with a stopwatch. For the probe trials, the platform was

removed from the pool, and the videotapes were post-processed by a video-tracking software (SMART-Spontaneous Motor Activity Recording & Tracking; San Diego Instruments, San Diego) to determine the percentage of time spend in each quadrant during the 1 minute test.

During the first two days of visible platform training (Fig III-4A, visible days), the platform location was indicated by a circular mini-flag that was readily visible to the swimming animal. A total of 4 trials were performed with each animal and a maximum of 1 minute was allowed for each trial with an approximate 5 minutes intertrial interval. The latency to reach the platform was recorded and, if the animal failed to reach to platform, a latency of 60 s was recorded and the animal was then manually retrieved from the water and place onto the platform.

For the testing during invisible days (Fig III-4A, invisible days), the cue flag was removed, and the location of the platform was changed to novel locations which is randomized for individual mice. These locations for respective mice were then remained constant throughout the rest of the test. Other procedures were similar to the visible days, including 4 trials per day and approximately 5 minutes intertrial interval. The test lasted until all mice had memorized the location of the platform, after which the probe trial was performed for only once.

Rotarod performance test

The rotarod apparatus consisted of a steel cylinder covered with cardboard paper roll and mounted onto a rotating pump (Masterflex) from which its rotation was driven. The angular velocity was set to 12 rpm and while the mouse was placed onto

the rotating rod, two plastic circular disks from either side which rotates together with the rotarod keeps the animal from turning around, forcing it to perform a treadmill-like walking on the rod while trying to maintain balance. A circular plexiglass bowl filled with soft bedding material was placed underneath the rotarod in order to catch the animal once it falls off. A maximum of 90 s was allowed for each trial and the latency to fall off was recorded using a stopwatch. 3 trials were performed on each day of testing and an approximate 15 minutes intertrial interval separates the trials.

Forced swim test

The forced swim test was performed using a transparent glass cylinder (18 cm in diameter) of water filled up to 30 cm in depth. Mice were gently placed into the cylinder individually and its behavior was videotaped in front of a camera for 4 minutes, and time of immobility, which is defined as exhibiting no movements beyond those required to keep afloat was recorded using a stopwatch. Only one trial per mouse was performed on the first day, and another trial was performed for each mouse on the following day.

Preparation of intestinal samples and H&E stain

Two months old Fbxl15$^{+/+}$ and Fbxl15$^{-/-}$ mice were sacrificed by cervical dislocation and their intestine was dissected out and washed in PBS. The intestine was then sectioned with a pair of scissors into four parts, corresponding to duodenum,

jejunum, ileum and colon, respectively. The intestines were subsequently flushed with PBS, cut open, and then gently rolled using a tooth pick to form a Swiss roll. The Swiss roll was transferred into a tissue processing cassette (VWR) and immersed in 10% formalin for overnight, followed by dehydration in gradient ethanol, xylene, and eventually imbedded in wax.

After collecting sections of the imbedded Swiss roll using a microtome (Leica), slides were dewaxed by heating at 55 degrees for 15 minutes followed by rinsing in xyline and then rehydrated in gradient ethanol. After washing in water for 5 minutes, slides were incubated in the Mayer's Hematoxylin solution (Sigma) for exactly 1 min, followed by washing in running tap water for 15 minutes. The slides were briefly tapped dry and then dipped in Eosin solution (Sigma), followed by tap water washing and dehydration via gradient ethanol. The slides were then transferred into xylene solution and mounted by Permount (Fisher Scientific).

MicroCT analysis of trabacular bone tissue

We used micro-computed tomography (Skyscan 1172 high-resolution micro-CT, Rutgers Robert Wood Johnson Medical School core facility) to analyze bone volume percentage of the trabecular bone at the proximal tibia. Mice were sacrificed by cervical dislocation, and the tibia was removed and stored in 70% ethanol temporarily and later transferred into a scanning tube containing saline solution before the CT scan. The scanning pixel size was set to 5 μm and after 3D reconstruction of the scanned images, Skyscan CTan software was used to select the region of interest (ROI) of trabular bone, which we define as commencing 220 μm from the growth plate level

in the direction of the metaphysic, and extending a further 1 mm. Within the ROI, a circular contour was manually drawn to outline the trabular region, and a three dimensional batch analysis was performed within the CTan software to measure bone volume fraction (bone volume over tissue volume).

REFERENCES

Aboul-Enein, F., Rauschka, H., Kornek, B., Stadelmann, C., Stefferl, A., Bruck, W., . . . Lassmann, H. (2003). Preferential loss of myelin-associated glycoprotein reflects hypoxia-like white matter damage in stroke and inflammatory brain diseases. *J Neuropathol Exp Neurol, 62*(1), 25-33.

Acs, P., & Komoly, S. (2012). Selective ultrastructural vulnerability in the cuprizone-induced experimental demyelination. *Ideggyogy Sz, 65*(7-8), 266-270.

Acs, P., Selak, M. A., Komoly, S., & Kalman, B. (2013). Distribution of oligodendrocyte loss and mitochondrial toxicity in the cuprizone-induced experimental demyelination model. *J Neuroimmunol, 262*(1-2), 128-131. doi: 10.1016/j.jneuroim.2013.06.012

Antion, M. D., Christie, L. A., Bond, A. M., Dalva, M. B., & Contractor, A. (2010). Ephrin-B3 regulates glutamate receptor signaling at hippocampal synapses. *Molecular and Cellular Neuroscience, 45*(4), 378-388. doi: https://doi.org/10.1016/j.mcn.2010.07.011

Armstrong, J. N., Saganich, M. J., Xu, N.-J., Henkemeyer, M., Heinemann, S. F., & Contractor, A. (2006). B-Ephrin Reverse Signaling Is Required for NMDA-Independent Long-Term Potentiation of Mossy Fibers in the Hippocampus. *The Journal of Neuroscience, 26*(13), 3474-3481. doi: 10.1523/jneurosci.4338-05.2006

Arnett, H. A., Wang, Y., Matsushima, G. K., Suzuki, K., & Ting, J. P. (2003). Functional genomic analysis of remyelination reveals importance of inflammation in oligodendrocyte regeneration. *J Neurosci, 23*(30), 9824-9832.

Asano, M., Wakabayashi, T., Ishikawa, K., & Kishimoto, H. (1978). Mechanism of the formation of megamitochondria by copper-chelating agents. IV. Role of fusion phenomenon in the cuprizone-induced megamitochondrial formation. *Acta Pathol Jpn, 28*(2), 205-213.

Barres, B. A., Koroshetz, W. J., Swartz, K. J., Chun, L. L., & Corey, D. P. (1990). Ion channel expression by white matter glia: the O-2A glial progenitor cell. *Neuron, 4*(4), 507-524.

Barres, B. A., & Raff, M. C. (1993). Proliferation of oligodendrocyte precursor cells depends on electrical activity in axons. *Nature, 361*, 258. doi: 10.1038/361258a0

Bauer, J., Bradl, M., Klein, M., Leisser, M., Deckwerth, T. L., Wekerle, H., & Lassmann, H. (2002). Endoplasmic reticulum stress in PLP-overexpressing transgenic rats: gray matter oligodendrocytes are more vulnerable than white matter oligodendrocytes. *J Neuropathol Exp Neurol, 61*(1), 12-22.

Benetti, F., Ventura, M., Salmini, B., Ceola, S., Carbonera, D., Mammi, S., . . . Spisni, E. (2010). Cuprizone neurotoxicity, copper deficiency and neurodegeneration. *Neurotoxicology, 31*(5), 509-517. doi: 10.1016/j.neuro.2010.05.008

Bengtsson, S. L., Nagy, Z., Skare, S., Forsman, L., Forssberg, H., & Ullen, F. (2005). Extensive piano practicing has regionally specific effects on white matter development. *Nat Neurosci, 8*(9), 1148-1150. doi: 10.1038/nn1516

Benson, M. D., Romero, M. I., Lush, M. E., Lu, Q. R., Henkemeyer, M., & Parada, L. F. (2005). Ephrin-B3 is a myelin-based inhibitor of neurite outgrowth. *Proc Natl Acad Sci U S A, 102*(30), 10694-10699. doi: 10.1073/pnas.0504021102

Bergles, D. E., Roberts, J. D., Somogyi, P., & Jahr, C. E. (2000). Glutamatergic synapses on oligodendrocyte precursor cells in the hippocampus. *Nature, 405*(6783), 187-191. doi: 10.1038/35012083

Biancotti, J. C., Kumar, S., & de Vellis, J. (2008). Activation of inflammatory response by a combination of growth factors in cuprizone-induced demyelinated brain leads to myelin repair. *Neurochem Res, 33*(12), 2615-2628. doi: 10.1007/s11064-008-9792-8

Blakemore, W. F. (1972). Observations on oligodendrocyte degeneration, the resolution of status spongiosus and remyelination in cuprizone intoxication in mice. *Journal of Neurocytology, 1*(4), 413-426. doi: 10.1007/bf01102943

Bourin, M., & Hascoet, M. (2003). The mouse light/dark box test. *Eur J Pharmacol, 463*(1-3), 55-65.

Bradl, M., & Lassmann, H. (2010). Oligodendrocytes: biology and pathology. *Acta Neuropathol, 119*(1), 37-53. doi: 10.1007/s00401-009-0601-5

Bradl, M., & Lassmann, H. (2010). Oligodendrocytes: biology and pathology. *Acta Neuropathol, 119*(1), 37-53. doi: 10.1007/s00401-009-0601-5

Brogi, A., Strazza, M., Melli, M., & Costantino-Ceccarini, E. (1997). Induction of intracellular ceramide by interleukin-1 beta in oligodendrocytes. *J Cell Biochem, 66*(4), 532-541.

Brosnan, C. F., Stoner, G. L., Bloom, B. R., & Wisniewski, H. M. (1977). Studies on demyelination by activated lymphocytes in the rabbit eye. II. Antibody-dependent cell-mediated demyelination. *J Immunol, 118*(6), 2103-2110.

Busino, L., Bassermann, F., Maiolica, A., Lee, C., Nolan, P. M., Godinho, S. I., . . . Pagano, M. (2007). SCFFbxl3 controls the oscillation of the circadian clock by directing the degradation of cryptochrome proteins. *Science, 316*(5826), 900-904. doi: 10.1126/science.1141194

Cahoy, J. D., Emery, B., Kaushal, A., Foo, L. C., Zamanian, J. L., Christopherson, K. S., . . . Barres, B. A. (2008). A transcriptome database for astrocytes, neurons, and oligodendrocytes: a new resource for understanding brain development and function. *J Neurosci, 28*(1), 264-278. doi: 10.1523/jneurosci.4178-07.2008

Cammer, W., & Zhang, H. (1993). Atypical localization of the oligodendrocytic isoform (PI) of glutathione-S-transferase in astrocytes during cuprizone intoxication. *J Neurosci Res, 36*(2), 183-190. doi: 10.1002/jnr.490360208

Capello, E., & Mancardi, G. L. (2004). Marburg type and Balo's concentric sclerosis: rare and acute variants of multiple sclerosis. *Neurol Sci, 25 Suppl 4*, S361-363.

Carlton, W. W. (1966). Response of mice to the chelating agents sodium diethyldithiocarbamate, α-benzoinoxime, and biscyclohexanone oxaldihydrazone. *Toxicol Appl Pharmacol, 8*(3), 512-521.

Charles, P., Hernandez, M. P., Stankoff, B., Aigrot, M. S., Colin, C., Rougon, G., . . . Lubetzki, C. (2000). Negative regulation of central nervous system myelination by polysialylated-neural cell adhesion molecule. *Proceedings of the National Academy of Sciences, 97*(13), 7585-7590. doi: 10.1073/pnas.100076197

Chen, L. P., Li, Z. F., Ping, M., Li, R., Liu, J., Xie, X. H., . . . Guo, L. (2012). Regulation of Olig2 during astroglial differentiation in the subventricular zone of a cuprizone-induced demyelination mouse model. *Neuroscience, 221*, 96-107. doi: http://dx.doi.org/10.1016/j.neuroscience.2012.06.063

Chen, M.-K., & Guilarte, T. s. R. (2006). Imaging the Peripheral Benzodiazepine

Receptor Response in Central Nervous System Demyelination and Remyelination. *Toxicological Sciences, 91*(2), 532-539. doi: 10.1093/toxsci/kfj172

Chen, Y., Wu, H., Wang, S., Koito, H., Li, J., Ye, F., . . . Lu, Q. R. (2009). The oligodendrocyte-specific G protein-coupled receptor GPR17 is a cell-intrinsic timer of myelination. *Nat Neurosci, 12*(11), 1398-1406. doi: 10.1038/nn.2410

Cheng, N., Brantley, D. M., & Chen, J. (2002). The ephrins and Eph receptors in angiogenesis. *Cytokine & Growth Factor Reviews, 13*(1), 75-85. doi: http://dx.doi.org/10.1016/S1359-6101(01)00031-4

Connor, J. R., & Menzies, S. L. (1996). Relationship of iron to oligodendrocytes and myelination. *Glia, 17*(2), 83-93. doi: 10.1002/(SICI)1098-1136(199606)17:2<83::AID-GLIA1>3.0.CO;2-7

Cooper, M. A., Crockett, D. P., Nowakowski, R. S., Gale, N. W., & Zhou, R. (2009). Distribution of EphA5 receptor protein in the developing and adult mouse nervous system. *J Comp Neurol, 514*(4), 310-328. doi: 10.1002/cne.22030

Cui, Y., He, S., Xing, C., Lu, K., Wang, J., Xing, G., . . . Zhang, L. (2011). SCFFBXL(1)(5) regulates BMP signalling by directing the degradation of HECT-type ubiquitin ligase Smurf1. *Embo j, 30*(13), 2675-2689. doi: 10.1038/emboj.2011.155

Dardente, H., Mendoza, J., Fustin, J. M., Challet, E., & Hazlerigg, D. G. (2008). Implication of the F-Box Protein FBXL21 in circadian pacemaker function in mammals. *PLoS One, 3*(10), e3530. doi: 10.1371/journal.pone.0003530

De Biase, L. M., Nishiyama, A., & Bergles, D. E. (2010). Excitability and synaptic communication within the oligodendrocyte lineage. *J Neurosci, 30*(10), 3600-3611. doi: 10.1523/jneurosci.6000-09.2010

de Castro, F., & Bribian, A. (2005). The molecular orchestra of the migration of oligodendrocyte precursors during development. *Brain Res Brain Res Rev, 49*(2), 227-241. doi: 10.1016/j.brainresrev.2004.12.034

Demerens, C., Stankoff, B., Logak, M., Anglade, P., Allinquant, B., Couraud, F., . . . Lubetzki, C. (1996). Induction of myelination in the central nervous system by electrical activity. *Proc Natl Acad Sci U S A, 93*(18), 9887-9892.

Doeppner, T. R., Bretschneider, E., Doehring, M., Segura, I., Sentürk, A., Acker-Palmer, A., . . . Bähr, M. (2011). Enhancement of endogenous neurogenesis in ephrin-B3 deficient mice after transient focal cerebral ischemia. *Acta Neuropathol, 122*(4), 429. doi: 10.1007/s00401-011-0856-5

Dugas, J. C., Cuellar, T. L., Scholze, A., Ason, B., Ibrahim, A., Emery, B., . . . Barres, B. A. (2010). Dicer1 and miR-219 Are required for normal oligodendrocyte differentiation and myelination. *Neuron, 65*(5), 597-611. doi: 10.1016/j.neuron.2010.01.027

Egea, J., & Klein, R. (2007). Bidirectional Eph–ephrin signaling during axon guidance. *Trends in Cell Biology, 17*(5), 230-238. doi: http://dx.doi.org/10.1016/j.tcb.2007.03.004

Emery, B. (2010). Regulation of oligodendrocyte differentiation and myelination. *Science, 330*(6005), 779-782. doi: 10.1126/science.1190927

Emery, B. (2010). Regulation of Oligodendrocyte Differentiation and Myelination. *Science, 330*(6005), 779-782. doi: 10.1126/science.1190927

Emery, B., Agalliu, D., Cahoy, J. D., Watkins, T. A., Dugas, J. C., Mulinyawe, S. B., . . . Barres, B. A. (2009). Myelin gene regulatory factor is a critical transcriptional regulator required for CNS myelination. *Cell, 138*(1), 172-185. doi: 10.1016/j.cell.2009.04.031

Eph Nomenclature, C. (1997). Unified Nomenclature for Eph Family Receptors and Their Ligands, the Ephrins. *Cell, 90*(3), 403-404. doi: http://dx.doi.org/10.1016/S0092-8674(00)80500-0

Fancy, S. P., Baranzini, S. E., Zhao, C., Yuk, D. I., Irvine, K. A., Kaing, S., . . . Rowitch, D. H. (2009). Dysregulation of the Wnt pathway inhibits timely myelination and remyelination in the mammalian CNS. *Genes Dev, 23*(13), 1571-1585. doi: 10.1101/gad.1806309

Fields, R. D. (2005). Myelination: an overlooked mechanism of synaptic plasticity? *Neuroscientist, 11*(6), 528-531. doi: 10.1177/1073858405282304

Franco-Pons, N., Torrente, M., Colomina, M. T., & Vilella, E. (2007). Behavioral deficits in the cuprizone-induced murine model of demyelination/remyelination. *Toxicol Lett, 169*(3), 205-213. doi: 10.1016/j.toxlet.2007.01.010

Franklin, K. B. J. (1997). *The mouse brain in stereotaxic coordinates / Keith B.J. Franklin, George Paxinos*. San Diego: Academic Press.

Frohman, E. M., Racke, M. K., & Raine, C. S. (2006). Multiple sclerosis--the plaque and its pathogenesis. *N Engl J Med, 354*(9), 942-955. doi: 10.1056/NEJMra052130

Frost, E., Kiernan, B. W., Faissner, A., & ffrench-Constant, C. (1996). Regulation of oligodendrocyte precursor migration by extracellular matrix: evidence for substrate-specific inhibition of migration by tenascin-C. *Dev Neurosci, 18*(4), 266-273.

Fu, H., Cai, J., Clevers, H., Fast, E., Gray, S., Greenberg, R., . . . Stiles, C. D. (2009). A Genome-Wide Screen for Spatially Restricted Expression Patterns Identifies Transcription Factors That Regulate Glial Development. *The Journal of Neuroscience, 29*(36), 11399-11408. doi: 10.1523/jneurosci.0160-09.2009

Fulmer, C. G., VonDran, M. W., Stillman, A. A., Huang, Y., Hempstead, B. L., & Dreyfus, C. F. (2014). Astrocyte-Derived BDNF Supports Myelin Protein Synthesis after Cuprizone-Induced Demyelination. *The Journal of Neuroscience, 34*(24), 8186-8196. doi: 10.1523/JNEUROSCI.4267-13.2014

Gallo, V., Zhou, J., McBain, C., Wright, P., Knutson, P., & Armstrong, R. (1996). Oligodendrocyte progenitor cell proliferation and lineage progression are regulated by glutamate receptor-mediated K+ channel block. *The Journal of Neuroscience, 16*(8), 2659-2670.

Garzillo, C. L., & Mello, L. E. (2002). Characterization of reactive astrocytes in the chronic phase of the pilocarpine model of epilepsy. *Epilepsia, 43 Suppl 5*, 107-109.

Genain, C. P., Cannella, B., Hauser, S. L., & Raine, C. S. (1999). Identification of autoantibodies associated with myelin damage in multiple sclerosis. *Nat Med, 5*(2), 170-175. doi: 10.1038/5532

Godinho, S. I., Maywood, E. S., Shaw, L., Tucci, V., Barnard, A. R., Busino, L., . . . Nolan, P. M. (2007). The after-hours mutant reveals a role for Fbxl3 in determining mammalian circadian period. *Science, 316*(5826), 897-900. doi: 10.1126/science.1141138

Heiman, M., Schaefer, A., Gong, S., Peterson, J. D., Day, M., Ramsey, K. E., . . . Heintz, N. (2008). A translational profiling approach for the molecular characterization of CNS cell types. *Cell, 135*(4), 738-748. doi: 10.1016/j.cell.2008.10.028

Hemm, R. D., Carlton, W. W., & Welser, J. R. (1971). Ultrastructural changes of cuprizone encephalopathy in mice. *Toxicol Appl Pharmacol, 18*(4), 869-882.

Hershko, A., & Ciechanover, A. (1998). The ubiquitin system. *Annu Rev Biochem, 67*, 425-479. doi: 10.1146/annurev.biochem.67.1.425

Hesse, A., Wagner, M., Held, J., Bruck, W., Salinas-Riester, G., Hao, Z., . . . Kuhlmann, T. (2010). In toxic demyelination oligodendroglial cell death occurs early and is FAS independent. *Neurobiol Dis, 37*(2), 362-369. doi: 10.1016/j.nbd.2009.10.016

Himanen, J.-P., Chumley, M. J., Lackmann, M., Li, C., Barton, W. A., Jeffrey, P. D., . . . Nikolov, D. B. (2004). Repelling class discrimination: ephrin-A5 binds to and activates EphB2 receptor signaling. *Nat Neurosci, 7*(5), 501-509. doi: http://www.nature.com/neuro/journal/v7/n5/suppinfo/nn1237_S1.html

Hirano, A., Yumimoto, K., Tsunematsu, R., Matsumoto, M., Oyama, M., Kozuka-Hata, H., . . . Fukada, Y. (2013). FBXL21 regulates oscillation of the circadian clock through ubiquitination and stabilization of cryptochromes. *Cell, 152*(5), 1106-1118. doi: 10.1016/j.cell.2013.01.054

Hiremath, M. M., Saito, Y., Knapp, G. W., Ting, J. P., Suzuki, K., & Matsushima, G. K. (1998). Microglial/macrophage accumulation during cuprizone-induced demyelination in C57BL/6 mice. *J Neuroimmunol, 92*(1-2), 38-49.

Horiuchi, M., Itoh, A., Pleasure, D., & Itoh, T. (2006). MEK-ERK signaling is involved in interferon-gamma-induced death of oligodendroglial progenitor cells. *J Biol Chem, 281*(29), 20095-20106. doi: 10.1074/jbc.M603179200

Hu, Y., Li, S., Jiang, H., Li, M. T., & Zhou, J. W. (2014). Ephrin-B2/EphA4 forward signaling is required for regulation of radial migration of cortical neurons in the mouse. *Neurosci Bull, 30*(3), 425-432. doi: 10.1007/s12264-013-1404-1

Ishibashi, T., Dakin, K. A., Stevens, B., Lee, P. R., Kozlov, S. V., Stewart, C. L., & Fields, R. D. (2006). Astrocytes promote myelination in response to electrical impulses. *Neuron, 49*(6), 823-832. doi: 10.1016/j.neuron.2006.02.006

Jarjour, A. A., Manitt, C., Moore, S. W., Thompson, K. M., Yuh, S. J., & Kennedy, T. E. (2003). Netrin-1 is a chemorepellent for oligodendrocyte precursor cells in the embryonic spinal cord. *J Neurosci, 23*(9), 3735-3744.

Jin, J., Cardozo, T., Lovering, R. C., Elledge, S. J., Pagano, M., & Harper, J. W. (2004). Systematic analysis and nomenclature of mammalian F-box proteins. *Genes Dev, 18*(21), 2573-2580. doi: 10.1101/gad.1255304

Jurewicz, A., Matysiak, M., Tybor, K., Kilianek, L., Raine, C. S., & Selmaj, K. (2005). Tumour necrosis factor-induced death of adult human oligodendrocytes is mediated by apoptosis inducing factor. *Brain, 128*(Pt 11), 2675-2688. doi: 10.1093/brain/awh627

Juurlink, B. H. (1997). Response of glial cells to ischemia: roles of reactive oxygen species and glutathione. *Neurosci Biobehav Rev, 21*(2), 151-166.

König, R., Stillfried, M., Aperdannier, P., Clarner, T., Beyer, C., Kipp, M., & Mey, J. (2012). Expression of retinoid X receptor beta is induced in astrocytes during corpus callosum demyelination. *Journal of Chemical Neuroanatomy, 43*(2), 120-132. doi: http://dx.doi.org/10.1016/j.jchemneu.2012.01.002

Kamphuis, W., Mamber, C., Moeton, M., Kooijman, L., Sluijs, J. A., Jansen, A. H., . . . Hol, E. M. (2012). GFAP isoforms in adult mouse brain with a focus on neurogenic astrocytes and reactive astrogliosis in mouse models of Alzheimer disease. *PLoS One, 7*(8), e42823. doi: 10.1371/journal.pone.0042823

Kessaris, N., Fogarty, M., Iannarelli, P., Grist, M., Wegner, M., & Richardson, W. D. (2005). Competing waves of oligodendrocytes in the forebrain and postnatal elimination of an embryonic lineage. *Nature Neuroscience, 9*, 173. doi: 10.1038/nn1620

https://www.nature.com/articles/nn1620#supplementary-information

Kiernan, B. W., Gotz, B., Faissner, A., & ffrench-Constant, C. (1996). Tenascin-C inhibits oligodendrocyte precursor cell migration by both adhesion-dependent and adhesion-independent mechanisms. *Mol Cell Neurosci, 7*(4), 322-335. doi: 10.1006/mcne.1996.0024

Kipp, M., Clarner, T., Dang, J., Copray, S., & Beyer, C. (2009). The cuprizone animal model: new insights into an old story. *Acta Neuropathol, 118*(6), 723-736. doi: 10.1007/s00401-009-0591-3

Kipreos, E. T., & Pagano, M. (2000). The F-box protein family. *Genome Biol, 1*(5), Reviews3002. doi: 10.1186/gb-2000-1-5-reviews3002

Kister, I., Bacon, T. E., Chamot, E., Salter, A. R., Cutter, G. R., Kalina, J. T., & Herbert, J. (2013). Natural History of Multiple Sclerosis Symptoms. *International Journal of MS Care, 15*(3), 146-156. doi: 10.7224/1537-2073.2012-053

Klein, R. (2009). Bidirectional modulation of synaptic functions by Eph/ephrin signaling. *Nat Neurosci, 12*(1), 15-20.

Koh, K., Zheng, X., & Sehgal, A. (2006). JETLAG Resets the Drosophila Circadian Clock by Promoting Light-Induced Degradation of TIMELESS. *Science, 312*(5781), 1809-1812. doi: 10.1126/science.1124951

Kullander, K., & Klein, R. (2002). Mechanisms and functions of eph and ephrin signalling. *Nat Rev Mol Cell Biol, 3*(7), 475-486.

Langer-Gould, A., Brara, S. M., Beaber, B. E., & Zhang, J. L. (2013). Incidence of multiple sclerosis in multiple racial and ethnic groups. *Neurology, 80*(19), 1734-1739. doi: 10.1212/WNL.0b013e3182918cc2

Lassmann, H., Bruck, W., & Lucchinetti, C. (2001). Heterogeneity of multiple sclerosis pathogenesis: implications for diagnosis and therapy. *Trends Mol Med, 7*(3), 115-121.

Lennon, V. A., Wingerchuk, D. M., Kryzer, T. J., Pittock, S. J., Lucchinetti, C. F., Fujihara, K., . . . Weinshenker, B. G. (2004). A serum autoantibody marker of neuromyelitis optica: distinction from multiple sclerosis. *Lancet, 364*(9451), 2106-2112. doi: 10.1016/s0140-6736(04)17551-x

Li, D., Xie, P., Zhao, F., Shu, J., Li, L., Zhan, Y., & Zhang, L. (2015). F-box protein Fbxo3 targets Smurf1 ubiquitin ligase for ubiquitination and degradation. *Biochem Biophys Res Commun, 458*(4), 941-945. doi: 10.1016/j.bbrc.2015.02.089

Liberto, C. M., Albrecht, P. J., Herx, L. M., Yong, V. W., & Levison, S. W. (2004). Pro-regenerative properties of cytokine-activated astrocytes. *J Neurochem, 89*(5), 1092-1100. doi: 10.1111/j.1471-4159.2004.02420.x

Liebetanz, D., & Merkler, D. (2006). Effects of commissural de- and remyelination on motor skill behaviour in the cuprizone mouse model of multiple sclerosis. *Exp Neurol, 202*(1), 217-224. doi: 10.1016/j.expneurol.2006.05.032

Lin, S. C., & Bergles, D. E. (2002). Physiological characteristics of NG2-expressing glial cells. *J Neurocytol, 31*(6-7), 537-549.

Linington, C., Bradl, M., Lassmann, H., Brunner, C., & Vass, K. (1988). Augmentation of demyelination in rat acute allergic encephalomyelitis by circulating mouse monoclonal antibodies directed against a myelin/oligodendrocyte glycoprotein. *Am J Pathol, 130*(3), 443-454.

Love, S. (1988). Cuprizone neurotoxicity in the rat: morphologic observations. *J Neurol Sci, 84*(2-3), 223-237.

Lu, Q. R., Sun, T., Zhu, Z., Ma, N., Garcia, M., Stiles, C. D., & Rowitch, D. H. (2002).

Common developmental requirement for Olig function indicates a motor neuron/oligodendrocyte connection. *Cell, 109*(1), 75-86.

Lublin, F. D., & Reingold, S. C. (1996). Defining the clinical course of multiple sclerosis: results of an international survey. National Multiple Sclerosis Society (USA) Advisory Committee on Clinical Trials of New Agents in Multiple Sclerosis. *Neurology, 46*(4), 907-911.

Lublin, F. D., Reingold, S. C., Cohen, J. A., Cutter, G. R., Sørensen, P. S., Thompson, A. J., . . . Polman, C. H. (2014). Defining the clinical course of multiple sclerosis: The 2013 revisions. *Neurology, 83*(3), 278-286. doi: 10.1212/wnl.0000000000000560

Lublin, F. D., Reingold, S. C., & Sclerosis*, N. M. S. S. A. C. o. C. T. o. N. A. i. M. (1996). Defining the clinical course of multiple sclerosis: Results of an international survey. *Neurology, 46*(4), 907-911. doi: 10.1212/wnl.46.4.907

Lucchinetti, C., Bruck, W., Parisi, J., Scheithauer, B., Rodriguez, M., & Lassmann, H. (2000). Heterogeneity of multiple sclerosis lesions: implications for the pathogenesis of demyelination. *Ann Neurol, 47*(6), 707-717.

Lucchinetti, C. F., Bruck, W., Rodriguez, M., & Lassmann, H. (1996). Distinct patterns of multiple sclerosis pathology indicates heterogeneity on pathogenesis. *Brain Pathol, 6*(3), 259-274.

Lucchinetti, C. F., Mandler, R. N., McGavern, D., Bruck, W., Gleich, G., Ransohoff, R. M., . . . Lassmann, H. (2002). A role for humoral mechanisms in the pathogenesis of Devic's neuromyelitis optica. *Brain, 125*(Pt 7), 1450-1461.

Ludwin, S. K. (1978). Central nervous system demyelination and remyelination in the mouse: an ultrastructural study of cuprizone toxicity. *Lab Invest, 39*(6), 597-612.

Luxey, M., Jungas, T., Laussu, J., Audouard, C., Garces, A., & Davy, A. (2013). Eph:ephrin-B1 forward signaling controls fasciculation of sensory and motor axons. *Dev Biol, 383*(2), 264-274. doi: 10.1016/j.ydbio.2013.09.010

Mason, J. L., Jones, J. J., Taniike, M., Morell, P., Suzuki, K., & Matsushima, G. K. (2000). Mature oligodendrocyte apoptosis precedes IGF-1 production and oligodendrocyte progenitor accumulation and differentiation during demyelination/remyelination. *J Neurosci Res, 61*(3), 251-262. doi: 10.1002/1097-4547(20000801)61:3<251::aid-jnr3>3.0.co;2-w

Matsushima, G. K., & Morell, P. (2001). The neurotoxicant, cuprizone, as a model to study demyelination and remyelination in the central nervous system. *Brain Pathol, 11*(1), 107-116.

Matute, C., Torre, I., Perez-Cerda, F., Perez-Samartin, A., Alberdi, E., Etxebarria, E., . . . Domercq, M. (2007). P2X(7) receptor blockade prevents ATP excitotoxicity in oligodendrocytes and ameliorates experimental autoimmune encephalomyelitis. *J Neurosci, 27*(35), 9525-9533. doi: 10.1523/jneurosci.0579-07.2007

McFarland, H. F., & Martin, R. (2007). Multiple sclerosis: a complicated picture of autoimmunity. *Nat Immunol, 8*(9), 913-919. doi: 10.1038/ni1507

McTigue, D. M., & Tripathi, R. B. (2008). The life, death, and replacement of oligodendrocytes in the adult CNS. *J Neurochem, 107*(1), 1-19. doi: 10.1111/j.1471-4159.2008.05570.x

Mi, S., Miller, R. H., Lee, X., Scott, M. L., Shulag-Morskaya, S., Shao, Z., . . . Pepinsky, R. B. (2005). LINGO-1 negatively regulates myelination by oligodendrocytes. *Nature Neuroscience, 8*, 745. doi: 10.1038/nn1460

Miller, D. H., & Leary, S. M. (2007). Primary-progressive multiple sclerosis. *Lancet*

Neurol, 6(10), 903-912. doi: 10.1016/s1474-4422(07)70243-0

Milner, R., Frost, E., Nishimura, S., Delcommenne, M., Streuli, C., Pytela, R., & Ffrench-Constant, C. (1997). Expression of alpha vbeta3 and alpha vbeta8 integrins during oligodendrocyte precursor differentiation in the presence and absence of axons. *Glia, 21*(4), 350-360.

Misu, T., Fujihara, K., & Itoyama, Y. (2008). [Neuromyelitis optica and anti-aquaporin 4 antibody--an overview]. *Brain Nerve, 60*(5), 527-537.

Moll, N. M., Hong, E., Fauveau, M., Naruse, M., Kerninon, C., Tepavcevic, V., . . . Nait Oumesmar, B. (2013). SOX17 is expressed in regenerating oligodendrocytes in experimental models of demyelination and in multiple sclerosis. *Glia, 61*(10), 1659-1672. doi: 10.1002/glia.22547

Mukhopadhyay, G., Doherty, P., Walsh, F. S., Crocker, P. R., & Filbin, M. T. (1994). A novel role for myelin-associated glycoprotein as an inhibitor of axonal regeneration. *Neuron, 13*(3), 757-767. doi: https://doi.org/10.1016/0896-6273(94)90042-6

Murayama, S., & Saito, Y. (2007). [Neuropathology of progressive multifocal leukoencephalopathy]. *Brain Nerve, 59*(2), 119-124.

Na, S. Y., Cao, Y., Toben, C., Nitschke, L., Stadelmann, C., Gold, R., . . . Hunig, T. (2008). Naive CD8 T-cells initiate spontaneous autoimmunity to a sequestered model antigen of the central nervous system. *Brain, 131*(Pt 9), 2353-2365. doi: 10.1093/brain/awn148

Nave, K. A. (2010). Myelination and the trophic support of long axons. *Nat Rev Neurosci, 11*(4), 275-283. doi: 10.1038/nrn2797

Niehaus, A., Stegmuller, J., Diers-Fenger, M., & Trotter, J. (1999). Cell-surface glycoprotein of oligodendrocyte progenitors involved in migration. *J Neurosci, 19*(12), 4948-4961.

Nilsson, G. (1950). A New Colour Reaction on Copper and Certain Carbonyl Compounds (Vol. 4, pp. 205-205): MUNKSGAARD INT PUBL LTD 35 NORRE SOGADE, PO BOX 2148, DK-1016 COPENHAGEN, DENMARK.

Noseworthy, J. H., Lucchinetti, C., Rodriguez, M., & Weinshenker, B. G. (2000). Multiple sclerosis. *N Engl J Med, 343*(13), 938-952. doi: 10.1056/nejm200009283431307

Nyenhuis, D. L., Rao, S. M., Zajecka, J. M., Luchetta, T., Bernardin, L., & Garron, D. C. (1995). Mood disturbance versus other symptoms of depression in multiple sclerosis. *J Int Neuropsychol Soc, 1*(3), 291-296.

Obeid, L. M., Linardic, C. M., Karolak, L. A., & Hannun, Y. A. (1993). Programmed cell death induced by ceramide. *Science, 259*(5102), 1769-1771.

Olah, M., Amor, S., Brouwer, N., Vinet, J., Eggen, B., Biber, K., & Boddeke, H. W. G. M. (2012). Identification of a microglia phenotype supportive of remyelination. *Glia, 60*(2), 306-321. doi: 10.1002/glia.21266

Othman, A., Frim, D. M., Polak, P., Vujicic, S., Arnason, B. G., & Boullerne, A. I. (2011). Olig1 is expressed in human oligodendrocytes during maturation and regeneration. *Glia, 59*(6), 914-926. doi: 10.1002/glia.21163

Pasquale, E. B. (2004). Eph-ephrin promiscuity is now crystal clear. *Nat Neurosci, 7*(5), 417-418.

Pasquini, L. A., Calatayud, C. A., Bertone Una, A. L., Millet, V., Pasquini, J. M., & Soto, E. F. (2007). The neurotoxic effect of cuprizone on oligodendrocytes depends on the presence of pro-inflammatory cytokines secreted by microglia. *Neurochem Res, 32*(2), 279-292. doi: 10.1007/s11064-006-9165-0

Patel, J. R., McCandless, E. E., Dorsey, D., & Klein, R. S. (2010). CXCR4 promotes

differentiation of oligodendrocyte progenitors and remyelination. *Proceedings of the National Academy of Sciences, 107*(24), 11062-11067. doi: 10.1073/pnas.1006301107

Poliakov, A., Cotrina, M., & Wilkinson, D. G. (2004). Diverse Roles of Eph Receptors and Ephrins in the Regulation of Cell Migration and Tissue Assembly. *Developmental Cell, 7*(4), 465-480. doi: http://dx.doi.org/10.1016/j.devcel.2004.09.006

Porsolt, R. D., Le Pichon, M., & Jalfre, M. (1977). Depression: a new animal model sensitive to antidepressant treatments. *Nature, 266*(5604), 730-732.

Praet, J., Guglielmetti, C., Berneman, Z., Van der Linden, A., & Ponsaerts, P. (2014). Cellular and molecular neuropathology of the cuprizone mouse model: Clinical relevance for multiple sclerosis. *Neuroscience & Biobehavioral Reviews, 47*(Supplement C), 485-505. doi: https://doi.org/10.1016/j.neubiorev.2014.10.004

Praet, J., Guglielmetti, C., Berneman, Z., Van der Linden, A., & Ponsaerts, P. (2014). Cellular and molecular neuropathology of the cuprizone mouse model: clinical relevance for multiple sclerosis. *Neurosci Biobehav Rev, 47*, 485-505. doi: 10.1016/j.neubiorev.2014.10.004

Prestoz, L., Chatzopoulou, E., Lemkine, G., Spassky, N., Lebras, B., Kagawa, T., . . . Thomas, J. L. (2004). Control of axonophilic migration of oligodendrocyte precursor cells by Eph-ephrin interaction. *Neuron Glia Biol, 1*(1), 73-83. doi: doi:10.1017/S1740925X04000109

Raasch, J., Zeller, N., van Loo, G., Merkler, D., Mildner, A., Erny, D., . . . Prinz, M. (2011). IκB kinase 2 determines oligodendrocyte loss by non-cell-autonomous activation of NF-κB in the central nervous system. *Brain, 134*(4), 1184-1198. doi: 10.1093/brain/awq359

Rao, P., & Segal, B. M. (2004). Experimental Autoimmune Encephalomyelitis. In A. Perl (Ed.), *Autoimmunity: Methods and Protocols* (pp. 363-375). Totowa, NJ: Humana Press.

Redwine, J. M., Blinder, K. L., & Armstrong, R. C. (1997). In situ expression of fibroblast growth factor receptors by oligodendrocyte progenitors and oligodendrocytes in adult mouse central nervous system. *J Neurosci Res, 50*(2), 229-237. doi: 10.1002/(sici)1097-4547(19971015)50:2<229::aid-jnr11>3.0.co;2-3

Remington, L. T., Babcock, A. A., Zehntner, S. P., & Owens, T. (2007). Microglial Recruitment, Activation, and Proliferation in Response to Primary Demyelination. *Am J Pathol, 170*(5), 1713-1724. doi: http://dx.doi.org/10.2353/ajpath.2007.060783

Robinson, A. P., Harp, C. T., Noronha, A., & Miller, S. D. (2014). The experimental autoimmune encephalomyelitis (EAE) model of MS: utility for understanding disease pathophysiology and treatment. *Handbook of clinical neurology, 122*, 173-189. doi: 10.1016/B978-0-444-52001-2.00008-X

Rossi-George, A., LeBlanc, F., Kaneta, T., Urbach, D., & Kusnecov, A. W. (2004). Effects of bacterial superantigens on behavior of mice in the elevated plus maze and light-dark box. *Brain Behav Immun, 18*(1), 46-54.

Salter, M. G., & Fern, R. (2005). NMDA receptors are expressed in developing oligodendrocyte processes and mediate injury. *Nature, 438*, 1167. doi: 10.1038/nature04301

https://www.nature.com/articles/nature04301#supplementary-information

Sanchez-Gomez, M. V., & Matute, C. (1999). AMPA and kainate receptors each

mediate excitotoxicity in oligodendroglial cultures. *Neurobiol Dis, 6*(6), 475-485. doi: 10.1006/nbdi.1999.0264

Sapkota, G., Alarcon, C., Spagnoli, F. M., Brivanlou, A. H., & Massague, J. (2007). Balancing BMP signaling through integrated inputs into the Smad1 linker. *Mol Cell, 25*(3), 441-454. doi: 10.1016/j.molcel.2007.01.006

Savaskan, N. E., Weinmann, O., Heimrich, B., & Eyupoglu, I. Y. (2009). High resolution neurochemical gold staining method for myelin in peripheral and central nervous system at the light- and electron-microscopic level. *Cell Tissue Res, 337*(2), 213-221. doi: 10.1007/s00441-009-0815-9

Schmued, L., Bowyer, J., Cozart, M., Heard, D., Binienda, Z., & Paule, M. (2008). Introducing Black-Gold II, a highly soluble gold phosphate complex with several unique advantages for the histochemical localization of myelin. *Brain Res, 1229*, 210-217. doi: 10.1016/j.brainres.2008.06.129

Schnadelbach, O., Blaschuk, O. W., Symonds, M., Gour, B. J., Doherty, P., & Fawcett, J. W. (2000). N-cadherin influences migration of oligodendrocytes on astrocyte monolayers. *Mol Cell Neurosci, 15*(3), 288-302. doi: 10.1006/mcne.1999.0819

Scholz, J., Klein, M. C., Behrens, T. E., & Johansen-Berg, H. (2009). Training induces changes in white-matter architecture. *Nat Neurosci, 12*(11), 1370-1371. doi: 10.1038/nn.2412

Senturk, A., Pfennig, S., Weiss, A., Burk, K., & Acker-Palmer, A. (2011). Ephrin Bs are essential components of the Reelin pathway to regulate neuronal migration. *Nature, 472*(7343), 356-360. doi: 10.1038/nature09874

Senturk, A., Pfennig, S., Weiss, A., Burk, K., & Acker-Palmer, A. (2011). Ephrin Bs are essential components of the Reelin pathway to regulate neuronal migration. *Nature, 472*(7343), 356-360. doi: http://www.nature.com/nature/journal/v472/n7343/abs/10.1038-nature09874-unlocked.html#supplementary-information

Sheleg, M., Yu, Q., Go, C., Wagner, G. C., Kusnecov, A. W., & Zhou, R. (2017). Decreased maternal behavior and anxiety in ephrin-A5-/- mice. *Genes Brain Behav, 16*(2), 271-284. doi: 10.1111/gbb.12319

Shen, S., Li, J., & Casaccia-Bonnefil, P. (2005). Histone modifications affect timing of oligodendrocyte progenitor differentiation in the developing rat brain. *J Cell Biol, 169*(4), 577-589. doi: 10.1083/jcb.200412101

Shin, D., Shin, J. Y., McManus, M. T., Ptacek, L. J., & Fu, Y. H. (2009). Dicer ablation in oligodendrocytes provokes neuronal impairment in mice. *Ann Neurol, 66*(6), 843-857. doi: 10.1002/ana.21927

Shiotsuki, H., Yoshimi, K., Shimo, Y., Funayama, M., Takamatsu, Y., Ikeda, K., . . . Hattori, N. (2010). A rotarod test for evaluation of motor skill learning. *J Neurosci Methods, 189*(2), 180-185. doi: 10.1016/j.jneumeth.2010.03.026

Skripuletz, T., Lindner, M., Kotsiari, A., Garde, N., Fokuhl, J., Linsmeier, F., . . . Stangel, M. (2008). Cortical demyelination is prominent in the murine cuprizone model and is strain-dependent. *Am J Pathol, 172*(4), 1053-1061. doi: 10.2353/ajpath.2008.070850

Slattery, D. A., & Cryan, J. F. (2012). Using the rat forced swim test to assess antidepressant-like activity in rodents. *Nat Protoc, 7*(6), 1009-1014. doi: 10.1038/nprot.2012.044

Smith, K. J., & Lassmann, H. (2002). The role of nitric oxide in multiple sclerosis. *Lancet Neurol, 1*(4), 232-241.

Soundarapandian, M. M., Selvaraj, V., Lo, U. G., Golub, M. S., Feldman, D. H.,

Pleasure, D. E., & Deng, W. (2011). Zfp488 promotes oligodendrocyte differentiation of neural progenitor cells in adult mice after demyelination. *Sci Rep, 1*, 2. doi: 10.1038/srep00002

Spassky, N., Heydon, K., Mangatal, A., Jankovski, A., Olivier, C., Queraud-Lesaux, F., . . . Zalc, B. (2001). Sonic hedgehog-dependent emergence of oligodendrocytes in the telencephalon: evidence for a source of oligodendrocytes in the olfactory bulb that is independent of PDGFRα signaling. *Development, 128*(24), 4993-5004.

Stevens, B., Porta, S., Haak, L. L., Gallo, V., & Fields, R. D. (2002). Adenosine: a neuron-glial transmitter promoting myelination in the CNS in response to action potentials. *Neuron, 36*(5), 855-868.

Stys, P. K., Zamponi, G. W., van Minnen, J., & Geurts, J. J. (2012). Will the real multiple sclerosis please stand up? *Nat Rev Neurosci, 13*(7), 507-514. doi: 10.1038/nrn3275

Suzuki, K., & Kikkawa, Y. (1969). Status spongiosus of CNS and hepatic changes induced by cuprizone (biscyclohexanone oxalyldihydrazone). *Am J Pathol, 54*(2), 307-325.

Tandler, B., & Hoppel, C. L. (1973). Division of giant mitochondria during recovery from cuprizone intoxication. *J Cell Biol, 56*(1), 266-272.

Tandler, B., & Hoppel, C. L. (1975). The failure of supplemental dietary copper to prevent cuprizone-induced alterations in mouse hepatocytes. *Beitr Pathol, 156*(1), 56-64.

Tansey, F. A., Zhang, H., & Cammer, W. (1997). Rapid upregulation of the Pi isoform of glutathione-S-transferase in mouse brains after withdrawal of the neurotoxicant, cuprizone. *Molecular and Chemical Neuropathology, 31*(2), 161-170. doi: 10.1007/bf02815240

Targett, M. P., Sussman, J., Scolding, N., O'Leary, M. T., Compston, D. A., & Blakemore, W. F. (1996). Failure to achieve remyelination of demyelinated rat axons following transplantation of glial cells obtained from the adult human brain. *Neuropathol Appl Neurobiol, 22*(3), 199-206.

Taylor, L. C., Gilmore, W., & Matsushima, G. K. (2009). SJL mice exposed to cuprizone intoxication reveal strain and gender pattern differences in demyelination. *Brain Pathol, 19*(3), 467-479. doi: 10.1111/j.1750-3639.2008.00230.x

Thorburne, S. K., & Juurlink, B. H. (1996). Low glutathione and high iron govern the susceptibility of oligodendroglial precursors to oxidative stress. *J Neurochem, 67*(3), 1014-1022.

Tiwari-Woodruff, S. K., Buznikov, A. G., Vu, T. Q., Micevych, P. E., Chen, K., Kornblum, H. I., & Bronstein, J. M. (2001). OSP/claudin-11 forms a complex with a novel member of the tetraspanin super family and beta1 integrin and regulates proliferation and migration of oligodendrocytes. *J Cell Biol, 153*(2), 295-305.

Torkildsen, O., Brunborg, L. A., Myhr, K. M., & Bo, L. (2008). The cuprizone model for demyelination. *Acta Neurol Scand Suppl, 188*, 72-76. doi: 10.1111/j.1600-0404.2008.01036.x

Trapp, B. D. (1990). Myelin-associated glycoprotein. Location and potential functions. *Ann N Y Acad Sci, 605*, 29-43.

Trapp, B. D., & Quarles, R. H. (1984). Immunocytochemical localization of the myelin-associated glycoprotein. Fact or artifact? *J Neuroimmunol, 6*(4), 231-249.

Voß, E. V., Škuljec, J., Gudi, V., Skripuletz, T., Pul, R., Trebst, C., & Stangel, M. (2012). Characterisation of microglia during de- and remyelination: Can they create a repair promoting environment? *Neurobiol Dis, 45*(1), 519-528. doi: http://dx.doi.org/10.1016/j.nbd.2011.09.008

Wagner, T., & Rafael, J. (1977). Biochemical properties of liver megamitochondria induced by chloramphenicol or cuprizone. *Exp Cell Res, 107*(1), 1-13.

Wakabayashi, T., Asano, M., Ishikawa, K., & Kishimoto, H. (1978). Mechanism of the formation of megamitochondria by copper-chelating agents. V. Further studies on isolated megamitochondria. *Acta Pathol Jpn, 28*(2), 215-223.

Wakabayashi, T., Asano, M., & Kurono, C. (1975). Mechanism of the formation of megamitochondria induced by copper-chelating agents. II. Isolation and some properties of megamitochondria from the cuprizone-treated mouse liver. *Acta Pathol Jpn, 25*(1), 39-49.

Walf, A. A., & Frye, C. A. (2007). The use of the elevated plus maze as an assay of anxiety-related behavior in rodents. *Nat Protoc, 2*(2), 322-328. doi: 10.1038/nprot.2007.44

Wang, C., Rougon, G., & Kiss, J. Z. (1994). Requirement of polysialic acid for the migration of the O-2A glial progenitor cell from neurohypophyseal explants. *J Neurosci, 14*(7), 4446-4457.

Wang, S., Sdrulla, A. D., diSibio, G., Bush, G., Nofziger, D., Hicks, C., . . . Barres, B. A. (1998). Notch receptor activation inhibits oligodendrocyte differentiation. *Neuron, 21*(1), 63-75.

Watkins, T. A., Emery, B., Mulinyawe, S., & Barres, B. A. (2008). Distinct stages of myelination regulated by gamma-secretase and astrocytes in a rapidly myelinating CNS coculture system. *Neuron, 60*(4), 555-569. doi: 10.1016/j.neuron.2008.09.011

Wegner, M. (2008). A matter of identity: transcriptional control in oligodendrocytes. *J Mol Neurosci, 35*(1), 3-12. doi: 10.1007/s12031-007-9008-8

Wisniewski, H. M., & Bloom, B. R. (1975). Primary demyelination as a nonspecific consequence of a cell-mediated immune reaction. *J Exp Med, 141*(2), 346-359.

Wolswijk, G. (2000). Oligodendrocyte survival, loss and birth in lesions of chronic-stage multiple sclerosis. *Brain, 123 (Pt 1)*, 105-115.

Woodruff, R. T., Schorpp, K. M., Lawrenczyk, A. J., Chakraborty, T., & Kusnecov, A. W. (2011). Effects of acute and repeated administration of Staphylococcal enterotoxin A on Morris water maze learning, corticosterone and hippocampal IL-1beta and TNFalpha. *Brain Behav Immun, 25*(5), 938-946. doi: 10.1016/j.bbi.2010.10.005

Xiao, L., Xu, H., Zhang, Y., Wei, Z., He, J., Jiang, W., . . . Li, X. M. (2008). Quetiapine facilitates oligodendrocyte development and prevents mice from myelin breakdown and behavioral changes. *Mol Psychiatry, 13*(7), 697-708. doi: 10.1038/sj.mp.4002064

Xing, L., Zhang, M., & Chen, D. (2010). Smurf control in bone cells. *J Cell Biochem, 110*(3), 554-563. doi: 10.1002/jcb.22586

Xu, C., Bailly-Maitre, B., & Reed, J. C. (2005). Endoplasmic reticulum stress: cell life and death decisions. *J Clin Invest, 115*(10), 2656-2664. doi: 10.1172/jci26373

Xu, H., Yang, H. J., McConomy, B., Browning, R., & Li, X. M. (2010). Behavioral and neurobiological changes in C57BL/6 mouse exposed to cuprizone: effects of antipsychotics. *Front Behav Neurosci, 4*, 8. doi: 10.3389/fnbeh.2010.00008

Xu, H., Yang, H. J., Zhang, Y., Clough, R., Browning, R., & Li, X. M. (2009).

Behavioral and neurobiological changes in C57BL/6 mice exposed to cuprizone. *Behav Neurosci*, *123*(2), 418-429. doi: 10.1037/a0014477

Xu, N.-J., & Henkemeyer, M. (2009). Ephrin-B3 reverse signaling through Grb4 and cytoskeletal regulators mediates axon pruning. *Nat Neurosci*, *12*(3), 268-276. doi: http://www.nature.com/neuro/journal/v12/n3/suppinfo/nn.2254_S1.html

Xu, N.-J., Sun, S., Gibson, J. R., & Henkemeyer, M. (2011). A dual shaping mechanism for postsynaptic ephrin-B3 as a receptor that sculpts dendrites and synapses. *Nat Neurosci*, *14*(11), 1421-1429. doi: http://www.nature.com/neuro/journal/v14/n11/abs/nn.2931.html#supplementary-information

Yamashita, M., Ying, S. X., Zhang, G. M., Li, C., Cheng, S. Y., Deng, C. X., & Zhang, Y. E. (2005). Ubiquitin ligase Smurf1 controls osteoblast activity and bone homeostasis by targeting MEKK2 for degradation. *Cell*, *121*(1), 101-113. doi: 10.1016/j.cell.2005.01.035

Yan, H., & Rivkees, S. A. (2002). Hepatocyte growth factor stimulates the proliferation and migration of oligodendrocyte precursor cells. *J Neurosci Res*, *69*(5), 597-606. doi: 10.1002/jnr.10323

Ye, F., Chen, Y., Hoang, T., Montgomery, R. L., Zhao, X. H., Bu, H., . . . Lu, Q. R. (2009). HDAC1 and HDAC2 regulate oligodendrocyte differentiation by disrupting the beta-catenin-TCF interaction. *Nat Neurosci*, *12*(7), 829-838. doi: 10.1038/nn.2333

Ye, J. N., Chen, X. S., Su, L., Liu, Y. L., Cai, Q. Y., Zhan, X. L., . . . Yao, Z. X. (2013). Progesterone alleviates neural behavioral deficits and demyelination with reduced degeneration of oligodendroglial cells in cuprizone-induced mice. *PLoS One*, *8*(1), e54590. doi: 10.1371/journal.pone.0054590

Yokoyama, N., Romero, M. I., Cowan, C. A., Galvan, P., Helmbacher, F., Charnay, P., . . . Henkemeyer, M. (2001). Forward Signaling Mediated by Ephrin-B3 Prevents Contralateral Corticospinal Axons from Recrossing the Spinal Cord Midline. *Neuron*, *29*(1), 85-97. doi: https://doi.org/10.1016/S0896-6273(01)00182-9

Zaaraoui, W., Deloire, M., Merle, M., Girard, C., Raffard, G., Biran, M., . . . Dousset, V. (2008). Monitoring demyelination and remyelination by magnetization transfer imaging in the mouse brain at 9.4 T. *Magnetic Resonance Materials in Physics, Biology and Medicine*, *21*(5), 357-362. doi: 10.1007/s10334-008-0141-3

Zatta, P., Raso, M., Zambenedetti, P., Wittkowski, W., Messori, L., Piccioli, F., . . . Beltramini, M. (2005). Copper and zinc dismetabolism in the mouse brain upon chronic cuprizone treatment. *Cell Mol Life Sci*, *62*(13), 1502-1513. doi: 10.1007/s00018-005-5073-8

Zhao, M., Qiao, M., Harris, S. E., Oyajobi, B. O., Mundy, G. R., & Chen, D. (2004). Smurf1 inhibits osteoblast differentiation and bone formation in vitro and in vivo. *J Biol Chem*, *279*(13), 12854-12859. doi: 10.1074/jbc.M313294200

Zhao, M., Qiao, M., Oyajobi, B. O., Mundy, G. R., & Chen, D. (2003). E3 ubiquitin ligase Smurf1 mediates core-binding factor alpha1/Runx2 degradation and plays a specific role in osteoblast differentiation. *J Biol Chem*, *278*(30), 27939-27944. doi: 10.1074/jbc.M304132200

Zhao, X., He, X., Han, X., Yu, Y., Ye, F., Chen, Y., . . . Lu, Q. R. (2010). MicroRNA-mediated control of oligodendrocyte differentiation. *Neuron*, *65*(5), 612-626. doi: 10.1016/j.neuron.2010.02.018

Zhou, Q., Choi, G., & Anderson, D. J. (2001). The bHLH transcription factor Olig2

promotes oligodendrocyte differentiation in collaboration with Nkx2.2. *Neuron, 31*(5), 791-807.

Ziskin, J. L., Nishiyama, A., Rubio, M., Fukaya, M., & Bergles, D. E. (2007). Vesicular release of glutamate from unmyelinated axons in white matter. *Nat Neurosci, 10*(3), 321-330. doi: 10.1038/nn1854